50272-101

REPORT DOCUMENTATION PAGE	1. REPORT NO. NCEER-89-0025	2.	3. Recipient's Accession No.

4. Title and Subtitle
DYNA1D A Computer Program for Nonlinear Seismic Site Response Analysis Technical Documentation

5. Report Date
September 14, 1989

6.

7. Author(s)
Jean H. Prevost

8. Performing Organization Rept. No.

9. Performing Organization Name and Address

10. Project/Task/Work Unit No.

11. Contract(C) or Grant(G) No.
(C) 86-2021 and 87-1307
ECE 86-07591
(G)

12. Sponsoring Organization Name and Address
National Center for Earthquake Engineering Research
State University of New York at Buffalo
Red Jacket Quadrangle
Buffalo, New York 14261

13. Type of Report & Period Covered
Technical Report

14.

15. Supplementary Notes
This research was conducted at Princeton University and was partially supported by the National Science Foundation under Grant No. ECE 86-07591.

16. Abstract (Limit: 200 words)

This report describes DYNA1D, a finite element computer program for nonlinear seismic site response analysis. Dry, saturated and partially saturated deposits can be analyzed. DYNA1D has been developed to allow site response analyses to be performed taking into account: (1) the nonlinear, anisotropic and hysteretic stress-strain behavior of the soil materials; and (2) the effects of the transient flow of the pore water through the soil strata. The procedures used (field and constitutive equations) are general and applicable to multidimensional situations. The goal was to provide a realistic and reliable analysis procedure for use in engineering design practice. Therefore, although no sacrifices have been made as to the rigor and generality of the field and constitutive equations used, attempts have been made to simplify the use of the code. For that purpose, features such as automatic initialization procedures have been implemented. Also, required material constitutive parameters are identified in terms of classical soil mechanics parameters. In order to ease the interpretation of the analysis results, graphic display capabilities which allow plots of spatial and temporal variations of field components have been implemented.

17. Document Analysis a. Descriptors

b. Identifiers/Open-Ended Terms

EARTHQUAKE ENGINEERING
SITE RESPONSE ANALYSIS
SEISMIC RISK ANALYSIS
SOIL STRUCTURE INTERACTION
GEOTECHNICAL RESEARCH
COMPUTER PROGRAMS
DYNA1D
GROUND MOTIONS

c. COSATI Field/Group

18. Availability Statement	19. Security Class (This Report)	21. No. of Pages
Release Unlimited	Unclassified	138
	20. Security Class (This Page) Unclassified	22. Price A07

(See ANSI-Z39.18) See instructions on Reverse OPTIONAL FORM 272 (4-77)

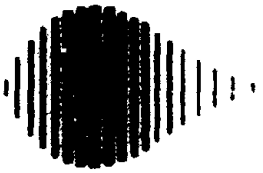

NATIONAL CENTER FOR EARTHQUAKE ENGINEERING RESEARCH
State University of New York at Buffalo

DYNA1D
A COMPUTER PROGRAM FOR NONLINEAR SEISMIC SITE RESPONSE ANALYSIS TECHNICAL DOCUMENTATION

by

Jean H. Prevost
Department of Civil Engineering and Operations Research
Princeton University
Princeton, New Jersey 08544

Technical Report NCEER-89-0025

September 14, 1989

This research was conducted at Princeton University and was partially supported by the National Science Foundation under Grant No. ECE 86-07591.

NOTICE

This report was prepared by Princeton University as a result of research sponsored by the National Center for Earthquake Engineering Research (NCEER). Neither NCEER, associates of NCEER, its sponsors, Princeton University, or any person acting on their behalf:

a. makes any warranty, express or implied, with respect to the use of any information, apparatus, method, or process disclosed in this report or that such use may not infringe upon privately owned rights; or

b. assumes any liabilities of whatsoever kind with respect to the use of, or the damage resulting from the use of, any information, apparatus, method or process disclosed in this report.

DYNAID
A COMPUTER PROGRAM FOR NONLINEAR SEISMIC SITE RESPONSE ANALYSIS
TECHNICAL DOCUMENTATION

by

Jean H. Prevost[1]

September 14, 1989

Technical Report NCEER-89-0025

NCEER Contract Numbers 86-2021 and 87-1307

NSF Master Contract Number ECE 86-07591

1 Professor, Dept. of Civil Engineering and Operations Research, Princeton University

NATIONAL CENTER FOR EARTHQUAKE ENGINEERING RESEARCH
State University of New York at Buffalo
Red Jacket Quadrangle, Buffalo, NY 14261

PREFACE

The National Center for Earthquake Engineering Research (NCEER) is devoted to the expansion and dissemination of knowledge about earthquakes, the improvement of earthquake-resistant design, and the implementation of seismic hazard mitigation procedures to minimize loss of lives and property. The emphasis is on structures and lifelines that are found in zones of moderate to high seismicity throughout the United States.

NCEER's research is being carried out in an integrated and coordinated manner following a structured program. The current research program comprises four main areas:

- Existing and New Structures
- Secondary and Protective Systems
- Lifeline Systems
- Disaster Research and Planning

This technical report pertains to Program 1, Existing and New Structures, and more specifically to geotechnical studies.

The long term goal of research in Existing and New Structures is to develop seismic hazard mitigation procedures through rational probabilistic risk assessment for damage or collapse of structures, mainly existing buildings, in regions of moderate to high seismicity. The work relies on improved definitions of seismicity and site response, experimental and analytical evaluations of systems response, and more accurate assessment of risk factors. This technology will be incorporated in expert systems tools and improved code formats for existing and new structures. Methods of retrofit will also be developed. When this work is completed, it should be possible to characterize and quantify societal impact of seismic risk in various geographical regions and large municipalities. Toward this goal, the program has been divided into five components, as shown in the figure below:

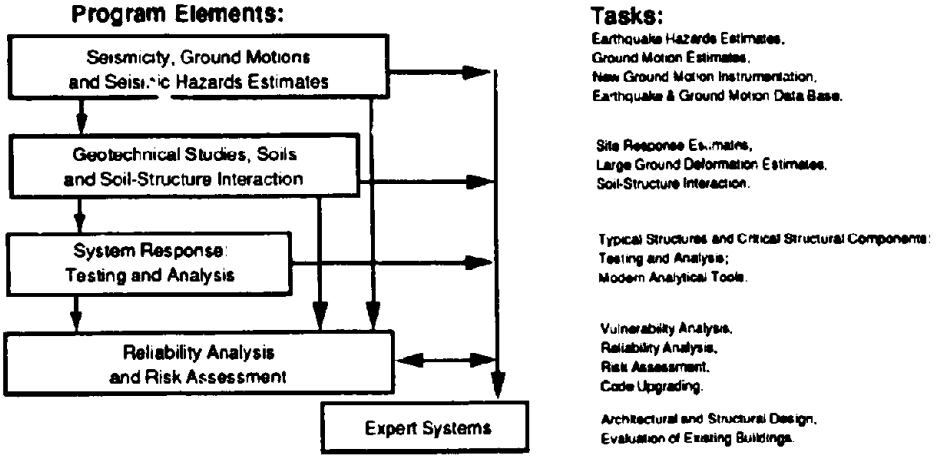

Geotechnical studies constitute one of the important areas of research in Existing and New Structures. Current research activities include the following:

1. Development of linear and nonlinear site response estimates.
2. Development of liquefaction and large ground deformation estimates.
3. Investigation of soil-structure interaction phenomena.
4. Development of computational methods.
5. Incorporation of local soil effects and soil-structure interaction into existing codes.

The ultimate goal of projects concerned with geotechnical studies is to develop methods of engineering estimation of large soil deformations, soil-structure interaction, and site response.

This report describes the development of DYNA1D, a finite element computer program for nonlinear site response analysis. The program can be used to analyze dry, saturated, and partially saturated soils. The program provides a user friendly interface and graphic displays of various output plots. It is intended to be a realistic and reliable procedure that can be used in engineering design practice.

ABSTRACT

This report describes DYNA1D, a finite element computer program for nonlinear seismic site response analysis. Dry, saturated and partially saturated deposits can be analyzed. DYNA1D has been developed to allow site response analyses to be performed taking into account: *(1)* the nonlinear, anisotropic and hysteretic stress-strain behavior of the soil materials; and *(2)* the effects of the transient flow of the pore water through the soil strata. The procedures used (field and constitutive equations) are general and applicable to *multidimensional* situations. The goal was to provide a realistic and reliable analysis procedure for use in engineering design practice. Therefore, although no sacrifices have been made as to the rigor and generality of the field and constitutive equations used, attemps have been made to simplify the use of the code. For that purpose, features such as automatic (*i.e.*, user transparent) initialization procedures have been implemented. Also, required material constitutive parameters are identified in terms of "classical" soil mechanics paramcters (*e.g.*, elastic moduli, friction angles, permeabilities, etc.). In order to ease the interpretation of the analysis results, graphic display capabilities which allow plots of spatial and temporal variations of field components have been implemented.

The program and its analysis capabilities are described in Section 1. The theoretical framework which forms the basis of the formulations used is summarized in Section 2. The numerical formulation employed for solving the coupled field equations is reviewed in Section 3. Special boundary conditions allow the seismic input motion to be prescribed as an incident vertically propagating motion, or as the sum of an incident and a reflected motion. The procedures implemented are *exact*, and explained in detail in Section 4. Each finite element is associated with a set of material properties. The material may be assumed linear (*i.e.*, isotropic linear elastic), or nonlinear, anisotropic and hysteretic. Two types of nonlinear soil models may be used, depending upon whether drainage or no drainage of the fluid phase are to take place, *viz.*, depending upon whether the material response is to be assumed dependent on the mean effective stress. Both nonlinear soil models are based on multi-yield plasticity constitutive theory. The pressure dependent model is fully described in Section 5. The required material parameters for both soil models are defined in terms of common soil mechanics parameters (*e.g.*, cohesion, friction angle, porosity, etc.). The procedures used to generate the required model parameters are detailed in Section 6. The integration algorithms used for integrating the nonlinear, anisotropic, hysteretic elastic-plastic constitutive equations are explained in Section 7. Output consists of nodal, element stresses, strains, and pore water pressures, etc. and time histories. The results are conveniently post-processed using the graphics post-processors, which allow selective plots of field components time histories, Fourier spectra, velocity spectra, etc., and spatial plots at selected times of field components variations.

TABLE OF CONTENTS

1. DYNA1D / PROGRAM DESCRIPTION 1-1
- 1.1 Introduction 1-1
- 1.2 Objectives and Goals 1-2
- 1.3 Analysis Capabilities 1-3
- 1.4 References 1-6

2. DYNAMICS OF POROUS MEDIA / BASIC THEORY 2-1
- 2.1 Introduction 2-1
- 2.2 Kinematics 2-3
- 2.3 Average Quantities 2-5
- 2.4 Balance Laws 2-7
  - 2.4.1 Balance of Mass 2-7
  - 2.4.2 Balance of Linear Momentum 2-7
  - 2.4.3 Entropy Inequality 2-9
- 2.5 Constitutive Assumptions 2-10
  - 2.5.1 Solid Grains 2-10
  - 2.5.2 Fluid Phase 2-10
  - 2.5.3 Solid Porous Skeleton 2-11
  - 2.5.4 Momentum Supplies 2-12
- 2.6 Coupled Field Equations 2-12
- 2.7 Applications/Special Cases 2-13
  - 2.7.1 Dynamics without Inertia and Convective Effects in Fluid 2-13
  - 2.7.2 Dynamics with Undrained Conditions 2-13
  - 2.7.3 Dynamics with Drained Conditions 2-15
  - 2.7.4 Pseudo-Static Loading Conditions 2-15
- 2.8 Appendix A: Wave Propagation with Diffusion 2-17
- 2.9 Appendix B: One-Dimensional Wave Propagation 2-22
- 2.10 References 2-32

3. DYNAMICS OF POROUS MEDIA / NUMERICAL FORMULATION 3-1
- 3.1 Introduction 3-1
- 3.2 Weak Form / Semi-Discrete Finite Element Equations 3-5
- 3.3 Time Integration 3-7
  - 3.3.1 One-Step Algorithms 3-7
  - 3.3.2 Implementation 3-8

3.3.3 Stability Conditions 3-11
3.4 Implementation 3-12
3.4.1 Wave Propagation Calculations 3-12
3.4.1 Vibration Type Calculations 3-13
3.4.1 Diffusion Type Calculations 3-17
3.4.1 Remarks 3-17
3.5 References 3-18

4. TRANSMITTING BOUNDARY 4-1
4.1 Introduction 4-1
4.2 One-Dimensional Vertical Propagation of Seismic Waves 4-2
4.3 Semi-Infinite Soil Column 4-4
4.4 Conclusions 4-8
4.5 References 4-8

5. PLASTICITY MODEL FOR FRICTIONAL SOILS 5-1
5.1 Introduction 5-1
5.2 Basic Theory 5-3
5.2.1 Constitutive Equations 5-3
5.2.2 Yield Function 5-3
5.2.3 Flow Rule 5-5
5.2.4 Hardening Rule 5-5
5.2.5 Consistency Condition 5-6
5.2.6 Remarks 5-7
5.3 Model Parameters Identification 5-9
5.3.1 "Triaxial" Soil Test 5-10
5.4 References 5-18

6. SHEAR STRESS-STRAIN CURVE GENERATION FROM SIMPLE MATERIAL PARAMETERS 6-1
6.1 Introduction 6-1
6.2 Hyperbolic Function 6-3
6.3 Modified Hyperbolic Function 6-4
6.4 Equivalent Viscous Damping 6-6
6.5 Conclusions 6-8
6.6 References 6-8

7. INTEGRATION ALGORITHMS

FOR ELASTIC-PLASTIC CONSTITUTIVE RELATIONS 7-1
7.1 Introduction 7-1
7.2 Theory 7-4
7.3 Algorithms 7-5
7.3.1 Algorithmic Set-up 7-8
7.3.2 Multi-Yield Surface Plasticity Case 7-11
7.3.3 Application / Examples 7-16
7.4 Extension to Visco-Plasticity 7-20
7.5 References 7-22

LIST OF FIGURES

1.1 Semi-Infinite Layered Soil Profile / Finite Element Mesh 1-4

2.1 Pore Fluid Pressure vs Position / Dynamically Compatible Case 2-25
(a) Time $\tau = 2.0$ 2-25
(b) Time $\tau = 5.0$ 2-25
(c) Time $\tau = 10.$ 2-26
(d) Time $\tau = 20.$ 2-26

4.1 Semi-Infinite Layered Soil Profile 4-5

5.1 Yield Surface in Principal Stress Space 5-4
5.2 Dilatational Plastic Flow 5-6
5.3 Yield Surface Translation 5-7
5.4 Model Calibration - Triaxial Soil Test 5-14

6.1 Shear Stress-Strain Curve - Notation Definition 6-9
6.2 Generated Shear Stress-Strain Curves 6-10
6.3 Secant Modulus vs Shear Strain Level 6-11
(a) G / G_0 *vs.* γ / γ_{max} 6-11
(b) $G / (\tau_{max} / \gamma_{max})$ *vs.* γ / γ_{max} 6-11
6.4 Hysteresis Loops - Equivalent Viscous Damping Definition 6-12
6.5 Equivalent Viscous Damping vs Shear Strain 6-13

7.1 Schematic of the Elastic Predictor / Plastic Stress Relaxation 7-7
7.2 Multi-Yield Plasticity Case - Schematic of the Correction 7-12
7.3 Multi-Yield Plasticity Case - Cutting Plane Algorithm 7-19
(a) Shear Stress-Strain Curves 7-19
(b) Effective Stress Paths 7-19

LIST OF FLOWCHARTS

3.1 Time Integration with Newton-Raphson Iterations 3-10

7.1 Cutting Plane Projections Iterations 7-10
7.2 Integration Algorithm - Multi-Yield Plasticity Case 7-14
7.3 Visco-Plastic Algorithm 7-21

SECTION 1
DYNA1D
PROGRAM DESCRIPTION

1.1 INTRODUCTION

Seismic site response analysis involves the determination of the spatial and temporal variation of ground motions at a given site. It also involves the determination of the effects of seismic waves, *e.g.*, potential liquefaction, at a given site. It is a most important and essential step in any seismic soil-structure interaction analysis, and is required to compute compatible motions at the boundaries of the discrete soil model in direct methods of analysis. To compute the site response, assumptions must be made regarding the types of waves propagated during the earthquake. The most common assumptions are that the soil is horizontally stratified and that the excitation consists of vertically propagating dilatational (P-waves) and shear (S-waves). The dilatational waves only produce vertical motions, and the problem then becomes one-dimensional. However, due to the presence of coupling between shear and volumetric deformations in soil media, the shear waves will, in general, produce both horizontal and vertical motions. These effects are usually disregarded, and the shear wave propagation is commonly analyzed as a one-dimensional problem (see e.g., Ref. [10]). Such an assumption is certainly valid for saturated soil media if no drainage of the pore fluid can take place within the time frame of the seismic excitation. However, for dry soil deposits and for saturated soil deposits of moderate permeabilities in which drainage can take place, horizontal motions will in general be accompanied with vertical motions and such effects should be accounted for in the analysis. Further, in cases in which potential liquefaction is of concern, a complete effective stress analysis which models directly the nonlinear

hysteretic stress-strain response of soils should be conducted. In such an analysis, the buildups in pore water pressures and their dissipation with time are computed, and their effects on the dynamic response are taken into account. Effective stress analysis based on the solution of *uncoupled* equations for the porous solid soil skeleton and the pore water fluid have been proposed (see e.g., Refs [5,6]). However, a rational and complete analysis should be based on the solution of the *fully coupled* (see e.g., Ref. [1]) solid soil skeleton/pore water fluid equations, such as proposed in Refs [2-4,9].

DYNA1D [8] has been developed to allow site response analyses to be performed taking into account: *(1)* the nonlinear, anisotropic and hysteretic stress-strain behavior of the soil materials; and *(2)* the effects of the transient flow of the pore water through the soil strata. The procedures used (field and constitutive equations) are general and applicable to *multidimensional* situations (see *e.g.*, Ref. [7]).

1.2 OBJECTIVES AND GOALS

DYNA1D is a finite element analysis program designed to perform nonlinear seismic site response calculations. The goal was to provide a realistic and reliable analysis procedure for use in engineering design practice. Therefore, although no sacrifices have been made as to the rigor and generality of the field and constitutive equation used, attempts have been made to simplify, as much as possible, the use of the code. For that purpose, features such as automatic (*i.e.*, user transparent) initialization procedures have been implemented. Also, required constitutive parameters are identified in terms of "classical" soil mechanics parameters (*e.g.*, elastic moduli, friction angles, permeabilities, etc...). In order to ease the interpretation of the analysis results, graphic display capabilities which allow plots of spatial and temporal variations of field components have been implemented.

1.3 ANALYSIS CAPABILITIES

Dry, saturated and partially saturated deposits can be analysed. The theoretical framework which forms the basis of the formulations used is summarized in Section 2. The numerical formulation employed for solving the coupled field equations is reviewed in Section 3.

Consider a typical situation such as illustrated in Fig. 1.1. A semi-infinite horizontally layered soil deposit is subjected to a seismic ground motion. The ground motion is attributed to the upward propagation of seismic waves from the underlying rock or rock-like layers. A complete site response analysis would require a model which also includes the source mechanism. However, for seismic excitations, the many uncertainties in the source mechanism and in the geological parameters along the transmission path, and the restrictions on the size of the numerical model, dictate a simpler approach:

- The semi-infinite domain is modeled by using a *finite* model, and the site response calculations are performed for a given seismic input motion prescribed in the form of an acceleration (or velocity, or displacement) time history to be applied at the base of the soil column. When an infinite domain is modelled by a finite model, there is danger that waves reflected from the free-surface will be reflected back off the artificial bottom boundary and cause errors in the response calculations, unless special boundary conditions can be imposed at the base of the soil column. In DYNA1D [8], special boundary conditions can be prescribed which allow the seismic input motion to be prescribed as an incident vertically propagating motion, or as the sum of an incident and a reflected motion. The procedures implemented are *exact*, and explained in detail in Section 4.

- The finite soil column is modeled by using finite elements. For that purpose, the horizontally-layered ground is divided into a number of finite elements as shown in Fig. 1.1. Each finite element is defined by two (2) nodes. The nodes need not be equally

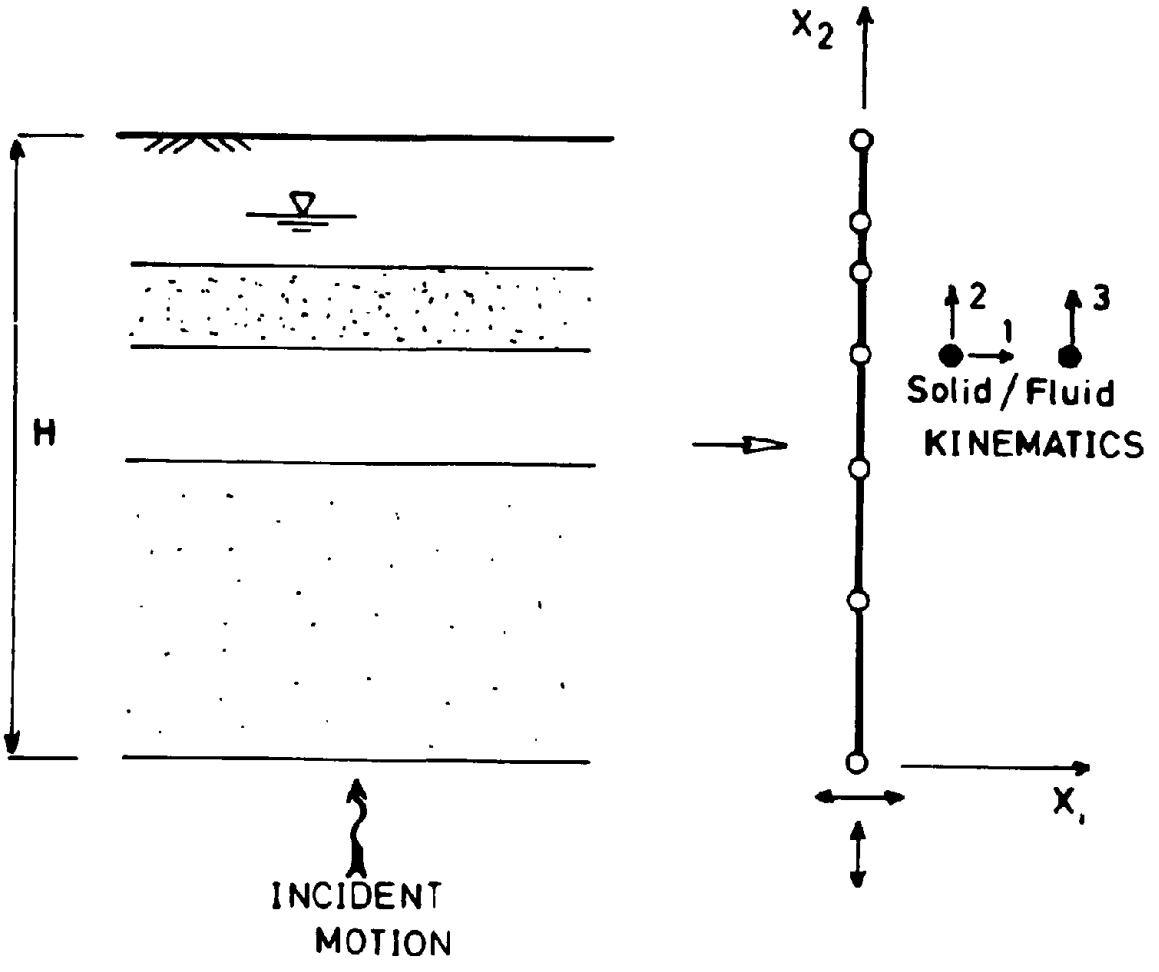

Figure 1.1 Semi-Infinite Layered Soil Profile / Finite Element Mesh

spaced, nor need to be input so as to follow any particular numbering pattern. If desired, the elements may be conveniently grouped into groups, *e.g.*, to selectively identify different soil layers.

- In the free-field conditions, soil skeleton motions can occur in both the horizontal and vertical directions. Therefore, to each nodes are assigned two solid kinematic degrees of freedom, in the horizontal (number 1) and vertical (2) directions, respectively. How-

ever, fluid motions can only occur in the vertical direction. Therefore, for saturated deposits in which fluid motions can take place, the third kinematic degree of freedom is assigned to the fluid motion in the vertical direction (number 3).

- To each element is associated a set of material properties. The material may be assumed linear (*i.e.*, isotropic linear elastic), or nonlinear. Two types of nonlinear soil models may be used, depending upon whether drainage or no drainage of the fluid phase are to take place, *viz.*, depending whether the material response is to be assumed dependent on the mean effective stress.

- Both nonlinear soil models, are based on multi-yield levels plasticity constitutive theory. The pressure dependent model is fully described in Section 5. The required material parameters for both soil models, are defined in terms of common soil mechanics parameters (*e.g.*, cohesion, friction angle, porosity, etc...). The procedures used to generate the required model parameters are detailed in Section 6.

- The integration algorithms used for integrating the nonlinear, anisotropic, hysteretic elastic-plastic constitutive equations are explained in Section 7.

- Output consists of nodal, element stresses, strains, and pore water pressures, etc... time histories. The results are conveniently post-processed using the graphics post-processors, which allow selective plots of field components time histories, Fourier spectra, velocity spectra, etc..., and spatial plots at selected times of field components variations.

1.4 REFERENCES:

1. Biot, M.A., "Theory of Propagation of Elastic Waves in a Fluid-Saturated Porous Solid," *J. Acous. Soc. Am.*, Vol. 28, 1956, pp. 168-191.
2. Dikmen, S.U., and J. Ghaboussi, "Effective Stress Analysis of Seismic Response and Liquefaction: Theory," *J. Geotech Eng.*, ASCE, Vol. 110, No. 5, May 1984, pp. 628-644.
3. Ghaboussi, J., and Dikmen, S.U., "LASS-II, Computer Program for Analysis of Seismic Response and Liquefaction of Horizontally Layered Sands," *Report No. UILU-ENG-77-2010*, Dept. of Civil Eng., Univ. of Illinois at Urbana-Champaign, Urbana, IL, 1977.
4. Ghaboussi, J., and Dikmen, S.U., "Liquefaction Analysis of Horizontally Layered Sands," *J. Geotech. Eng. Div.*, ASCE, Vol. 104, No. GT3, March 1978, pp. 341-356.
5. Lee, M.K.W., and Finn, N.D., Liam, "DESRA-1: Program for the Dynamic Effective Stress Response Analysis of Soil Deposits Including Liquefaction Evaluation," *Soil Mechanics Series Report No. 38*, Dept. of Civil Eng., Univ. of British Columbia, Vancouver, B.C., 1975.
6. Martin, P.O., and Seed, H.B., "Simplified Procedure for Effective Stress Analysis of Ground Response," *J. Geotech. Eng. Div.*, ASCE, Vol. 105, No GT6, 1979, pp. 739-758.
7. Prevost, J.H., "DYNAFLOW: A Nonlinear Transient Finite Element Analysis Program," Dept. of Civil Engineering, Princeton University, 1981, last update, 1987.
8. Prevost, J.H., "DYNA1D: A Computer Program for Nonlinear Site Response Analysis - User's Manual," Department of Civil Engineering and Operations Research, Princeton University, July 1988.
9. Prevost, J.H., "Effective Stress Analysis of Seismic Site Response," *Int. J. Num. Analyt. Meth. Geomechanics*, Vol. 10, No. 6, 1986, pp. 653-665.
10. Schnabel, P.B., Lysmer, J., and Seed, H.B., "SHAKE - A computer Program for Earthquake Response Analysis of Horizontally Layered Sites," *Report EERC 72-12*, Univ. of California, Berkeley, CA, 1972.

SECTION 2
DYNAMICS OF POROUS MEDIA
BASIC THEORY

2.1 INTRODUCTION

Soils consist of an assemblage of particles with different sizes and shapes which form a skeleton whose voids are filled with water and air or gas. The word "soil" therefore implies a mixture of assorted mineral grains with various fluids. Hence, soil in general must be looked at as a one (dry soil) or two (saturated soil) or multiphase (partially saturated soil) material whose state is to be described by the stresses and displacements (velocities) within each phase. There are still great uncertainties on how to deal analytically with partly saturated soils. Attention is therefore restricted in the following to dry and fully saturated soils. The stresses carried by the soil skeleton are conventionally called "effective stresses" in the soil mechanics literature (see e.g., Terzaghi [1943]), and those in the fluid phase are called the "pore fluid pressures".

In a saturated soil, when free drainage conditions prevail, the steady state pore-fluid pressures depend only on the hydraulic conditions and are independent of the soil skeleton response to external loads. Therefore, in that case, a single phase continuum description of soil behavior is certainly adequate. Similarly, a single phase description is also adequate when no drainage (i.e., no flow) conditions prevail. However, in intermediate cases in which some flow can take place, there is an interaction between the skeleton strains and the pore-fluid flow. The solution of these problems requires that soil behavior be analyzed by incorporating the effects of the transient flow of the pore-fluid through the voids, and therefore requires that a two phase continuum formulation be available for porous media. Such a theory was first developed by Biot [5-10] for an elastic porous

medium. However, it is observed experimentally that the stress-strain strength behavior of the soil skeleton is strongly non-linear, anisotropic, hysteretic and path-dependent. An extension of Biot's theory into the non-linear anelastic range is therefore necessary in order to analyze the transient response of soil deposits. This extension has acquired considerable importance in recent years due to the increased concern with the dynamic behavior of saturated soil deposits and associated liquefaction of saturated sand deposits under seismic loading conditions. Such an extension of Biot's formulation [26] is presented herein. For that purpose, soil is viewed as a multi-phase medium and the modern theories of mixtures developed by Green and Naghdi [21], and Eringen and Ingram [19], are used. General mixture results can be shown through formal linearization of the field and constitutive equations, to reduce to Biot's linear poroelastic model (see e.g. [12]).

The general theoretical framework which forms the basis of mixtures' theories was first developed by Truesdell and Toupin [28] early in 1960. Since then, the theoretical description of multiphase materials has received repeated attention in the literature, and fundamental equations for a dynamic theory of interacting continua have been derived [see e.g. Refs 16, 19-24, 28, 29, 34-36]. The most recent findings are summarized in Refs 2, 3 and 11 which contain many references to relevant works. In the following, the general mixture equations are first summarized and applied to describe the flow of water through saturated anelastic porous soil media. Special attention is given in particular to the physical meaning of the partial stresses which appear in the general field equations, and an effort is made to relate them to physical quantities measurable in the field.

During deformations, the solid particles which form the soil skeleton undergo irreversible motions such as slips at grain boundaries, creations of voids by particles coming out of a packed configuration, and combinations of such irreversible motions. When the particulate nature and the microscopic origin of the phenomena involved are

not sought, phenomenological equations then provide an adequate description of the behavior of the various phases which form the soil medium. In multiphase theories, the conceptual model is thus one in which each phase (or constituent) enters through its averaged properties obtained as if the particles were smeared out in space. In other words, the particulate nature of the constituents is described in terms of phenomenological laws as the particles behave collectively as a continuum. Soil is thus viewed herein as consisting of a solid skeleton interacting with the pore fluids. In order to be able to derive multiphase field and constitutive equations for such a medium, a technique for obtaining local average quantities is necessary. Furthermore, the basic kinematics and balance equations for each constituent and for the mixture as a whole must be defined.

2.2 KINEMATICS

Soil is viewed herein as a mixture consisting of m ($1 \leq m \leq 2$) deformable media, each of which is regarded as a continuum (for saturated soils $m = 2$), and each following its own motion. It is assumed that at any time t each place x of the mixture is occupied simultaneously by m different particles $X^1, X^2, \cdots, X^m$, one for each constituent. As in single-phase theory, to each constituent is assigned a fixed but otherwise arbitrary reference configuration [18,25,31], and a motion

$$\mathbf{x} = \mathbf{x}^{\alpha}(\mathbf{X}^{\alpha}, t) \qquad \alpha = 1, \ldots, m \tag{1}$$

where $\mathbf{X}^{\alpha}$ denotes the position of the α^{th} -constituent in its reference configuration, and x the spatial position occupied at the time t by the particle labeled $\mathbf{X}^{\alpha}$. For simplicity in the following, both the reference and current configurations of each constituent are referred to rectangular Cartesian axes. Capital and lower case letters are used for the indices on coordinates and tensors referred to the undeformed and deformed configuration, respectively (see e.g., Refs 18 and 25). The usual continuity and differen-

tiability assumptions are made for the deformation functions $\mathbf{x}^\alpha$, and the following restrictions are imposed

$$\det [x^\alpha_{a,A}] = J^\alpha (\mathbf{X}^\alpha, t) \; ; \quad \det [x^\alpha_{a,b}] > 0 \qquad \alpha = 1, \ldots . m \tag{2}$$

for physically possible motions, in which det denotes the determinant and a comma (,) a partial derivative. The velocity and acceleration of $\mathbf{X}^\alpha$ at time t are obtained from Eq. 1 by time differentiation, viz.

$$\mathbf{v}^\alpha = \mathbf{v}^\alpha(\mathbf{x}, t) = \frac{\overset{\alpha}{D}}{Dt}(\mathbf{x}) = \dot{\mathbf{x}}^\alpha \; ; \qquad \mathbf{a}^\alpha = \mathbf{a}^\alpha(\mathbf{x}, t) = \frac{\overset{\alpha}{D}}{Dt}(\mathbf{v}^\alpha) = \ddot{\mathbf{x}}^\alpha \tag{3}$$

where a superimposed dot indicates differentiation with respect to time holding $\mathbf{X}^\alpha$ fixed (i.e., the material derivative following the motion of the α -constituent),

$$(\dot{})^\alpha = \frac{\overset{\alpha}{D}}{Dt}( ) = \frac{\partial}{\partial t}( ) + \mathbf{v}^\alpha \cdot \nabla ( ) \tag{4}$$

Here, and in the following, ∇ and $\bar{\nabla}$ are used to denote spatial and material derivatives, respectively. The deformation gradient for $\mathbf{X}^\alpha$ at time t is defined by

$$\mathbf{F}^\alpha = \mathbf{F}^\alpha (\mathbf{x}^\alpha, t) = \bar{\nabla} \mathbf{x}^\alpha = [F^\alpha_{aA}] = [x^\alpha_{a,A}] \tag{5}$$

and the velocity gradient is defined by

$$\mathbf{L}^\alpha = \mathbf{L}^\alpha(\mathbf{x}, t) = \nabla \mathbf{v}^\alpha = \dot{\mathbf{F}}^\alpha \cdot (\mathbf{F}^\alpha)^{-1} = [L^\alpha_{ab}] = [v^\alpha_{a,b}] \tag{6}$$

in which, $(\mathbf{F}^\alpha)^{-1}$ denotes the inverse of $\mathbf{F}^\alpha$. The symmetric and skew-symmetric parts of $\mathbf{L}^\alpha$ are referred to as the deformation rate, $\mathbf{d}^\alpha$, and spin tensor, $\mathbf{w}^\alpha$, respectively.

2.3 AVERAGE QUANTITIES

Average quantities are obtained by integrating microscopic quantities over an averaging volume or area. The averaging procedure is used to obtain a field of macroscopic quantities for each phase. In the macroscopic field, the averaging volume represents and characterizes a physical point. Because the averaging volume is macroscopically infinitesimal, it is denoted by dV. Similarly, the averaging area dA, represents and characterizes a physical point on the surface of dV, and is an infinitesimal element of area in the macroscopic field. The characteristic length, D, of the averaging volume or area is selected such that [34] $l \ll D \ll L$, where l is the microscopic scale of the porous medium and L is the scale of gross inhomogeneities. Typically, l = 50 micron in sands and l = 1 micron in clays, whereas L = 1cm. The part of dV occupied by the α-phase is denoted by dV^α, and the volume fraction, n^α, of the α-phase is the fraction of dV occupied by the α-phase defined by

$$n^\alpha = n^\alpha(\mathbf{x}, t) = \frac{dV^\alpha}{dV} \tag{7}$$

Cleary, n^α is constrained by $\sum_\alpha n^\alpha = 1$ and $0 \le n^\alpha \le 1$. Similarly, the part of dA lying in the α-phase is denoted by dA^α, and the areal fraction, $\bar{n}^\alpha$, of the α-phase is the fraction of dA which interest the α-phase defined by

$$\bar{n}^\alpha = \bar{n}^\alpha(\mathbf{x}, t) = \frac{dA^\alpha}{dA} \tag{8}$$

subject to $\sum_\alpha \bar{n}^\alpha = 1$ and $0 \le \bar{n}^\alpha \le 1$. In Ref. [24], arguments are presented which support the intuitively appealing identity, $\bar{n}^\alpha = n^\alpha$ [6,27], and in the following, that identity is assumed to hold.

A macroscopic average mass density function, ρ^α, is associated with each constituent and is defined as the volume average of the microscopic density function, ρ_α, as

[20]

$$\rho^{\alpha} = \frac{1}{dV}\int_{dV^{\alpha}} \rho_{\alpha}\, dv \tag{9}$$

where dv is the microscopic volume element. In this equation and in subsequent developments, the dependence of macroscopic and microscopic quantities on $\mathbf{x}$ and t is understood. The intrinsic volume average mass density is defined as

$$\bar{\rho}_{\alpha} = \frac{1}{dV^{\alpha}} \int_{dV^{\alpha}} \rho_{\alpha}\, dv = \frac{1}{n^{\alpha}}\, \rho^{\alpha} \tag{10}$$

Note that only when the mass density of the α-phase is microscopically constant, is the intrinsic volume average mass density function equal to the microscopic mass density. In the following, $\bar{\rho}_{\alpha} = \rho_{\alpha}$ and thus $\rho^{\alpha} = n^{\alpha}\, \rho_{\alpha}$.

The mass density, ρ, of the mixture is defined as

$$\rho = \rho\,(\mathbf{x}, t) = \sum_{\alpha} \rho^{\alpha} \tag{11}$$

and the mean (or barycentric) velocity, $\mathbf{v}$, for the mixture is defined as

$$\mathbf{v} = \mathbf{v}\,(\mathbf{x}, t) = \frac{1}{\rho} \sum_{\alpha} \rho^{\alpha}\, \mathbf{v}^{\alpha} \tag{12}$$

The velocity gradient for the mixture is then

$$\mathbf{L} = \nabla \mathbf{v} = [L_{ab}] = [v_{a,b}] \tag{13}$$

It is of importance to emphasize that the velocity $\mathbf{v}^{\alpha}$ of the α-constituent (Eq. 3) is its microscopic (intrinsic or seepage) velocity, and is different from the mean (or superficial) velocity $\bar{\mathbf{v}}^{\alpha}$, used for instance in Darcy's law [17], defined as

$$\int_{\partial R} \rho_{\alpha}\, \bar{\mathbf{v}}^{\alpha} \cdot \mathbf{n}\, dA = \int_{\partial R^{\alpha}} \rho_{\alpha}\, \mathbf{v}^{\alpha} \cdot \mathbf{n}\, dA = \int_{\partial R} \rho^{\alpha}\, \mathbf{v}^{\alpha} \cdot \mathbf{n}\, dA \tag{14}$$

where $\mathbf{n}$ denotes the unit outward normal to the surface ∂R, of area A, which encloses the fixed region in space R, of volume V. Clearly, $\bar{\mathbf{v}}^{\alpha} = n^{\alpha}\, \mathbf{v}^{\alpha}$.

2.4 BALANCE LAWS

All equations are postulated at the current time t, and all field quantities are functions of $\mathbf{x}$ and t. When discussing a constituent of the mixture, it is supposed that it can be isolated from the rest of the mixture, provided that allowance is made for the action upon it of the other constituent(s). The balance laws for the two-phase soil mixture are summarized as follows:

2.4.1 Balance of Mass:

No chemical interaction is assumed to take place between the solid soil skeleton and the fluid phase. The balance of mass of each α-constituent then takes the form

$$\overset{\alpha}{\frac{D}{Dt}} (\rho^\alpha) + \rho^\alpha \nabla \cdot \mathbf{v}^\alpha = 0 \tag{15}$$

Another version of Eq. 5 is obtained by recalling that $\rho^\alpha = n^\alpha \rho_\alpha$, and

$$\overset{\alpha}{\frac{D}{Dt}} (n^\alpha) + n^\alpha \nabla \cdot \mathbf{v}^\alpha = - \frac{n^\alpha}{\rho_\alpha} \overset{\alpha}{\frac{D}{Dt}} (\rho_\alpha) \tag{16}$$

in which $\overset{\alpha}{D} (\rho_\alpha) / Dt = 0$ if the grains which constitute the α-phase are incompressible. Eq. 16 will prove most useful in the following.

2.4.2 Balance of Linear Momentum:

Before postulating the balance of momentum laws for each α-constituent it is first necessary to consider the forces acting on this constituent within the region R. In addition to body forces, such as gravity forces, one must also account for the effect on the α-constituent of the mixture outside the region R. This effect is accounted for by introducing a vector field $\mathbf{T}^\alpha (\mathbf{n}, \mathbf{x}, t)$ defined on ∂R and measured per unit area of ∂R, such that $\int_{\partial R} \mathbf{T}\, dA$ represents the contact force exerted across ∂R by the α-constituents outside of

R on the α-constituent in R [23,32,35]. This notion of a stress vector is in accord with the stress vector notion for a single-substance continuous medium as introduced in classical continuum mechanics (see e.g., Refs 18,25,31-33). Corresponding to the partial stress vector $\mathbf{t}^\alpha$, there exists a partial stress tensor $\boldsymbol{\sigma}^\alpha$ [32,35], such that $\mathbf{t}^\alpha = \mathbf{n} \cdot \boldsymbol{\sigma}^\alpha$, where $\mathbf{n}$ denotes the unit outward normal to ∂R. Locally,

$$\mathbf{t}^\alpha = \frac{1}{dA} \int_{dA^\alpha} \mathbf{t}_\alpha \, dA \tag{17}$$

where $\mathbf{t}_\alpha$ denotes the intrinsic stress vector of the α-phase Note that: $\mathbf{t}^\alpha = n^\alpha \mathbf{t}_\alpha$ when $\mathbf{t}_\alpha$ is microscopically constant. From Eq. 17 and the above definition, it is apparent that the partial stress tensor corresponding to the fluid phase, $\boldsymbol{\sigma}^w$, is equal to n^w times the pore fluid stress, σ_w, i.e., $\boldsymbol{\sigma}^w = n^w \sigma_w$. However, the partial stess tensor corresponding to the solid phase, $\boldsymbol{\sigma}^s$, is *not* the effective stress, $\boldsymbol{\sigma}'^s$, of classical soil mechanics [30] but rather is

$$\boldsymbol{\sigma}^s = \boldsymbol{\sigma}'^s + n^s \sigma_w = n^s \sigma_s = (1 - n^w) \sigma_s \tag{18}$$

for a saturated porous medium, where $n^s \sigma_w$ accounts for the effects of the pore fluid stress on the individual solid grains which constitutes the solid skeleton. In deriving Eq. 18 it has been assumed that the contact areas between the solid grains are negligibly small [4,27], so that the pore fluid and associated stress completely surrounds each grain. Each solid grain is also subjected to intergranular forces that are in excess of the pore fluid stress and characterized by the effective stress $\boldsymbol{\sigma}'^s$. The global stress $\boldsymbol{\sigma}$ which is to appear in the general balance equations for the porous medium, is the sum of the partial stresses, $\boldsymbol{\sigma} = \sum_\alpha \boldsymbol{\sigma}^\alpha$, and is equal to:

$$\boldsymbol{\sigma} = \boldsymbol{\sigma}^s + \boldsymbol{\sigma}^w = \boldsymbol{\sigma}'^s + \sigma_w \tag{19}$$

for a saturated porous medium, as postulated in classical soil mechanics [30].

The local version of the balance of linear momentum equations for each constituent then simply writes (see e.g., Refs [2] and [11]):

$$\rho^{\alpha}\,\mathbf{a}^{\alpha} = \nabla\cdot\boldsymbol{\sigma}^{\alpha} + \hat{\mathbf{p}}^{\alpha} + \rho^{\alpha}\,\mathbf{b} \tag{20}$$

where $\mathbf{b}$ = body force per unit mass; $\hat{\mathbf{p}}^{\alpha}$ = momentum supply to the α - constituent from the rest of the mixture due to other interaction effects (for example due to the relative motions of the constituents), subject to $\sum_{\alpha}\hat{\mathbf{p}}^{\alpha} = 0$ [2,11]. It is further assumed that the mixture consists of non-polar constituents and that there are no moment of momentum supply between the phases. The balance laws of moment of momentum for each phase then yield that, as in single-substance media, the partial stress tensors must all be symmetric.

2.4.3 Entropy Inequality:

In setting up constitutive hypotheses for each constituents, one must ensure that they do not violate the entropy inequality which states that for a mixture in which each constituent has the same temperature θ [2],

$$-\sum_{\alpha}\rho^{\alpha}\frac{\overset{\alpha}{D}A^{\alpha}}{Dt} - \sum_{\alpha}\rho^{\alpha}s^{\alpha}\frac{\overset{\alpha}{D}\theta}{Dt} + \sum_{\alpha}\hat{\mathbf{p}}\cdot(\mathbf{v}^{\alpha}-\mathbf{v}) + \sum_{\alpha}\boldsymbol{\sigma}^{\alpha}:\mathbf{d}^{\alpha} - \frac{1}{\theta}\,\mathbf{q}\cdot\nabla\theta \geq 0 \tag{21}$$

in which $\boldsymbol{\sigma}^{\alpha}:\mathbf{d}^{\alpha} = tr\,(\boldsymbol{\sigma}^{\alpha}\mathbf{d}^{\alpha})$, A^{α} = partial Helmoltz free energy, s^{α} = partial entropy, and $\mathbf{q}$ = heat flux for the mixture.

2.5 CONSTITUTIVE ASSUMPTIONS

Constitutive equations must be provided for the state variables. This is accomplished as follows:

2.5.1 Solid Grains:

For all pratical applications of interest in soil mechanics, the solid grains may be assumed incompressible, and in the following ρ_s = constant. Eq. 16 for the solid phase then simplifies to:

$$\overset{s}{\frac{D}{Dt}}(n^w) = (1 - n^w)\,\nabla \cdot \mathbf{v}^s \tag{22}$$

where $n^w = (1 - n^s) =$ porosity, and Eqs. 16 and 22 may be combined to yield the so-called "storage equation", viz.

$$\nabla \cdot [\, n^w \mathbf{v}^w \,] + \nabla \cdot [\, n^s \mathbf{v}^s \,] = -\frac{n^w}{\rho_w} \overset{w}{\frac{D}{Dt}}(\rho_w) \tag{23}$$

2.5.2 Fluid Phase:

The following constitutive equation is assumed to describe the behavior of the fluid phase

$$\sigma_w = -p_w\,\delta \tag{24}$$

where p_w = pore-fluid pressure; i.e., it is assumed that the fluid has no <u>average</u> shear viscosity. Further, the fluid flow is assumed barotropic so that the fluid kinetic equation of state is independent of the temperature, viz.,

$$F(p_w, \rho_w) = 0 \tag{25}$$

from which it follows that

$$\frac{1}{\rho_w} \overset{w}{\frac{D}{Dt}}(\rho_w) = \frac{1}{\lambda^w} \overset{w}{\frac{D}{Dt}}(p_w) \tag{26}$$

where $\lambda^w = \rho_w \, \partial p_w / \partial \rho_w$ = bulk modulus of the fluid phase. The fluid pressure can thus be determined from Eq. 23 which now writes:

$$\frac{\overset{w}{D}}{Dt} (p_w) = - \frac{\lambda^w}{n^w} [\nabla \cdot (n^w \, \mathbf{v}^w) + \nabla \cdot (n^s \, \mathbf{v}^s)] \tag{27}$$

For soil media, the compressibility of the fluid phase is often much smaller than the compressibility of the solid skeleton. Therefore, the fluid phase may, in some applications, be regarded as incompressible, and Eq. 23 reduces in that case to

$$\nabla \cdot [n^w \, \mathbf{v}^w] + \nabla \cdot [n^s \, \mathbf{v}^s] = 0 \tag{28}$$

2.5.3 Solid Porous Skeleton

A rate-type constitutive equation is assumed to describe the behavior of the porous solid skeleton, of the following form:

$$\frac{\overset{\delta}{D}}{Dt} (\boldsymbol{\sigma}'^s) = \mathbf{D}^S : \mathbf{v}^s_{(}) + \mathbf{D}^G : \mathbf{v}^s_{[}] = \mathbf{D} : \nabla \, \mathbf{v}^s \tag{29}$$

where $\mathbf{v}^s_{(}$ and $\mathbf{v}^s_{[}$ = symmetric and skew-symmetric parts of the solid velocity gradient, respectively; $\mathbf{D}^S$ is the material constitutive tensor, an (objective) tensor valued function of, possible $\boldsymbol{\sigma}'^s$ and the solid deformation gradient; $\mathbf{D}^G$ is the contribution from the rotational component of the stress rate, viz.,

$$D^G_{ijkl} = \frac{1}{2} [\sigma'_{il} \, \delta_{jk} + \sigma'_{jl} \, \delta_{ik} - \sigma'_{ik} \, \delta_{jl} - \sigma'_{jk} \, \delta_{il}] \tag{30}$$

Many nonlinear material models of interest can be put in the above form (e.g., all nonlinear elastic and many elastic-plastic material models). Appropriate expressions for the effective modulus tensor $\mathbf{D}^S$ for soil media are discussed in Section 5. For a linear isotropic elastic porous skeleton:

$$D^S_{ijkl} = \lambda^s \, \delta_{ij} \, \delta_{kl} + \mu^s (\delta_{ik} \, \delta_{jl} + \delta_{il} \, \delta_{jk}) \tag{31}$$

where λ^s , μ^s = effective Lame's moduli, δ_{ij} = Kronecker delta.

2.5.4 Momentum Supplies

Momentum interaction between the solid skeleton and the fluid phase is assumed to consist of diffusive and dilatational contributions, viz.

$$\hat{\mathbf{p}}^s = -\hat{\mathbf{p}}^w = -\boldsymbol{\xi} \cdot (\mathbf{v}^s - \mathbf{v}^w) - p_w \nabla n^w \tag{32}$$

where $\boldsymbol{\xi}$ = symmetric, positive-definite second-order tensor. The first term accounts for the momentum transfer due to diffusion phenomena and is sometimes called the "stokes drag" [11]. The inclusion of such a term is basic to all porous media theories (see e.g., [5-10]). The second term is called a "buoyancy force" in mixture theories.

2.6 COUPLED FIELD EQUATIONS

Under the assumptions described above, the linear momentum equations (Eq. 20) simplify to:

$$\rho^s \mathbf{a}^s = \nabla \cdot \boldsymbol{\sigma}'^s - n^s \nabla p_w - \boldsymbol{\xi} \cdot (\mathbf{v}^s - \mathbf{v}^w) + \rho^s \mathbf{b} \tag{33a}$$

$$\rho^w \overset{s}{\frac{D}{Dt}} (\mathbf{v}^w) = \rho^w (\mathbf{v}^s - \mathbf{v}^w) \cdot \nabla \mathbf{v}^w - n^w \nabla p_w + \boldsymbol{\xi} \cdot (\mathbf{v}^s - \mathbf{v}^w) + \rho^w \mathbf{b} \tag{33b}$$

when the movement of the solid phase is used as the reference motion. When inertia and convective terms are neglected, Eq. 33b reduces to Darcy's law [17] as

$$n^w (\mathbf{v}^w - \mathbf{v}^s) = -(n^w)^2 \boldsymbol{\xi}^{-1} \cdot (\nabla p_w - \rho_w \mathbf{b}) \tag{34}$$

and thus $\mathbf{k} = (n^w)^2 \gamma_w \boldsymbol{\xi}^{-1}$ = Darcy permeability tensor (symmetric, positive-definite), (units: L/T); $\gamma_w = g \rho_w$ = unit weight of the fluid; g = acceleration of gravity.

2.7 APPLICATIONS / SPECIAL CASES

Several simplified situations of interest in soil mechanics can be obtained as special cases of the general theory presented previously (Eqs. 22, 23 and 33), as shown hereafter.

2.7.1 Dynamics Without Inertia and Convective Effects in Fluid

If inertia and convestive effects in the fluid phase are neglected, Eqs. 33a and 33b can be combined to yield:

$$\rho^s \mathbf{a}^s = \nabla \cdot (\boldsymbol{\sigma}'^s - p_w \boldsymbol{\delta}) + \rho b \tag{35}$$

where $\rho = \rho^s + \rho^w$ = total mass density of the mixture. Further, Eq. 33b simplifies to Eq. 34. Then taking the divergence of both sides of Eq. 34 and combining with Eq. 27, one gets

$$\begin{aligned} -\nabla \cdot [\, n^w (\mathbf{v}^w - \mathbf{v}^s) \,] &= \frac{n^w}{\lambda^w} \overset{w}{\frac{D}{Dt}} (p_w) + \nabla \cdot \mathbf{v}^s \\ &= -\nabla \cdot [\, \frac{1}{\gamma_w} \mathbf{k} \cdot (\nabla p_w - \rho_w \mathbf{b}) \,] \end{aligned} \tag{36}$$

and finally (rearranging terms):

$$\frac{n^w}{\lambda^w} \overset{w}{\frac{D}{Dt}} (p_w) - \nabla \cdot [\, \frac{1}{\gamma_w} \mathbf{k} \cdot (\nabla p_w - \rho_w \mathbf{b})] + \nabla \cdot \mathbf{v}^s = 0 \tag{37}$$

In many practical cases, the compressibility of the fluid phase is often much smaller than that of the solid soil skeleton. Eq. 37 can then be further simplified by assuming that the fluid compressibility can be neglected, as:

$$-\nabla \cdot \mathbf{k} \cdot [\, \nabla (\frac{p_w}{\gamma_w}) - \frac{1}{g} \mathbf{b} \,] + \nabla \cdot \mathbf{v}^s = 0 \tag{38}$$

The term $-\frac{1}{g} \mathbf{b}$ can conveniently be expressed in a cartesian reference frame as ∇y where y is the vertical coordinate (y -axis vertical, oriented upward).

2.7.2 Dynamics with Undrained Conditions

In that case $\mathbf{k} \approx 0$ relative to the rate of loading, the pore-fluid follows the motion of the solid phase (i.e., $\mathbf{v}^w = \mathbf{v}^s$) and Eq. 33 simplifies to:

$$\rho \mathbf{a} = \nabla \cdot (\boldsymbol{\sigma}'^{s} - p_w \boldsymbol{\delta}) + \rho \mathbf{b} \tag{39}$$

where $\mathbf{a}$ ($= \mathbf{a}^s = \mathbf{a}^w$) = acceleration of the mixture. The storage equation (Eq. 23) also simplifies, and

$$\nabla \cdot \mathbf{v}^s = - \frac{n^w}{\rho_w} \frac{D}{Dt} (\rho_w) = - \frac{n^w}{\lambda^w} \frac{D}{Dt} (p_w) \tag{40}$$

If it is further assumed that the fluid compressibility can be neglected, then (from Eqs. 22 and 40)

$$\frac{D}{Dt} (n^w) = 0 \quad \text{and} \quad \nabla \cdot \mathbf{v}^s = \nabla \cdot \mathbf{v}^w = 0 \tag{41}$$

Note that in general, changes in pore-fluid pressures will arise as a result of the strains in the solid soil skeleton.

2.7.3 Dynamics with Drained Conditions:

In that case $\mathbf{k} = \infty$ relative to the rate of loading, and no changes in pore-fluid pressures take place as a result of the strains in the solid soil skeleton. Eq. 33 then simplifies to:

$$\rho^s \mathbf{a}^s = \nabla \cdot (\boldsymbol{\sigma}'^{s} - p_w \boldsymbol{\delta}) + \rho \mathbf{b} \tag{42}$$

if the pore-fluid is assumed at steady-state, viz. (from Eq. 37),

$$- \nabla \cdot [\frac{1}{\gamma_w} \mathbf{k} \cdot (\nabla p_w - \rho_w \mathbf{b})] = 0 \tag{43}$$

If it is further assumed that no fluid flow is taking place (static fluid pressures), then Eq. 33a simplifies to:

$$\rho^s \mathbf{a}^s = \nabla \cdot \boldsymbol{\sigma}'^{s} + \rho'^{s} \mathbf{b} \tag{44}$$

where $\rho'^{s} = \rho - \rho_w = n^s (\rho_s - \rho_w)$ = buoyant mass density of the porous soil skeleton, and (from Eq. 33b)

$$\nabla p_w - \rho_w \mathbf{b} = 0 \tag{45}$$

2.7.4 Pseudo-static loading conditions:

In that case inertia (and convective) effects are neglected both in the solid and fluid phases. The corresponding field equations for the various cases are simply obtained from above by setting $\mathbf{a}^s = \mathbf{a}^w = 0$, viz.

2.7.4.1 "Partly" drained loading conditions (Consolidation Equations):

$$\nabla \cdot (\boldsymbol{\sigma}'^s - p_w \boldsymbol{\delta}) + \rho \mathbf{b} = 0 \tag{46a}$$

$$\frac{n^w}{\lambda^w} \overset{w}{\frac{D}{Dt}} (p_w) - \nabla \cdot [\frac{1}{\gamma_w} \mathbf{k} \cdot (\nabla p_w - \rho_w \mathbf{b})] + \nabla \cdot \mathbf{v}^s = 0 \tag{46b}$$

2.7.4.2 Undrained Loading Conditions:

$$\nabla \cdot (\boldsymbol{\sigma}'^s - p_w \boldsymbol{\delta}) + \rho \mathbf{b} = 0 \tag{47}$$

with $\nabla \cdot \mathbf{v}^s = \nabla \cdot \mathbf{v}^w = 0$ ($\frac{D}{Dt} n^w = 0$) if it is further assumed that the fluid compressibility can be neglected.

2.7.4.3 Drained Loading Conditions:

$$\nabla \cdot (\boldsymbol{\sigma}'^s - p_w \boldsymbol{\delta}) + \rho \mathbf{b} = 0 \tag{48a}$$

$$- \nabla \cdot [\frac{1}{\gamma_w} \mathbf{k} \cdot (\nabla p_w - \rho_w \mathbf{b})] = 0 \tag{48b}$$

or, if no fluid flow is taking place:

$$\nabla \cdot \boldsymbol{\sigma}'^s + \rho'^s \mathbf{b} = 0 \tag{49a}$$

$$\nabla p_w - \rho_w \mathbf{b} = 0 \tag{49b}$$

2.8 APPENDIX A : Wave P: opagation with Diffusion

In this section, results pertaining to the calculation of propagation speeds and decay properties of plane waves propagating in the porous medium model defined by Eqs. 33a and 33b are summarized. Small displacements are assumed and linearized equations are used. The solid skeleton is modeled as isotropic linear elastic (Eq. 31) and $\xi = \xi \delta$ in the following. One solid rotational and two dilatational diffusive waves will in general propagate thru the porous medium. It is convenient to first introduce results pertaining to *acceleration* waves. Readers interested in detailed derivations should consult Biot [1956], Bowen [1982]; Bowen and Chen [1975], and Bowen and Reinicke [1978] on that subject matter.

A1. Acceleration Waves:

(a) Rotational Wave: It propagates thru the solid skeleton with a wave speed C_s given by:

$$C_s^2 = \mu^s / \rho^s \tag{A1}$$

The wave is diffusive, and its amplitude decay is given by:

$$a(t) = a(0) \exp [- \xi t / 2 \rho^s] \tag{A2}$$

from which the attenuation distance δ_s ($\frac{1}{e}$ *decay*) can be computed as:

$$\delta_s = 2 \rho^s C_s / \xi \tag{A3}$$

(b) Dilatational Waves: Two dilatational waves may in general propagate thru the porous medium with speeds C_{p_1} and C_{p_2} given by:

$$C_{p_i}^2 = \frac{1}{2} \left[(C_1^2 + C_2^2) \pm [(C_1^2 - C_2^2) + 4 C_3^2]^{1/2} \right] \tag{A4}$$

where

$$C_1^2 = (\lambda^s + 2 \mu^s + \lambda^w \frac{(n^s)^2}{n^w}) / \rho^s \tag{A5a}$$

$$C_2^2 = (n^w \lambda^w) / \rho^w \tag{A5b}$$

$$C_3^2 = (n^s \lambda^w)^2 / (\rho^s \rho^w) \tag{A5c}$$

Note that Eq. A5 will always produce positive squared speeds and thus real speeds if $(\lambda^s + 2\mu^s) > 0$. The two waves are in general diffusive, and their amplitude decay is given by:

$$a_i(t) = a_i(0) \exp [- \xi \alpha_i t/2] \tag{A6}$$

$$\delta_{p_i} = 2 C_{p_i} / (\alpha_i \xi) \tag{A7}$$

where

$$\alpha_i = (\frac{1}{\rho^s} + \frac{1}{\rho^w}) \frac{| C_{p_i}^2 - C_0^2 |}{C_{p_1}^2 - C_{p_2}^2} \tag{A8}$$

and C_0 is the "frozen" mixture speed defined by:

$$C_0^2 = (\lambda^s + 2\mu^s + \frac{\lambda^w}{n^w}) / (\rho^s + \rho^w) \tag{A9}$$

with

$$C_{p_2}^2 < C_0^2 \leq C_{p_1}^2 \tag{A10}$$

Note that it is possible that $C_0 = C_{p_1}$ (dynamically compatible case). In that case:

$$\lambda^s + 2\mu^s = \frac{\lambda^w}{n^w} \frac{n^s (\rho_s - \rho_w)}{\rho_w} = \lambda^w [\frac{\rho^s}{\rho^w} - \frac{n^s}{n^w}] \tag{A11}$$

and,

$$C_{p_1} = C_0 = \sqrt{\frac{\lambda^w}{\rho^w}} ; \qquad \alpha_1 = 0 \tag{A12}$$

$$C_{p_2} = \sqrt{\frac{n^w (\lambda^s + 2\mu^s)}{\rho^s}} ; \qquad \alpha_2 = (\frac{1}{\rho^s} + \frac{1}{\rho^w}) \tag{A13}$$

Note that the wave of the first kind is nondiffusive in that case.

A2. Harmonic Waves:

The propagation of plane progressive waves in the porous medium model was first analyzed by Biot [1956] and later by Atkin [1968]. Solutions of the form

$$\phi(\mathbf{x}, t) = \phi_0 \exp[\, i(\eta\, \mathbf{n}\cdot\mathbf{x} - \omega t)\,] \tag{A14}$$

are sought to the wave equations, where $\mathbf{n}$ is the (unit) propagation vector, η is the (complex) wave number and ω is the (real) frequency. The speed of propagation C and the attenuation coefficient q of the plane harmonic wave described by Eq. A14 are given by

$$\eta = \frac{\omega}{C} + i\, q \tag{A15}$$

It is convenient to introduce the following characteristic frequency

$$\omega_0 = \xi \left(\frac{1}{\rho^s} + \frac{1}{\rho^w} \right) \tag{A16}$$

in terms of the drag coefficient, such that $1/\omega_0$ is the characteristic time of diffusion. The characteristic frequency ω_0 controls the transition from low-frequency to high-frequency behavior.

(a) Rotational Waves: The dispersion relation takes the following form:

$$C_s^2\, (\eta/\omega_0)^2\, (f - i\, X) - X^2\, (1 - i\, X) = 0 \tag{A17}$$

where

$$f = \frac{\rho^s}{\rho^s + \rho^w} \qquad X = \frac{\omega}{\omega_0} \tag{A18}$$

from which the propagation speed and attenuation coefficient are obtained as:

$$C = C_s \sqrt{2} \left\{ \left(\frac{1 + X^2}{f^2 + X^2} \right)^{1/2} + \frac{f + X^2}{f^2 + X^2} \right\}^{-1/2} \tag{A19}$$

$$q = \frac{\omega_0 X}{C_s \sqrt{2}} \left\{ \left(\frac{1 + X^2}{f^2 + X^2} \right)^{1/2} - \frac{f + X^2}{f^2 + X^2} \right\}^{1/2} \tag{A20}$$

At low frequencies ($\omega/\omega_0 << 1$)

$$C = C_s f^{1/2}\left\{1 + \frac{1}{8} f^{-2}(1-f)(3+f) X^2 + 0(X^4)\right\} \qquad \text{(A21)}$$

$$q = \frac{1}{2}(\omega_0/C_s) f^{-3/2}(1-f) X^2 + 0(X^4) \qquad \text{(A22)}$$

and at high frequencies ($\omega/\omega_0 >> 1$)

$$C = C_s\left\{1 - \frac{1}{8}(1-f)(1+3f) X^{-2} + 0(X^{-4})\right\} \qquad \text{(A23)}$$

$$q = \frac{1}{2}(\omega_0/C_s)(1-f)\left\{1 - \frac{1}{8}(1+2f+5f^2) X^{-2} + 0(X^{-4})\right\} \qquad \text{(A24)}$$

The transition from low- to high-frequency behavior is found to take place in the range $10^{-1} < X = \frac{\omega}{\omega_0} < 10$.

In the porous medium model, plane harmonic rotational disturbances thus take the form of progressive waves which are dampled and dispersed. The behavior of these waves at low frequencies differs from their behavior at high frequencies, the transition between the two regimes occurring fairly sharply at frequencies near the characteristic frequency ω_0.

(b) Dilatational Waves: The dispersion relation takes the following form:

$$i\omega\omega_0[\eta^2 C_0^2 - \omega^2] - (\eta^2 C_{p_1}^2 - \omega^2)(\eta^2 C_{p_2}^2 - \omega^2) = 0 \qquad \text{(A25)}$$

and is studied in detail by Atkin [1]. In general, two dilational waves (dispersive and diffusive) will propagate with speeds C_1 and C_2 such that

$$0 \le C_2 \le C_{p_2} < C_0 \le C_1 \le C_{p_1} \qquad \text{(A26)}$$

and correspond to Biot's waves of the first and second kind [1956], respectively.

Low-Frequency Behavior: In the low-frequency regime, the dilatational mode associated with the first root has the character of a progressive wave, while the second root is diffused. The propagation speed and attenuation coefficient of the wave-like mode are given by

$$C_1 = C_0\left\{1 + \frac{1}{8}(\lambda_1 - 1)(1 - \lambda_2)(1 + 3\lambda_1 + 3\lambda_2 - 7\lambda_1\lambda_2)X^2 + 0(X^4)\right\} \quad \text{(A27)}$$

$$q_1 = \frac{1}{2}(\omega_0/C_0)(\lambda_1 - 1)(1 - \lambda_2)X^2 + 0(X^4) \quad \text{(A28)}$$

where

$$\lambda_1 = (C_{p_1}/C_0)^2 \qquad \lambda_2 = (C_{p_2}/C_0)^2 \quad \text{(A29)}$$

High-Frequency Behavior: In the high-frequency regime, both dilatational modes are wave-like. Their propagation speeds and attenuation coefficients are given by

$$C_i = C_{p_i}\left\{1 - \frac{|\lambda_i - 1|}{8(\lambda_1 - \lambda_2)^2}(3\lambda_i + \lambda_k - 5\lambda_i\lambda_k + \lambda_i^2)X^{-2} + 0(X^{-4})\right\} \quad \text{(A30)}$$

$$q_i = \frac{1}{2}\frac{\omega_0}{C_{p_i}}\frac{|\lambda_i - 1|}{(\lambda_1 - \lambda_2)}\left[1 - \frac{1}{8(\lambda_1 - \lambda_2)^4}\left\{\lambda_i^2(\lambda_i^2 - 6\lambda_i\lambda_k + 21\lambda_k^2) + 2\lambda_i(\lambda_i^2 - 10\lambda_i\lambda_k - 7\lambda_k^2) + (5\lambda_i^2 + 10\lambda_i\lambda_k + \lambda_k^2)\right\}X^{-2} + 0(X^{-4})\right] \quad \text{(A31)}$$

where $i, k = 1, 2$ and $i \neq k$.

2.9 APPENDIX B : One-Dimensional Wave Propagation

In the analysis to follow, the initial-value problem consists of a semi-infinite saturated porous medium, initially at rest, and subjected at time zero to an arbitrary time-dependent disturbance at its free-boundary $x = 0$. Upon impact, two dilatational waves (in general both dispersive and diffusive) propagate thru the saturated porous medium with wave speeds C_1 and C_2 such that:

$$0 \leq C_2 \leq C_{p_2} < C_0 \leq C_1 \leq C_{p_1} \tag{B1}$$

where the propagation speeds C_{p_1} and C_{p_2} are the the propagation speeds associated with the characteristic manifolds corresponding to Eqs 2.33a and 2.33b, and C_0 is the "frozen" mixture speed (see Section 2.8, Appendix A). At the speed C_0 there is no relative motion between the two phases, the material is nondispersive and behaves like a single continuum. A closed form analytical solution (Simon and Zienkiewicz, 1984) for the one-dimensional propagation of transient dilatational pulses in a semi-infinite fluid-saturated elastic porous medium is possible when the solid and fluid are "dynamically compatible" *i.e.*, when $C_1 = C_0 = C_{p_1}$, *viz.*, when:

$$\lambda^s + 2\mu^s = \frac{\lambda^w}{n^w} \frac{n^s (\rho_s - \rho_w)}{\rho_w} = \lambda^w \left[\frac{\rho^s}{\rho^w} - \frac{n^s}{n^w} \right] \tag{B2}$$

In that case, the wave of the first kind is nondiffusive, and propagates with the speed:

$$C_1 = C_0 = C_{p_1} = \sqrt{\frac{\lambda^w}{\rho^w}} ; \qquad \alpha_1 = 0 \tag{B3}$$

whereas the wave of the second kind is diffusive, and propagates with the speed:

$$C_2 = C_{p_2} = \sqrt{\frac{n^w (\lambda^s + 2\mu^s)}{\rho^s}} ; \qquad \alpha_2 = \left(\frac{1}{\rho^s} + \frac{1}{\rho^w} \right) \tag{B4}$$

Note that in that case:

$$C_2 = \sqrt{\frac{n^w (\rho_s - \rho_w)}{\rho_s}} \; C_1 = \frac{C_1}{a^{1/2}} \; (< C_1) \tag{B5}$$

where:

$$a = \frac{\rho_s}{n^w (\rho_s - \rho_w)} \quad (> 1) \tag{B6}$$

The saturated porous medium is assumed initially at rest, and subjected at time $t = 0$ to an arbitrary time-dependent disturbance at its free boundary. Specifically, the following boundary conditions are assumed at the free boundary $x = 0$:

$$\sigma(0, t) = F(t) \qquad p_w(0, t) = 0 \tag{B7}$$

where $F(t)$ is an arbitrary function of time describing the prescribed stress at the free boundary. Free flow conditions (i.e., full drainage) are assumed at the free boundary. The solution is obtained using Laplace transforms (see Simon and Zienkiewicz (1984) for details) and is conveniently expressed in terms of the following parameters:

$$\zeta = \frac{x}{\rho K C_0} \qquad \tau = \frac{t}{\rho K} \tag{B8}$$

where $K = k / \gamma_w$, and in terms of the displacement w of the fluid *relative* to the solid (corresponding to the Darcy velocity), *viz.*,

$$w = n^w (u^w - u^s) \tag{B9}$$

Then the solution has the following form:

$$w = w(\zeta, \tau) = \frac{1}{(1-c)\sqrt{a}} \int_0^\tau f(\tau - \bar{\tau})\, e^{-\frac{b\bar{\tau}}{2a}} I_0\left[\frac{b\sqrt{\bar{\tau}^2 - a\zeta^2}}{2a}\right] 1(\bar{\tau} - \zeta\sqrt{a})\, d\bar{\tau} \tag{B10}$$

$$u^s = u^s(\zeta, \tau) = -\int_0^\tau f(\tau - \bar{\tau})\, 1(\bar{\tau} - \zeta)\, d\bar{\tau} - cw(\zeta, \tau) \tag{B11}$$

where

$$f(\tau) = \frac{K}{C_0}\sigma(0, \tau) = \frac{K}{C_0} F(\rho K \tau) = \frac{K}{C_0} F(t) \tag{B12}$$

$$a = \frac{\rho_s}{n^w (\rho_s - \rho_w)} \qquad b = \frac{1}{c(1-c)} \qquad c = \frac{\rho_w}{\rho} \tag{B13}$$

and $1(\tau)$ = unit step function; $I_0(z)$ = modified Bessel function of zero order. The pore fluid pressure, total stress and effective stress are obtained as:

$$p_w = p_w(\zeta, \tau) = -c \frac{C_0}{K} [\, n^s u^s_{,\zeta} + n^w u^w_{,\zeta} \,] = -c \frac{C_0}{K} [\, u^s_{,\zeta} + w_{,\zeta} \,] \quad \text{(B14)}$$

$$\sigma = \sigma(\zeta, \tau) = \frac{C_0}{K} f(\tau - \zeta)\, 1(\tau - \zeta) \quad \text{(B15)}$$

$$\sigma'^s = \sigma'^s(\zeta, \tau) = \sigma + p_w \quad \text{(B16)}$$

The spatial derivatives of w and u^s are computed as:

$$w_{,\zeta} = \frac{-1}{1-c} \left\{ f(\tau - \zeta\sqrt{a})\, e^{-\frac{b\zeta}{2\sqrt{a}}}\, 1(\tau - \zeta\sqrt{a}) + \right.$$

$$\left. + \frac{b\zeta}{2\sqrt{a}} \int_0^{\tau} f(\tau - \bar{\tau}) \frac{e^{-\frac{b\bar{\tau}}{2a}} I_1\!\left[\frac{b\sqrt{\bar{\tau}^2 - a\zeta^2}}{2a}\right]}{(\bar{\tau}^2 - a\zeta^2)^{1/2}}\, 1(\bar{\tau} - \zeta\sqrt{a})\, d\bar{\tau} \right\} \quad \text{(B17)}$$

$$u^s_{,\zeta} = f(\tau - \zeta)\, e^{-\frac{b}{2}(\tau - \zeta)} - c w_{,\zeta} \quad \text{(B18)}$$

where $I_1(z)$ = modified Bessel function of order one. In the following, the prescribed stress at the free boundary is assumed to be a step function, *viz.*,

$$\sigma(0, t) = F(t) = \sigma_0\, 1(t) \quad \text{(B19)}$$

where $\sigma_0 < 0$ (compressive wave). In order to illustrate the general features of the transient wave propagation, typical results are presented in Fig. 2.1. Upon impact at the free end, a double wave pattern traveling with non-dimensional velocities of 1 (C_1) and $a^{-1/2}$ (C_2) is established. The first wave is undamped whereas the second wave is damped. The total stress propagates with the first wave, and triggers changes in pore fluid pressure and solid effective stress. From Eqs B14 and B15, the jumps in pore fluid pressure and solid effective stress upon arrival of the first wave ($\tau = \zeta$) are given by:

$$[\, p_w \,] = -c\ \sigma_0 \qquad [\, \sigma'^s \,] = (1-c)\,\sigma_0 \tag{B20}$$

No further changes take place until arrival of the second wave. The jumps in pore fluid pressure and solid effective stress upon arrival of the second wave ($\tau = \zeta \sqrt{a}$) are given by:

$$[\, p_w \,] = c\ \sigma_0\, e^{-\frac{b\zeta}{2\sqrt{a}}} \qquad [\, \sigma'^s \,] = c\ \sigma_0\, e^{-\frac{b\zeta}{2\sqrt{a}}} \tag{B21}$$

The second wave is present only in the near field, and eventually disappears in the far field. This is illustrated in Fig. 2.1 which shows the pore fluid pressure as a function of position at various non-dimensional times: $\tau = 2.0;\ 5.0;\ 10.0;\ 20.0$. For the example reported in Fig. 2.1, the material parameters were selected as follows:

$$a = 9 \qquad b = \frac{1}{c\,(c-1)} = \frac{16}{3} \qquad c = \frac{3}{4}$$

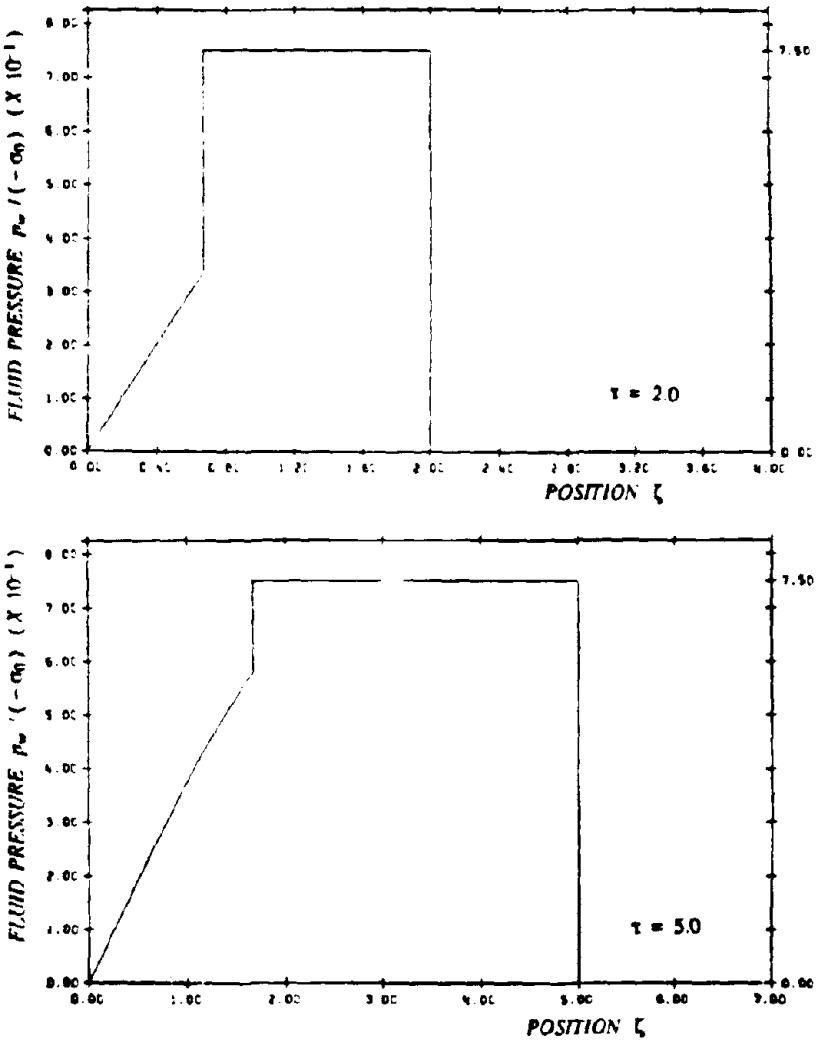

Figure 2.1 Pore fluid pressure vs. non-dimensional position
Dynamically compatible case: (a) $\tau = 2.0$; (b) $\tau = 5.0$.

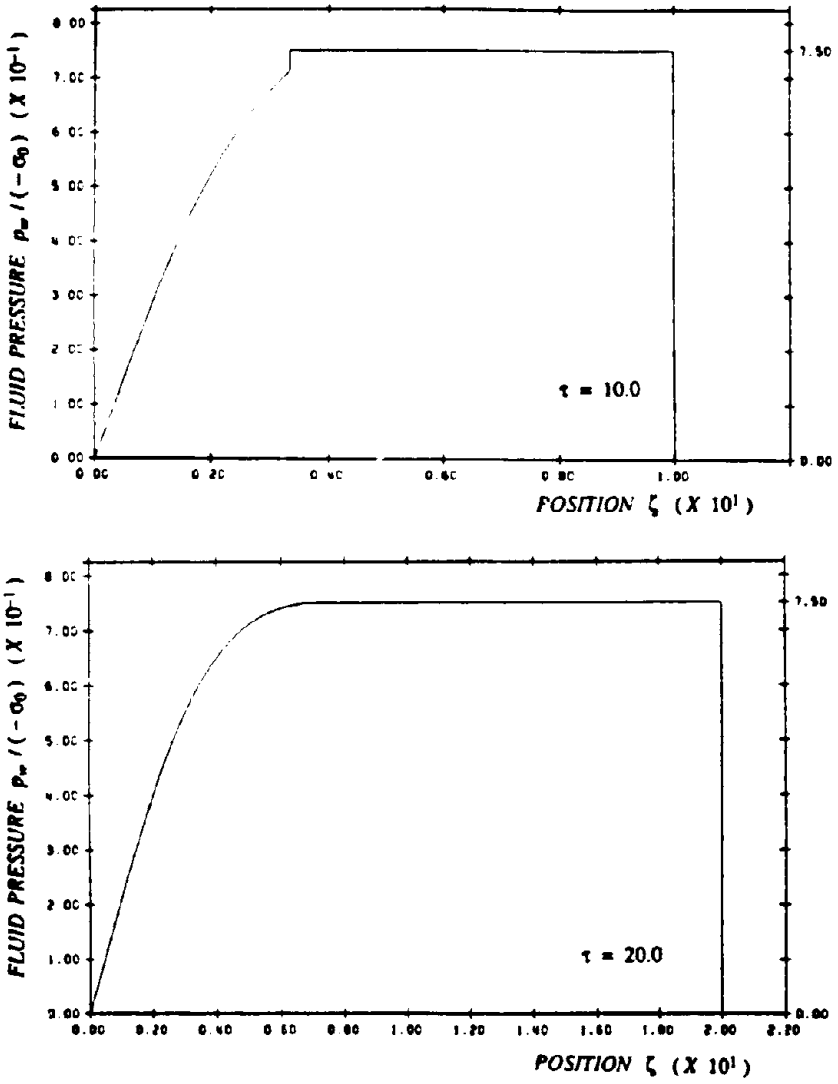

Figure 2.1 Pore fluid pressure vs. non-dimensional position
Dynamically compatible case: (c) $\tau = 10.0$; (d) $\tau = 20.0$.

2.10 REFERENCES

1. Atkin, R.J., "Completeness Theorems for Linearized Theories of Interacting Continua," *Quart. J. Mech. Appl. Math.*, Vol. 21, 1968, pp. 171-193.
2. Atkin, R.J. and Craine, R.E., "Continuum Theories of Mixtures: Basic Theory and Historical Development," *Quarterly J. of Mechanics and Applied Mathematics*, Vol. 29, 1976, pp. 209-244.
3. Atkin, R.J. and Craine, R.E., "Continuum Theories of Mixtures Applications," *Journal of the Institute of Mathematics and its Applications*, Vol. 17, 1976, pp. 153-207.
4. Bazant, Z.P. and R.J. Krizek, "Saturated Sand as an Inelastic Two-Phase Medium," *J. of the Eng. Mech. Div.*, ASCE, Vol. 101, No. EM4, 1975, pp. 317-332.
5. Biot, M.A., Theory of Elasticity and Consolidation for a Porous Anisotropic Solid," *J. of Applied Physics*, Vol. 26, 1955, pp. 182-185.
6. Biot, M.A., "Theory of Propagation of Elastic Waves in a Fluid- Saturated Porous Solid, I. Low Frequency Range," *J.of the Acoustical Society of America*, Vol. 28, 1956, pp. 168-178.
7. Biot, M.A., "Theory of Finite Deformations of Porous Solids," *Indiana University Mathematics Journal*, Vol. 21, No. 7, 1972, pp. 597-620.
8. Biot, M.A., "Variational Lagrangian Thermodynamics of Non-Isothermal Finite Strain Mechanics of Porous Solids and Thermomolecular Diffusion," *International Journal of Solids and Structures*, Vol. 13, 1977, pp. 579-597.
9. Biot, M.A., "Variational Irreversible Thermodynamics of Heat and Mass Transfer in Porous Solids: New Concepts and Methods," *Quarterly of Applied Mathematics*, Vol. 36, 1978, pp. 19-38.
10. Biot, M.A. and D.G. Willis, "The Elastic Coefficients of a Theory of Consolidation," *J. of Applied Mechanics*, ASME, Vol. 79, 1957, pp. 594-601.
11. Bowen, R.M., "Theory of Mixtures," in *Continuum Physics*, Vol. 3, A.C. Eringen (Ed.), Academic Press, New York, 1975, pp. 1-127.
12. Bowen, R.M., "Compressible Porous Media Models by Use of the Theory of Mixtures," *Int. Journal of Eng. Science*, Vol. 20, No. 6, 1982, pp. 697-735.
13. Bowen, R.M., and Chen, P.J., "Waves in a Binary Mixture of Linear Elastic Materials," *J. Mecanique*, Vol. 14, No. 2, 1975, pp. 237-266.
14. Bowen, R.M., and Reinicke, K.M., "Plane Progressive Waves in a Binary Mixture of Linear Elastic Materials," *J. Appl. Mech.*, ASME, Vol. 45, 1978, pp. 493-499.
15. Bowen, R.M., and Lockett, R.R., "Inertial Effects in Poroelasticity," *J. Appl. Mech.*, ASME, Vol. 50, 1983, pp. 334-342.
16. Crochet, M.J. and P.M. Naghdi, "On Constitutive Equations for Flow of Fluid Through an Elastic Solid," *Int. J. of Engineering Science*, Vol. 4, 1966, pp. 383-401.
17. Darcy, HJ., *Les Fontaines Publiques de la ville de Dijon*, V. Dalmont, Paris, 1856.
18. Eringen, A.C. *Nonlinear Theory of Continuous Media*, McGraw-Hill, New York, 1962.
19. Eringen, A.C. and J.D. Ingram, "A Continuum Theory of Chemically Reacting Media I and II," *Int. J. of Engineering Science*, Vol. .3, 1965, pp. 197-212, and Vol. 5, 1967, pp. 289-322.
20. Gray, W.G. and P.C.Y. Lee, "On the Theorems for Local Volume Averaging of Multiphase Systems," *Int. Journal of Multiphase Flow*, Vol. 3, 1977, pp. 333-340.

21. Green, A.E. and P.M. Naghdi, "A Dynamical Theory of Interacting Continua," *Int. J. of Eng. Science*, Vol. 3, 1965, pp. 231-241.

22. Green, A.E. and T.R. Steel, "Constitutive Equations for Interacting Continua," *Int. J. of Eng. Science*, Vol. 4, 1966, pp. 483-500.

23. Gurtin, M.E., Oliver, M.L. and W.O. Williams, "On Balance of Forces for Mixtures," *Quarterly of Applied Mathematics*, Vol. 30, 1972, pp. 527-530.

24. Hassanizadeh, M. and W.G. Gray, "General Balance Equations for Multiphase Systems," Princeton University, October, 1978.

25. Malvern, L.E., *Introduction to the Mechanics of a Continuous Medium*, Prentice-hall, 1969.

26. Prevost, J.H., "Mechanics of Continuous Porous Media," *Int. J. of Engineering Science*, Vol. 18, No. 5, 1980, pp. 787-800.

27. Schiffman, R.L., "Stress Components of a Porous Medium," *J. of Geophysical Research*, Vol. 75, 1970, pp. 4035-4038.

27b. Simon, B.R., and Zienkiewicz, O.C., "An Analytical Solution for the Transient Response of Saturated Porous Elastic Solids," *Int. J. Num. Meth. Eng.*, Vol. 8, No. 4, 1984, pp. 381-398.

28. Steel, T.R., "Applications of a Theory of Interacting Continua," *Quarterly Journal of Mechanics and Applied Mathematics*, Vol. 20, 1967, pp. 57-72.

29. Tabaddor, F. and R.W. Little, "Interacting Continuous Medium Composed of an Elastic Solid and an Incompressible Newtonian Fluid," *Int. J. of Eng. Science*, Vol. 7, 1971, pp. 825-841.

30. Terzaghi, K., *Theoretical Soil Mechanics*, John Wiley and Sons, N.Y., 1943.

31. Truesdell, C., *The Elements of Continuum Mechanics*, Springer-Verlag, New york, 1965.

32. Truesdell, C. and R.. Toupin, *The Classical Field Theories*, Handbuch der Physik, S. Flugge, Editor, Springer-Verlag, Berlin, Vol. III/1, 1960.

33. Truesdell, C. and W. Noll, *The Non-Linear Field Theories of Mechanics*, Handbuch der Physik, S. Flugge, Editor, Springer-Verlag, Berlin, Vol. III/3, 1965.

34. Whitaker, S., "Advances in Theory of Fluid Motion in Porous Media," *Industrial and Engineering Chemistry*, Vol. 61, No. 12, 1969, pp. 14-28.

35. Williams, W.O., "On the Theory of Mixtures," *Archives for Rational Mechanics and Analysis*, Vol. 51, 1973, pp. 239-260.

36. Williams, W.O., "Constitutive Equations for Flow of an Incompressible Viscous Fluid Through a Porous Medium," *Quarterly of Applied Mathematics*, Vol. 36, October, 1978, pp. 255-267.

SECTION 3
DYNAMICS OF POROUS MEDIA
NUMERICAL FORMULATION

3.1 INTRODUCTION

The enormous complexities encountered in solving geotechnical engineering problems (complex geometries, geological strata, material behavior) make analytical closed-formed solutions very difficult if not impossible. Recent advances in digital computer technology and in numerical methods have now rendered possible, at least in principle, the solution of any properly posed boundary value problem in mechanics. Consequently, applications of numerical techniques to geotechnical engineering problems have grown at a rapid pace during the last decade. Finite element methods appear to be the most popular procedures employed in geotechnical engineering. A number of excellent books on finite element methods are available (see e.g., Refs [1, 3, 5, 14]), to which the reader is referred to for more details on the technique. It is not the purpose of this section to offer an exhaustive treatment on the subject matter, but rather to briefly present some applications of the technique to geotechnical engineering problems. It is convenient to classify the classes of problems encountered in geotechnical engineering according to the nature of the differential equations to be solved as follows:

> *(i) Hyperbolic :* this class includes transient wave propagation and vibration type problems (in both saturated and dry soils),
>
> *(ii) Parabolic :* this class includes transient consolidation type problems in saturated soil systems,
>
> *(iii) Elliptic :* this class includes steady state seepage flow problems and load/deformation (and failure) analysis of soil and soil-structure systems in saturated (fully drained or undrained conditions) and dry soil media.

Only the techniques employed for solving hyperbolic problems are briefly reviewed in

the following. The problem of the dynamic response of a two-phase soil system can be represented as the following initial-boundary value problem: Let Ω denote the domain occupied by the two-phase system and Γ its boundary. Find the soil displacement field $\mathbf{u}^s(\mathbf{x},t)$ and the fluid velocity field $\mathbf{v}^w(\mathbf{x},t)$ in the domain $\Omega \in \mathbf{R}^{NSD}$ (NSD = number of space dimensions), such that:

$$\rho^s \mathbf{a}^s = \nabla\cdot\boldsymbol{\sigma}'^s - n^s \nabla p_w - \xi\cdot(\mathbf{v}^s - \mathbf{v}^w) + \rho^s \mathbf{b} \tag{1}$$

$$\rho^w \frac{D^s}{Dt}(\mathbf{v}^w) = \rho^w (\mathbf{v}^s - \mathbf{v}^w)\cdot\nabla\mathbf{v}^w - n^w \nabla p_w + \xi\cdot(\mathbf{v}^s - \mathbf{v}^w) + \rho^w \mathbf{b} \tag{2}$$

$$\frac{D^s}{Dt}(\boldsymbol{\sigma}'^s) = \mathbf{D} : \nabla\mathbf{v}^s \tag{3}$$

$$\frac{D^s}{Dt}(n^w) = (1 - n^w)\nabla\cdot\mathbf{v}^s \tag{4}$$

$$\frac{D^w}{Dt}(p_w) = -\frac{\lambda^w}{n^w}\left[\nabla\cdot(n^s \mathbf{v}^s) + \nabla\cdot(n^w \mathbf{v}^w)\right] \tag{5}$$

together with the boundary conditions

$$\mathbf{u}^s = \bar{\mathbf{u}}^s \quad on \quad \Gamma_{g^s} \tag{6a}$$

$$\mathbf{v}^w = \bar{\mathbf{v}}^w \quad on \quad \Gamma_{g^w} \tag{6b}$$

$$(\boldsymbol{\sigma}'^s - n^s p_w \delta)\cdot\mathbf{n} = \bar{\mathbf{h}}^s \quad on \quad \Gamma_{h^s} \tag{7a}$$

$$-n^w p_w \mathbf{n} = \bar{\mathbf{h}}^w \quad on \quad \Gamma_{h^w} \tag{7b}$$

and the initial conditions

$$\mathbf{u}^s(0) = \mathbf{u}_0^s \tag{8a}$$

$$\mathbf{v}^\alpha(0) = \mathbf{v}_0^\alpha \tag{8b}$$

Γ_{g^s}, Γ_{h^s} and Γ_{g^w}, Γ_{h^w} are the parts of the boundary on which the displacement and traction for the solid and fluid respectively are prescribed. They satisfy the following conditions:

$$\overline{\Gamma_{g^s} \cup \Gamma_{h^s}} = \Gamma \qquad \Gamma_{g^s} \cap \Gamma_{h^s} = 0 \tag{9a}$$

$$\overline{\Gamma_{g^w} \cup \Gamma_{h^w}} = \Gamma \qquad \Gamma_{g^w} \cap \Gamma_{h^w} = 0 \tag{9b}$$

When inertia and convective terms are neglected, Eq. 2 reduces to Darcy's law [2]:

$$n^w(\mathbf{v}^w - \mathbf{v}^s) = -(n^w)^2 \xi^{-1}\cdot(\nabla p_w - \rho_w \mathbf{b}) \tag{10}$$

and thus $\mathbf{k} = (n^w)^2 \gamma_w \xi^{-1}$ = Darcy permeability tensor (symmetric, positive-definite); $\gamma_w = g\ \rho_w$ = unit weight of the fluid, and g = acceleration of gravity.

REMARKS:

In the case of a *compressible* fluid (Eq. 5) the fluid pressure is determined (as the effective stress, Eq. 3) from the computed velocities through time integration of Eq. 5. In the case of an *incompressible* fluid, Eq. 5 is no longer available but is replaced by the continuity requirement,

$$\nabla\cdot(n^s \mathbf{v}^s) + \nabla\cdot(n^w \mathbf{v}^w) = 0 \tag{11}$$

In order to reduce the number of unknowns, it is convenient in that case to eliminate the fluid pressure from the list of unknowns. For that purpose, a *penalty-function* formulation of the continuity constraint expressed by Eq. 11 is used to compute the fluid pressure as:

$$p_w = -\frac{\lambda^w}{n^w}\left[\nabla\cdot(n^s \mathbf{v}^s) + \nabla\cdot(n^w \mathbf{v}^w)\right] \tag{12}$$

where λ^w is *not* the effective fluid bulk modulus appearing in Eq. 5, but rather is a *penalty parameter*. The penalty parameter is to be selected as a large number. This is further discussed in Ref. [12].

When fluid inertia and convection terms are neglected, the problem is expressed as follows: Find the soil displacement field $\mathbf{u}^s(\mathbf{x},t)$ and the fluid pressure field $p_w(\mathbf{x},t)$ in the domain $\Omega \in R^{NSD}$ such that:

$$\rho^s \mathbf{a}^s = \nabla\cdot(\sigma'^s - p_w \delta) + \rho \mathbf{b} \tag{13}$$

$$\frac{n^w}{\lambda^w}\frac{D^w}{Dt}p_w - \nabla\cdot\left[\frac{1}{\gamma_w}\mathbf{k}\cdot(\nabla p_w - \rho_w \mathbf{b})\right] + \nabla\cdot\mathbf{v}^s = 0 \tag{14}$$

$$\frac{D^s}{Dt}(\sigma'^s) = \mathbf{D} : \nabla\mathbf{v}^s \tag{15}$$

$$\frac{D^s}{Dt}(n^w) = (1 - n^w)\nabla\cdot\mathbf{v}^s \tag{16}$$

together with the boundary conditions:

$$\mathbf{u}^s = \bar{\mathbf{u}}^s \quad on \quad \Gamma_{g^s} \tag{17a}$$

$$p_w = \bar{p}_w \quad on \quad \Gamma_{g^w} \tag{17b}$$

$$(\sigma'^s - p_w \delta)\cdot \mathbf{n} = \bar{\mathbf{h}}^s \quad on \quad \Gamma_{h^s} \quad (\textit{total traction}) \tag{18a}$$

$$\mathbf{n}\cdot\frac{\mathbf{k}}{\gamma_w}\cdot(\nabla p_w - \rho_w \mathbf{b}) = \bar{h}^w \quad on \quad \Gamma_{h^w} \quad (\textit{flow rate}) \tag{18b}$$

and the initial conditions:

$$\mathbf{u}^s(0) = \mathbf{u}_0^s \tag{19a}$$

$$p_w(0) = p_{w\,0} \tag{19b}$$

$$\mathbf{v}^s(0) = \mathbf{v}_0^s \tag{19c}$$

where $\rho = \rho^s + \rho^w$ = total mass density of the mixture. This formulation is expressed in terms of the solid displacement and the fluid pressure only ($\mathbf{u}^s$ and p_w). However, the resulting semi-discrete finite element matrix equations form a nonsymmetrical system. Taking advantage of the symmetry of the full system of equations, including fluid inertia and convection terms, allows substantial reduction in computations, which may be greater than those resulting from neglecting fluid inertia and convection. In the following, the full system of equations is used.

3.2 WEAK FORM / SEMI-DISCRETE FINITE ELEMENT EQUATIONS

The weak formulation associated with the initial boundary value problem is obtained by proceeding along standard lines (see e.g., Refs. 1, 10, 23). The associated matrix problem is obtained by discretizing the domain occupied by the porous medium into non-overlapping finite elements. Each element is defined by nodal points at which shape functions are prescribed. In general, two sets of shape functions are required for the solid displacement and the fluid velocity field, respectively. However, since attention in the following is restricted to low order finite elements which are the most efficient in nonlinear analysis, the same shape functions are used for both the solid and the fluid. The shape functions for the solid displacement and fluid velocity associated with node A are denoted by N^A in the following. They satisfy the relation $N^A(\mathbf{x}^B) = \delta_{AB}$ in which

$\mathbf{x}^B$ denotes the position vector of node B and δ_{AB} = Kronecker delta. The Galerkin counterpart of the weak formulation is expressed in terms of the shape functions and gives rise to the following system of equations

$$\begin{bmatrix} \mathbf{M}^s & 0 \\ 0 & \mathbf{M}^w \end{bmatrix} \begin{Bmatrix} \mathbf{a}^s \\ \mathbf{a}^w \end{Bmatrix} + \begin{bmatrix} \mathbf{Z} & -\mathbf{Z} \\ -\mathbf{Z}^T & \mathbf{Z} \end{bmatrix} \begin{Bmatrix} \mathbf{v}^s \\ \mathbf{v}^w \end{Bmatrix} + \begin{Bmatrix} \mathbf{n}^s \\ \mathbf{n}^w \end{Bmatrix} = \begin{Bmatrix} \mathbf{f}^{s\ ext} \\ \mathbf{f}^{w\ ext} \end{Bmatrix} \tag{20}$$

where $\mathbf{M}^\alpha$, $\mathbf{a}^\alpha$, $\mathbf{v}^\alpha$, $\mathbf{n}^\alpha$, and $\mathbf{f}^{\alpha\ ext}$ represent the (generalized) mass matrix, acceleration, velocity and force vectors, respectively ($\alpha = s, w$ for the soil and fluid phases, respectively). The element contributions to node A from node B for direction i and j to the matrices appearing in Eq. 20 are defined below. The terms are integrated over the spatial domain occupied by the element Ω^e. For computational simplicity a diagonal "lumped" mass matrix is used,

$$(m_{ij}^{AB})^\alpha = \delta_{ij}\delta^{AB}\int_{\Omega^e}\rho^\alpha N^A\, d\Omega \qquad (no \sum on\ A) \tag{21}$$

The momentum transfer terms give rise to the damping matrix $\mathbf{Z}$:

$$(Z_{ij}^{AB}) = \int_{\Omega^e} N^A \xi_{ij} N^B\, d\Omega \tag{22}$$

The external force $\mathbf{f}^{\alpha\ ext}$ (i.e., body force, surface traction) is computed as follows:

$$(f_i^A)^{\alpha\ ext} = \int_{\Omega^e}\rho^\alpha b_i N^A\, d\Omega + boundary\ terms \tag{23}$$

The internal stress forces $\mathbf{n}^\alpha$ are computed as follows:

$$(n_i^A)^s = \int_{\Omega^e}(\sigma'^s_{ij} - n^s p_w \delta_{ij})N^A_{,j}\, d\Omega \tag{24a}$$

and

$$(n_i^A)^w = \int_{\Omega^e}\rho^w N^A (v_j^w - v_j^s) v_{i,j}^w\, d\Omega - \int_{\Omega^e} N^A_{,i} n^w p_w\, d\Omega \tag{24b}$$

3.3 TIME INTEGRATION

Time integration of the semi-discrete finite element equations is accomplished by a finite difference time stepping algorithm. In general, implicit and explicit integration procedures are available. Explicit procedures are computationally the simplest since they do not require (for a diagonal mass matrix) equation solving to advance the solution. However, stability restricts the size of the allowable time step. On the other hand, unconditional stability can usually be achieved in implicit procedures but they do require solution of a system of equations at each time step. For the problem at hand, a purely explicit procedure is not usually appropriate because of the unreasonably stringent time step restriction resulting from the presence of the very stiff fluid in the mixture (even for highly nonlinear solid material models). Recently developed methods combine the attractive features of explicit and implicit integration. The method used here falls under the category of "split operator methods". Different portions of the system of equations are treated implicitly and explicitly, reducing the system of equations to be solved. The specific split to be made is obviously problem dependent, and the appropriate implicit/explicit splits for the problem at hand are summarized thereafter.

3.3.1 One-Step Algorithms

The discretized equations of motion (Eq. 20) can be written symbolically as follows:

$$\mathbf{M}\,\mathbf{a} + \mathbf{C}\,\mathbf{v} + \mathbf{n}(\mathbf{d}, \mathbf{v}) = \mathbf{f}^{ext} \tag{25}$$

where $\mathbf{M}$, $\mathbf{C}$ represent the generalized mass and damping matrices, $\mathbf{n}$ and $\mathbf{f}^{ext}$ represent generalized internal and external forces and $\mathbf{a}$, $\mathbf{v}$, and $\mathbf{d}$ represent the generalized acceleration, velocity and displacement vectors. Time integration is performed by using the implicit-explicit algorithm of Hughes, et al. (Refs. [6,7]), which consists of satisfying the following equations:

$$\mathbf{M}\,\mathbf{a}_{n+1} + \mathbf{C}^I\mathbf{v}_{n+1} + \mathbf{C}^E\tilde{\mathbf{v}}_{n+1} + \mathbf{n}^I(\mathbf{d}_{n+1},\mathbf{v}_{n+1}) + \mathbf{n}^E(\tilde{\mathbf{d}}_{n+1},\tilde{\mathbf{v}}_{n+1}) = \mathbf{f}^{ext}_{n+1} \quad (26)$$

$$\mathbf{d}_{n+1} = \tilde{\mathbf{d}}_{n+1} + \beta\,\Delta t^2\,\mathbf{a}_{n+1} \quad (27)$$
$$\mathbf{v}_{n+1} = \tilde{\mathbf{v}}_{n+1} + \gamma\,\Delta t\,\mathbf{a}_{n+1}$$

where

$$\tilde{\mathbf{d}}_{n+1} = \mathbf{d}_n + \Delta t\,\mathbf{v}_n + (1-2\beta)\frac{\Delta t^2}{2}\mathbf{a}_n \quad (28)$$
$$\tilde{\mathbf{v}}_{n+1} = \mathbf{v}_n + (1-\gamma)\Delta t\,\mathbf{a}_n$$

The superscripts I and E refer to the parts of C and n which are treated implicitly and explicitly, respectively. Δt = time step; $\mathbf{f}^{ext}_n = \mathbf{f}^{ext}(t_n)$; $\mathbf{d}_n$, $\mathbf{v}_n$, and $\mathbf{a}_n$ are the approximations to $\mathbf{d}(t_n)$, $\mathbf{v}(t_n)$ and $\mathbf{a}(t_n)$; γ and β are algorithmic parameters which control accuracy and stability of the method. It may be recognized that when all terms are treated implicitly the procedure corresponds to the Newmark method (Ref. [8]). The quantities $\tilde{\mathbf{d}}_{n+1}$ and $\tilde{\mathbf{v}}_{n+1}$ are "predictor" values, while $\mathbf{d}_{n+1}$ and $\mathbf{v}_{n+1}$ are "corrector" values. From Eqs 26-28 it is apparent that the calculations are rendered partly explicit by evaluating part of the viscous term, $\mathbf{C}^E\tilde{\mathbf{v}}_{n+1}$, and the force $\mathbf{n}^E$ in terms of predictor values based on data known from the previous step. Calculations commence with the given initial data ($\mathbf{d}_0$ and $\mathbf{v}_0$) and $\mathbf{a}_0$ which is defined by:

$$\mathbf{M}\,\mathbf{a}_0 = \mathbf{f}^{ext}_0 - \mathbf{C}\,\mathbf{v}_0 - \mathbf{n}(\mathbf{d}_0, \mathbf{v}_0) \quad (29)$$

Since M is diagonal, the solution of Eq. 29 is trivial.

3.3.2 Implementation

At each time step Eqs 26-28 constitute a nonlinear algebraic problem which is solved by an iterative procedure. An "effective static problem" is formed in terms of $\mathbf{a}_{n+1}$ which is then linearized. Within each time step the calculations are performed iteratively as summarized in Flowchart 1 for a Newton-Raphson type implementation. In Flowchart 1,

$$\mathbf{K}^I = \partial \mathbf{n}^I / \partial \mathbf{d} \tag{30a}$$

$$\mathbf{C}^I = \mathbf{C} + \partial \mathbf{n}^I / \partial \mathbf{v} \tag{30b}$$

denote the parts of the tangent stiffness and damping matrices, respectively, to be treated implicitly. Implicit treatment of nonlinear terms usually requires matrix reformation and factorization at each time step (and for every iteration to be performed if Newton Raphson iterations are used). In general, it is therefore desirable to treat nonlinearities explicitly; γ and β in Eqs 27 and 28 are then selected to achieve unconditional stability in the implicit group. Then the maximum stable time step for the problem is determined from a Courant condition which must be satisfied in the explicit group. However, if any portion of the explicit group requires extremely small time steps, it becomes more efficient to treat that portion implicitly. The appropriate implicit-explicit split for the hyperbolic problem is discussed in Refs [10, 12], and is summarized thereafter.

FLOWCHART 1

1. Set Iteration Counter $i = 0$

2. Predictor Phase:

$$\mathbf{d}_{n+1}^{(i)} = \tilde{\mathbf{d}}_{n+1}$$
$$\mathbf{v}_{n+1}^{(i)} = \tilde{\mathbf{v}}_{n+1}$$
$$\mathbf{a}_{n+1}^{(i)} = 0$$

3. Form Out-of-Balance Force:

$$\Delta \mathbf{f}^{(i)} = \mathbf{f}_{n+1}^{ext} - \mathbf{M}\,\mathbf{a}_{n+1}^{(i)} - \mathbf{C}\,\mathbf{v}_{n+1}^{(i)} - \mathbf{n}(\mathbf{d}_{n+1}^{(i)}, \mathbf{v}_{n+1}^{(i)})$$

4. Form Effective Mass: (Reform and factorize only if required)

$$\mathbf{M}^* = \mathbf{M} + \Delta t\,\gamma\,\mathbf{C}^I + \Delta t^2\beta\,\mathbf{K}^I$$

5. Solution Phase:

$$\mathbf{M}^*\,\Delta\mathbf{a}^{(i)} = \Delta\mathbf{f}^{(i)}$$

6. Corrector Phase:

$$\mathbf{a}_{n+1}^{(i+1)} = \mathbf{a}_{n+1}^{(i)} + \Delta\mathbf{a}^{(i)}$$
$$\mathbf{v}_{n+1}^{(i+1)} = \tilde{\mathbf{v}}_{n+1} + \Delta t\,\gamma\,\mathbf{a}_{n+1}^{(i+1)}$$
$$\mathbf{d}_{n+1}^{(i+1)} = \tilde{\mathbf{d}}_{n+1} + \Delta t^2\beta\,\mathbf{a}_{n+1}^{(i+1)}$$

7. Convergence Check: (only if $i > 0$)

$$IF\left[\frac{\|\Delta\mathbf{f}^{(i)}\|}{\|\Delta\mathbf{f}^{(0)}\|} \le TOL^* \text{ . and . } \frac{\|\Delta\mathbf{a}^{(i)}\|}{\|\Delta\mathbf{a}^{(0)}\|}\,Q \le (1-Q)\,TOL^*\right] \quad GOTO\ 8$$

$$where \qquad Q = \max\left[\frac{\|\Delta\mathbf{a}^{(i)}\|}{\|\Delta\mathbf{a}^{(i-1)}\|},\ \frac{\|\Delta\mathbf{a}^{(i-1)}\|}{\|\Delta\mathbf{a}^{(i-2)}\|}\right]$$

$$OTHERWISE \quad i \Rightarrow i+1 \ \text{and}\ GOTO\ 3$$

8. $n \Rightarrow n+1$ and $GOTO$ 1

---

*Typically, $TOL = 10^{-3}$

3.3.3 Stability Conditions

Linearized stability analysis of implicit / explicit algorithms have been reported in Ref. [6]. The resulting stability conditions are summarized as follows (see Refs. [5-7]): In all cases $\gamma \geq 1/2$:

1. *Implicit Treatment:* unconditional stability is achieved if $\beta \geq \gamma/2$ and it is recommended (Ref. [4]) that

$$\beta = (\gamma + \tfrac{1}{2})^2 / 4 \tag{31}$$

to maximize high-frequency numerical dissipation.

2. *Explicit Treatment:* The time step restriction is

$$\Delta t \leq \frac{2}{\omega} (1 - \zeta) / (\gamma + \tfrac{1}{2}) \tag{32}$$

to maximize high-frequency numerical dissipation; ω = highest natural frequency present in the system of equations; ζ = damping ratio. The maximum expected frequency may be bounded by the frequency of the smallest element, viz., for a two node linear element,

$$\omega = 2 \frac{C}{L} \tag{33}$$

where L = dimension of the element and C = maximum wave speed.

3. *Implicit-Explicit Treatment:* The stability characteristics are determined by the conditions that render the following $\mathbf{B}$ matrix positive-definitive:

$$\mathbf{B} = \mathbf{M} + \Delta t \, (\gamma - \tfrac{1}{2}) \, \mathbf{C}^I + \Delta t^2 (\beta - \tfrac{\gamma}{2}) \, \mathbf{K}^I - \tfrac{1}{2} \Delta t \, \mathbf{C}^E - \tfrac{\gamma}{2} \Delta t^2 \, \mathbf{K}^E \tag{34}$$

Evidently, stability restrictions are dependent upon the specific choices adopted in the implicit-explicit split. As shown hereafter, it is convenient to always treat the damping terms implicitly (since they are linear). The resulting stability restrictions are then determined by the conditions which render the following $\mathbf{B}$ matrix

positive-definite:

$$\mathbf{B} = \mathbf{M} + \Delta t\,(\gamma - \tfrac{1}{2})\,\mathbf{C}^I + \Delta t^2\,(\beta - \tfrac{\gamma}{2})\,\mathbf{K}^I - \tfrac{\gamma}{2}\,\Delta t^2\,\mathbf{K}^E \qquad (35)$$

REMARK:

For vibration calculations optimum accuracy is obtained with $\gamma = 1/2$. Increasing γ serves to dissipate high frequency numerical noise. The purely diffusive part (consolidation part) of the problem can be captured "dynamically" using the hyperbolic system developed by setting $\gamma = 3/2$ and $\beta = 1$ and using implicit-explicit integration (Refs [10,12]). This choice damps out all dynamic transients.

3.4 IMPLEMENTATION

Depending upon the specifics of the particular problem to be studied, different computational strategies are to be adopted as discussed in the following.

3.4.1 Wave Propagation Calculations:

Very short time scale (and high frequency) solutions are sought and a purely explicit integration of the equations of motions is found most appropriate in that case. The time step size is restricted from stability considerations, and the calculations are to be carried out at a time step close to the time step corresponding to the propagation of the fastest compressional wave. The time step restriction is (from Eq. 32):

$$\Delta t \le \frac{2}{\omega}\,(1 - \frac{\alpha_i\,\xi}{2\,\omega})\,/\,(\gamma + \frac{1}{2}) \qquad (36)$$

where

$$\alpha_i = (\frac{1}{\rho^s} + \frac{1}{\rho^w})\,\frac{|\,C_{p_i}{}^2 - C_0{}^2\,|}{C_{p_1}{}^2 - C_{p_2}{}^2} \qquad (37)$$

and C_{p_i} = wave speeds of the two dilatational waves which may in general propagate thru the porous medium, C_0 = "frozen" mixture speed with,

$$C_{p_2}{}^2 < C_0{}^2 \le C_{p_1}{}^2 \qquad (38)$$

i.e., for the linear model:

$$C_0^2 = (\lambda^s + 2\mu^s + \frac{\lambda^w}{n^w}) / (\rho^s + \rho^w) \tag{39}$$

and the speeds C_{p_i} are given by:

$$C_{p_i}^2 = \frac{1}{2} \left[(C_1^2 + C_2^2) \pm [(C_1^2 - C_2^2) + 4 C_3^2]^{1/2} \right] \tag{40a}$$

where

$$C_1^2 = (\lambda^s + 2\mu^s + \lambda^w \frac{(n^s)^2}{n^w}) / \rho^s \tag{40b}$$

$$C_2^2 = (n^w \lambda^w) / \rho^w \tag{40c}$$

$$C_3^2 = (n^s \lambda^w)^2 / (\rho^s \rho^w) \tag{40d}$$

REMARKS:

(1) Second-order accuracy is achieved by selecting $\gamma = 1/2$ and $\beta = 0$ (Central difference integrator).

(2) If only rotational (shear) waves are to be present, the time step restriction is:

$$\Delta t \leq \frac{2}{\omega} (1 - \frac{\xi}{2 \omega \rho^s}) / (\gamma + \frac{1}{2})$$

and the wave speed associated with the shear wave is given as:

$$C_s = \sqrt{\frac{\mu^s}{\rho^s}} .$$

3.4.2 Vibration Type Calculations:

Since the frequencies to be captured are usually much smaller than above, an implicit integrator is usually most convenient in that case since it allows the time step to be selected following accuracy considerations only. Unconditional stability is to be achieved by proper selection of the algorithmic parameters as discussed in Section 3.3.3. In the following,

$$\gamma \geq 1/2 \quad \text{and} \quad \beta = (\gamma + \frac{1}{2})^2 / 4 \tag{41}$$

The damping term contains the momentum transfer contribution to the equations of motion, *viz.*,

$$\mathbf{C}^I = \begin{bmatrix} \mathbf{Z} & -\mathbf{Z} \\ -\mathbf{Z}^T & \mathbf{Z} \end{bmatrix} \tag{42}$$

The fluid convective force (Eq. 24b) is usually small and therefore is treated explicitly with no resulting computational difficulty. The fluid pressure contribution (Eqs 5 and 24) is treated implicitly. For that purpose, a fluid stiffness matrix is defined through linearization of Eq. 24 as:

$$\mathbf{K}_w = \begin{bmatrix} \mathbf{C}^{ss} & \mathbf{C}^{sw} \\ \mathbf{C}^{ws} & \mathbf{C}^{ww} \end{bmatrix} \tag{43}$$

where $\mathbf{C}^{\alpha\beta}(\alpha,\beta = s,w)$ are matrices defined as follows (from Eq. 5):

$$(C_{ij}^{AB})^{\alpha\beta} = \int_{\Omega^w} \lambda^w \frac{n^\alpha n^\beta}{n^w} N_{,i}^A N_{,j}^B \, d\Omega \tag{44}$$

Note that since $\mathbf{C}^{sw} = (\mathbf{C}^{ws})^T$ the resulting $\mathbf{K}_w$ is symmetric.

As for the solid effective stress contribution to the equations of motion (Eqs 3 and 24a), three options are possible: *explicit, implicit, or implicit-explicit* treatments.

(a) *Explicit:* in that case

$$\mathbf{K}^I = \mathbf{K}_w \tag{45}$$

and unconditional stability cannot be achieved. The resulting stability restrictions are as follows (from Section 2.3):

$$\Delta t \leq \frac{2}{\omega} / (\gamma + \frac{1}{2}) \tag{46}$$

where the maximum expected frequency ω may be bounded by the frequency of the smallest element, *viz.*, for the two-node linear element with a linear solid

effective stress model,

$$\omega = 2\frac{C}{L} \qquad C = \sqrt{\frac{\lambda^s + 2\mu^s}{\rho^s}} \tag{47}$$

where L = smallest dimension of the element.

(b) *Implicit:* in that case unconditional stability is to achieved. A solid effective stiffness operator is defined from Eq. 24a through linearization as:

$$\mathbf{K}_s = \begin{bmatrix} \mathbf{K}^S + \mathbf{K}^G & 0 \\ 0 & 0 \end{bmatrix} \tag{48}$$

where $\mathbf{K}^S$ is the material tangent part, and $\mathbf{K}^G$ is the initial stress or geometric part, formed from the tensors $\mathbf{D}^S$ and $\mathbf{D}^G$ (Eq. 2.29) in the usual manner, *e.g.*,

$$(K_{ij}^{AB})^S = \int_{\Omega^e} D_{ikjl}^S N_{,k}^A N_{,l}^B \, d\Omega \tag{49}$$

and (from Eqs 43 and 48):

$$\mathbf{K}^I = \frac{\partial \mathbf{n}}{\partial \mathbf{d}} = \mathbf{K}_s + \mathbf{K}_w \tag{50}$$

(c) *Implicit-Explicit:* For nonlinear effective stress solid models a purely implicit treatment of the effective stress solid contribution (Eqs 3 and 24a) requires a matrix reform / factorize at each time step (and for every iteration to be performed if Newton-Raphson iterations are used), thus producing a considerable computational burden. In that case it is convenient to adopt an implicit-explicit treatment of the effective stress contribution as follows: the linear part of the stress is treated implicitly while the remaining nonlinear part is treated explicitly. Thus, in the implicit-explicit procedure,

$$\mathbf{K}_s^I = \begin{bmatrix} \mathbf{K}_E^S & 0 \\ 0 & 0 \end{bmatrix} \tag{51}$$

where $\mathbf{K}_E^S$ is the linear contribution to the material tangent stiffness, and combining Eqs 43 and 51:

$$\mathbf{K}^I = \begin{bmatrix} \mathbf{K}_E^S + \mathbf{C}^{ss} & \mathbf{C}^{sw} \\ \mathbf{C}^{ws} & \mathbf{C}^{ww} \end{bmatrix} \tag{52}$$

which again is a symmetric matrix if $\mathbf{K}_E^S$ is symmetric. This choice does not always lead to unconditional stability. The difficulty is not usually associated with the explicit treatment of $\mathbf{K}^G$ (which contains terms of the stress order and therefore usually has a negligible impact on stability), but rather from the explicit treatment of the nonlinear term $(\mathbf{K}^S - \mathbf{K}_E^S)$ for materials with a locking tendency.

3.4.3 Diffusion Type Calculations:

It is sometimes desirable to capture the purely diffusive part (consolidation part) of the solution "dynamically". Such necessity arises in situations in which both short and long time solutions to a dynamical problem are sought (such as in seismic or blast induced liquefaction simulations). As shown in Refs [10, 12], by switching to an appropriate choice of the Newmark parameters, $\gamma = 3/2$ and $\beta = 1$, and by using the implicit or implicit-explicit options described previously, all dynamic transients can be damped out, and purely diffusive (consolidation) solutions can be obtained "dynamically" by solving the dynamic equations.

3.5 REFERENCES

1. Bathe, K.J., and Wilson, E.L., *Numerical Methods in Finite Element Analysis*, Prentice-Hall, Inc., N.J., 1976.
2. Darcy, H., "Les Fontaines Publiques de la ville de Dijon," V. Dalmont, Paris, 1856.
3. Desai, C.S. and Abel, J.P., *Introduction to the Finite Element Method*, Van Nostrand Reinhold, New York, 1972.
4. Hilber, H.M., "Analysis and Design of Numerical Integration Methods in Structural Dynamics," Report No. EERC 76-29, Earthquake Engineering Research Center, University of California, Berkeley, Calif. 1976.
5. Hughes, T.J.R., *The Finite Element Method*, Prentice Hall, New Jersey, 1987.
6. Hughes, T.J.R., Pister, K.S. and Taylor, R.L., "Implicit-Explicit Finite Elements in Nonlinear Transient Analysis," *Comp. Method Appl. Mech. Engr.* Vol. 17/18, 1979, pp. 159-182.
7. Hughes, T.J.R. and Liu, W.K., "Implicit-Explicit Finite Elements in Transient Analysis: Implementation and Numerical Examples," *Journal of Applied Mechanics* Vol. 45, June 1978, pp. 375-378.
8. Newmark, N.M., "A Method of Computation for Structural Dynamics," *Journal of Engineering, Mechanics, Div.*, ASCE, Vol. 85, no. EM3, 1959, pp. 67-94.
9. Prevost, J.H. "Mechanics of Continuous Porous Media," *International Journal of Engineering Science*," Vol. 18, No. 5, 1980, pp. 787-800.
10. Prevost, J.H., "Nonlinear Transient Phenomena in Saturated Porous Media," *Comp. Meth. Appl. Mech. Eng.*, 1982, Vol. 30, pp. 3-18.
11. Prevost, J.H., "A Simple Plasticity Theory for Frictional Cohesionless Soils," *Soil Dynamics and Earthquake Engineering*, Vol. 4, No. 1, 1985, pp. 9-17.
12. Prevost, J.H., "Wave Propagation in Fluid-Saturated Porous Media: An Efficient Finite Element Procedure," *Soil Dynamics and Earthquake Engineering*, Vol. 4, No. 4, 1985, pp. 183-202.
13. Terzaghi, K., *Theoretical Soil Mechanics*, John Wiley and Sons, N.Y., 1943.
14. Zienkiewicz, O.C., *The Finite Element Method*, 3rd Edition, McGraw-Hill, London, 1977.

SECTION 4
TRANSMITTING BOUNDARY

4.1 INTRODUCTION

The application of finite elements to the solution of geotechnical problems involving the vertical propagation of seismic waves in a soil deposit requires the development of special boundary conditions referred to as transmitting, non-reflecting, silent or energy-absorbing boundaries. These boundary conditions are required to use at the base of the necessarily finite mesh to simulate the infinite extent of the soil domain in the vertical downward direction. When an infinite domain is modeled by a finite mesh, there is danger that waves reflected from the free-surface will be reflected back off the artificial bottom boundary and cause errors in the response calculations, unless special boundary conditions can be imposed at the base of the soil column. In the following, a rigorous formulation of an appropriate boundary condition is developed. The proposed boundary condition is frequency independent, and is local in space and time. It is exact for linear systems only, and therefore requires that the bottom boundary of the soil column be placed at a sufficiently large depth such that the soil response be linear at that depth.

Seismic site response calculations are usually performed for a given seismic input prescribed in the form of an acceleration time history to be applied at the base of the soil column. As discussed hereafter, the implementation of an appropriate boundary condition at the base of the soil column requires detailed knowledge of the nature of the prescribed seismic input, viz. whether it corresponds to an incident vertically propagating motion or is the sum of an incident and a reflected motion.

The salient features of one-dimensional wave propagation in a semi-infinite system are first reviewed before the boundary condition is developed.

4.2 ONE-DIMENSIONAL VERTICAL PROPAGATION OF SEISMIC WAVES

For the purpose of illustrating the salient features of the boundary formulation, the vertical propagation of shear waves is considered. The equation of motion may be expressed as:

$$\rho u_{,tt} = G u_{,xx} \tag{1}$$

where a comma is used to indicate partial differentiation; ρ = mass density; G = shear modulus; u = horizontal displacement; t = time; and x = depth coordinate, with the x-coordinate assumed oriented upwards positively. The fundamental solution of Eq. 1 can be expressed as:

$$u(x, t) = I(t - \frac{x}{C}) + R(t + \frac{x}{C}) \tag{2}$$

where

$$C = \sqrt{\frac{G}{\rho}} \tag{3}$$

and I and R are two arbitrary functions of their arguments: $I(t - \frac{x}{C})$ represents a wave motion propagating upwards in the positive x-direction with the velocity C, and is referred to as the *incident motion*; $R(t + \frac{x}{C})$ represents a wave motion propagating downwards in the negative x-direction with the velocity C, and is referred to as the *reflected motion*. The following two identities apply:

$$I_{,x} + \frac{1}{C} I_{,t} = 0 \tag{4a}$$

$$R_{,x} - \frac{1}{C} R_{,t} = 0 \tag{4b}$$

and therefore, if one differentiates Eq. 2 with respect to x and t in turn:

$$u_{,x} = \frac{1}{C}(-I_{,t} + R_{,t}) \tag{5}$$

$$u_{,t} = I_{,t} + R_{,t} \tag{6}$$

The shear stress $\tau(x, t)$ can therefore be expressed as

$$\tau(x, t) = G\, u_{,x} = \rho C(-I_{,t} + R_{,t}) \tag{7}$$

and upon elimination of $R_{,t}$, the following relation is obtained:

$$\tau(x, t) = \rho C(u_{,t} - 2I_{,t}) \tag{8}$$

At this stage it is instructive to study the total wave pattern when an incident wave motion $I(t - \frac{x}{C})$ encounters an artificial boundary at $x = h$. Three extreme cases can be considered as follows:

4.2.1 *The boundary at $x = h$ is fixed.* Setting $u(h, t) = 0$ in Eq. 2 leads to:

$$R(t + \frac{x-h}{C}) = -I(t - \frac{x-h}{C}) \tag{9}$$

resulting in the total wave motion:

$$u(x, t) = I(t - \frac{x-h}{C}) - I(t + \frac{x-h}{C}) \tag{10}$$

Therefore, at a fixed boundary, the incident wave is reflected back with the same shape but opposite sign.

4.2.2 *The boundary at $x = h$ is free.* Setting $\tau(h, t) = 0$ in Eq. 7 leads to:

$$R(t + \frac{x-h}{C}) = I(t - \frac{x-h}{C}) \tag{11}$$

resulting in the total wave motion:

$$u(x, t) = I(t - \frac{x-h}{C}) + I(t + \frac{x-h}{C}) \tag{12}$$

Therefore, at a free boundary, the incident wave is reflected back with the same shape and the same sign.

4.2.3 *The boundary at $x = h$ is silent.* Selecting Eq. 4a which is identically satisfied for I as the boundary condition for u at $x = h$

$$(u_{,x} + \frac{1}{C} u_{,t}) \Big|_{x=h} = 0 \tag{13}$$

results in $R = 0$. Eq. 13 is called the radiation condition. It is obtained by selecting:

$$\tau(h, t) = -\rho C \, u_{,t} \Big|_{x=h} \tag{14}$$

When the incident wave I encounters that boundary, it passes through it without modification and continues propagating towards $x = +\infty$. No reflected wave R, which would propagate back in the negative x-direction can arise.

4.3 SEMI-INFINITE SOIL COLUMN

Consider the situation shown in Fig. 4.1. An incident vertically propagating wave I (coming from infinity) arrives at the site, and it is sought to compute the site response for this incident motion. The finite element mesh has been selected to extend down to the depth h, and an appropriate boundary condition at the base of the soil column is sought to simulate the infinite extend of the soil domain in the vertical downward direction. For the purpose of illustration, it is assumed that the site consists in genera[illegible] two homogeneous deposits with material properties as follows:

- (ρ, C) above the base of the soil column: $0 \le x \le h$
- (ρ_∞, C_∞) below the base of the soil column: $-\infty < x < 0$

In order to separate the influence of the incident wave from the reflected wave on the site response, it is assumed that the incident motion disturbance spans over a duration T with:

$$0 < T \leq \frac{h}{C}$$

and that it reaches the location $x = 0$ at time $t = 0$. Several cases are considered as follows:

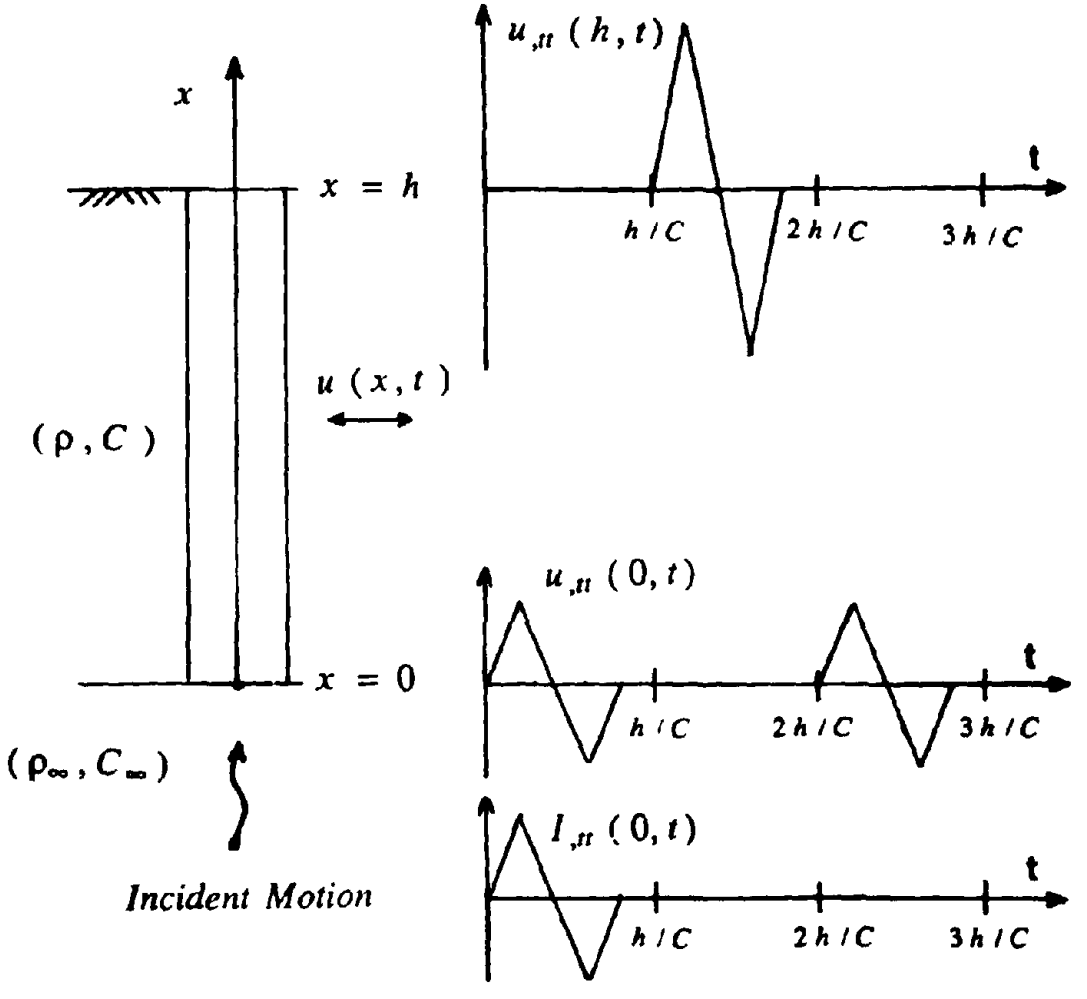

Figure 4.1 Semi-Infinite Layered Soil Profile

4.3.1 *Case 1*: Homogeneous semi-infinite deposit (viz., $\rho_m = \rho$; $C_m = C$): In that case the incident vertically propagating wave arriving at $x = 0$ at time $t = 0$, will reach the free surface $x = h$ at time $t = \frac{h}{C}$, will be reflected back from the free surface with the same shape and sign, and must cross the boundary at $x = 0$ (at times $t \geq \frac{2h}{C}$) without any further modification and continue propagating back towards infinity. The resulting motions are as follows:

- at $x = 0$

$$u(0, t) = I(t) + I(t - \frac{2h}{C}) H(t - \frac{2h}{C}) \tag{15}$$

- at $x = h$

$$u(h, t) = 2I(t - \frac{h}{C}) H(t - \frac{h}{C}) \tag{16}$$

where H is the Heaviside function. This is illustrated in Fig. 4.1. The desired response in the finite soil column can be achieved by prescribing at the base of the soil column either the total motion or the incident part of the motion only, as follows:

- *Prescribed motion (fixed base case)*: In that case the base input motion must be made up of the incident and reflected motions to reproduce the specified site response as

$$u(0, t) = I(t) + I(t - \frac{2h}{C}) H(t - \frac{2h}{C}) \tag{17}$$

The first part of the input corresponding to $I(t)$ in Eq. 17 will propagate towards the surface and reproduce the prescribed surface motion. It will then be reflected back off the free surface towards the fixed base where it will be reflected again with a negative amplitude:

$$-I(t - \frac{2h}{C}) H(t - \frac{2h}{C})$$

This reflected wave is canceled exactly by the second part of the input motion in Eq. 17 thereby preventing any further propagation of waves towards the surface. In other words, the incident wave $I(t)$ produces the surface motion and the reflected wave cancels the reflection from the rigid base.

REMARK: The total motion is the one computed in standard deconvolution procedures implemented in computer programs such as SHAKE (1972).

- *Prescribed traction (non-reflecting case)*: From Eq. 8 the stress in the semi-infinite soil deposit at location $x = 0$ can be expressed directly in terms of the motion at the location and the incident wave motion. Therefore, it suffices to apply at the artificial boundary $x = 0$, the traction:

$$\tau(0, t) = \rho C (2 I_{,t} - u_{,t}) \Big|_{(0,t)} \tag{18}$$

In that case, the incident input motion is absorbed exactly at the base after reflection from the surface. Eq. 18 is the most general boundary condition since it only requires knowledge of the incident motion.

4.3.2 *Case 2*: Non-homogeneous semi-infinite deposit: In that case only the incident motion is known as it arrives at location $x = 0$. In order to compute the site response for this incident motion, accounting for the effects of ensuing reflections (or no reflections if $C_\infty = C$ and $\rho_\infty = \rho$) at the boundary $x = 0$, one must prescribe the input at the base of the finite soil column in terms of prescribed tractions as:

$$\tau(0, t) = \rho_\infty C_\infty (2 I_{,t} - u_{,t}) \Big|_{(0,t)} \tag{19}$$

This will ensure proper simulation of the infinite extend of the soil domain in the downward direction.

4.4 CONCLUSIONS

A rigorous appropriate transmitting boundary condition was developed. The proposed boundary is frequency independent and is local in space and time. It is exact for vertically propagating wave motions and for linear systems only.

4.5 REFERENCES

[1] Schnabel, P. B., Lysmer, J., and Seed, H. B., "SHAKE: A Computer Program for Earthquake Response Analysis of Horizontally Layered Sites", *Report No. EERC 72-12*, University of California, Berkeley, (1972).

SECTION 5
PLASTICITY MODEL FOR FRICTIONAL SOILS

5.1 INTRODUCTION

Considerable attention has been given in the past decade to the development of constitutive equations for soil media, but although many different models have been proposed, there is not yet firm agreement among researchers. Elastic (see e.g., Duncan and Chang, 1970; Coon and Evans, 1971), endochronic (see e.g., Valanis and Read, 1982), and many elastic-plastic models with various degrees of sophistication and/or complexity have been proposed. Elastic-plastic models appear to be the most promising. The most popular and most widely used soil models are Cap models (Roscoe and Burland, 1968; Schofield and Wroth, 1968; DiMaggio and Sandler, 1971; Baladi and Rohani, 1979), based on classical isotropic plasticity theory with associated flow, and are variations and refinements of the basic Cap model pioneered by Drucker, Gibson and Henkel (1955). The most obvious limitations of these Cap models are:

(1) They do not adequately model soil stress-induced anisotropy;

(2) They are not applicable to cyclic loading conditions.

Similar limitations apply to the models presented in (Lade and Duncan, 1975; Nemat-Nasser, 1982). It may be argued that plastic models based on isotropic plastic hardening rules are adequate for situations in which only loading (and moderate unloading) occurs, however it is unlikely that such restrictions can be met at every point in general boundary value problems. In order to account for hysteretic effects, more elaborate plastic models based on a combination of isotropic and kinematic plastic hardening rules have recently been proposed. Some researchers prefer a two-yield surface plasticity (see e.g., Ghaboussi and Nomen, 1982; Mroz and Pietruszcak, 1983; Dafalias, 1987), while others

prefer a multi-yield surface plasticity (see e.g., Mroz, 1967; Prevost, 1977, 1978, 1985). Both theories suffer inherent limitations namely: storage requirements for the multi-surface theory, "a priori" selection of an evolution law for the two-surface theory. This is further discussed in Prevost (1982).

It is the purpose of this section to present a simple plasticity model for soils. The model is applicable to both cohesive and cohesionless soils. The model has been tailored (1) to retain the extreme versatility and accuracy of the simple multi-surface J_2-theory (see e.g., Prevost, 1977, 1978) in describing observed shear nonlinear hysteretic behavior, and shear stress-induced anisotropic effects; and (2) to reflect the strong dependency of the shear dilatancy on the effective stress ratio in both cohesionless (Rowe, 1962; Luong, 1980; Luong and Touati, 1983) and cohesive (Hicker, 1985) soils. Conical yield surfaces are used for that purpose. The theory is applicable to general three-dimensional stress-strain conditions, but its parameters can be derived entirely from the results of conventional triaxial soil tests. As for notation, boldface letters denote vectors, second- and fourth-order tensors in three-dimensions. A superposed dot denotes the (solid) material derivative, the symbol $|\ .\ |$ the norm of a vector or tensor, and the prefix tr the trace. The summation over repeated indices is implied, and the following notation is used: $\mathbf{a} : \mathbf{b} = tr\ \mathbf{a} \cdot \mathbf{b} = a_{ij}\, b_{ji}$. All stresses are *effective stresses*.

5.2 BASIC THEORY

5.2.1 Constitutive Equations:

The constitutive equations are written in the following form:

$$\dot{\boldsymbol{\sigma}} = \mathbf{E} : (\dot{\boldsymbol{\epsilon}} - \dot{\boldsymbol{\epsilon}}^{p}) \tag{1}$$

where $\boldsymbol{\sigma}$ = effective (Cauchy) stress tensor; $\dot{\boldsymbol{\epsilon}}$ = rate of deformation tensor (= symmetric part of the spatial solid velocity gradient); $\dot{\boldsymbol{\epsilon}}^{p}$ = plastic rate of deformation tensor; and a dot denotes the (solid) material derivative. In Eq. 1, $\mathbf{E}$ is the fourth-order isotropic elastic coefficient tensor, *viz.*,

$$E_{ijkl} = (B - \frac{2G}{3}) \delta_{ij} \delta_{kl} + G (\delta_{ik} \delta_{jl} + \delta_{il} \delta_{jk}) \tag{2}$$

where B = elastic bulk modulus; G = elastic shear modulus; and δ_{ij} = Kronecker delta.

5.2.2 Yield Function:

The yield function is selected of the following form:

$$f (\boldsymbol{\sigma}, \boldsymbol{\alpha}, M) = | \mathbf{s} - \bar{p} \boldsymbol{\alpha} | + \sqrt{\frac{2}{3}} M \bar{p} = 0 \tag{3}$$

where

$$| \mathbf{s} - \bar{p} \boldsymbol{\alpha} | = [tr (\mathbf{s} - \bar{p} \boldsymbol{\alpha})^{2}]^{1/2} = [(\mathbf{s} - \bar{p} \boldsymbol{\alpha}) : (\mathbf{s} - \bar{p} \boldsymbol{\alpha})]^{1/2} \tag{4a}$$

$$\mathbf{s} = \boldsymbol{\sigma} - p \boldsymbol{\delta} \qquad \textit{deviatoric stress tensor} \tag{4b}$$

$$p = \frac{1}{3} tr \boldsymbol{\sigma} \qquad \textit{effective mean normal stress} \tag{4c}$$

and $\bar{p} = (p - a)$ with a = attraction ($= c / tan \phi$; c = cohesion; ϕ = friction angle); $\boldsymbol{\alpha}$ = kinematic deviatoric tensor defining the coordinates of the yield surface center in deviatoric stress subspace; M = material parameter. The yield function plots as a conical yield surface in stress space with its apex located along the hydrostatic axis

at the attraction. For cohesionless soils $a = 0$ and the apex of the cone is at the origin. Unless $\alpha = 0$, the axis of the cone does not coincide with the space diagonal. The cross section of the yield surface by any deviatoric plane ($\bar{p}$ = constant) is circular with radius $R = -\sqrt{\frac{2}{3}}\, M\, \bar{p}$. Its center does not generally coincide with the origin but is shifted by the amount $\bar{p}\ \alpha$. This is illustrated by Fig. 5.1 in the principal stress space. The outer normal $\mathbf{Q}$ to the yield surface:

$$\mathbf{Q} = \mathbf{Q}' + Q''\ \delta \tag{5}$$

is computed as follows (from Eq. 3):

$$\mathbf{Q} := \partial_\sigma f = \frac{(\mathbf{s} - \bar{p}\ \alpha)}{|\mathbf{s} - \bar{p}\ \alpha|} + \frac{1}{3}\left[\sqrt{\frac{2}{3}}\, M - \frac{(\mathbf{s} - \bar{p}\ \alpha) : \alpha}{|\mathbf{s} - \bar{p}\ \alpha|}\right]\delta \tag{6}$$

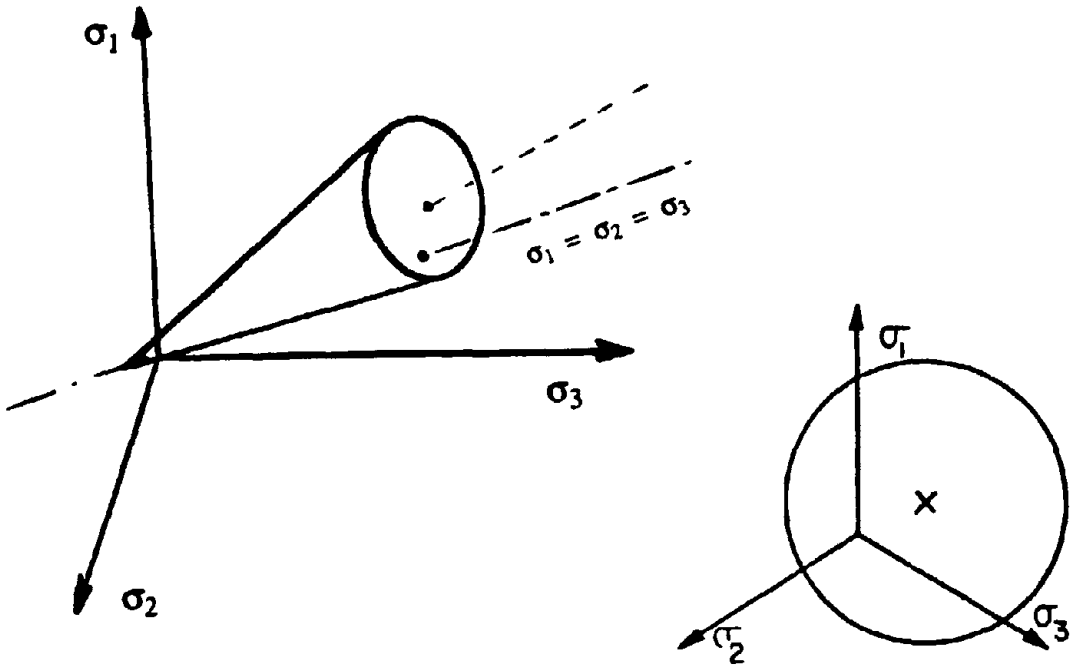

Figure 5.1 Yield Surface in Principal Stress Space

5.2.3 Flow Rule:

The plastic strain rate is defined as follows:

$$\dot{\boldsymbol{\varepsilon}}^{p} = \langle \dot{\lambda} \rangle \mathbf{P} \qquad \textit{where} \qquad \mathbf{P} = \mathbf{P}' + P'' \boldsymbol{\delta} \tag{7}$$

and $\dot{\lambda}$ = plastic loading function. The plastic potential is selected such that the deviatoric plastic flow be associative. However, a non-associative flow rule is used for its dilatational component, and in the following:

$$\mathbf{P}' = \mathbf{Q}' \qquad 3P'' = \frac{(\eta / \bar{\eta})^2 - 1}{(\eta / \eta)^2 + 1} \tag{8}$$

where $\eta = (\frac{3}{2}\mathbf{s} : \mathbf{s})^{1/2} / \bar{p}$ = mobilized stress ratio; and $\bar{\eta}$ = material parameter. When $\eta < \bar{\eta}$, $3P'' < 0$ and plastic compaction takes place, whereas when $\eta > \bar{\eta}$, $3P'' > 0$ and plastic dilation takes place. The case $\eta = \bar{\eta}$ corresponds to no plastic volumetric strains. This is illustrated in Fig. 5.2. In the following, $\bar{\eta} = \bar{\eta}_C$ when $tr\ \mathbf{s}^3 < 0$, and $\bar{\eta} = \bar{\eta}_E$ when $tr\ \mathbf{s}^3 > 0$.

5.2.4 Hardening Rule:

A purely deviatoric kinematic hardening rule is adopted and in the following,

$$\bar{p}\,\dot{\boldsymbol{\alpha}} = \langle \dot{\lambda} \rangle \frac{H'}{\mathbf{Q}' : \boldsymbol{\mu}}\,\boldsymbol{\mu} \tag{9}$$

where H' = plastic modulus; and $\boldsymbol{\mu}$ = (deviatoric) tensor defining the direction of translation. Note that the direction of translation remains arbitrary at this stage, and thus may be selected independently of any formal plasticity constraints.

In order to allow for the adjustment of the plastic hardening rule to any kind of experimental data, for example, data obtained from axial or simple shear soil tests, a collection of nested yield surfaces (Mroz, 1967) is used. The yield surfaces are all similar conical surfaces. Upon contact, the yield surfaces are to be translated by the stress point.

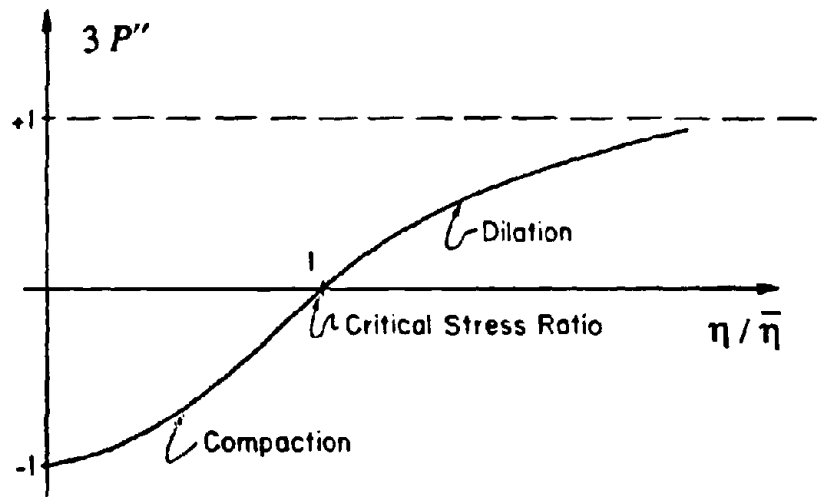

Figure 5.2 Dilatational Plastic Flow

In order to avoid overlappings of the surfaces (which would lead to a non-unique definition of the constitutive theory), the direction of translation μ of the active yield surface is selected such that

$$\mu = \frac{M'}{M} (s - \bar{p}\,\alpha) - (s - \bar{p}\,\alpha') \tag{10}$$

where M' and α' are the plastic parameters associated with the next outer surface ($M' > M$). This is illustrated in Fig. 5.3.

5.2.5 Consistency Condition:

The plastic loading function $\dot{\lambda}$ (Eqs 7 and 9) is determined by the consistency condition which emanates from time differentiation of Eq. 3, viz.,

$$\dot{f} = \mathbf{Q} : \dot{\sigma} - \bar{p}\,\mathbf{Q}' : \dot{\alpha} = 0 \tag{11}$$

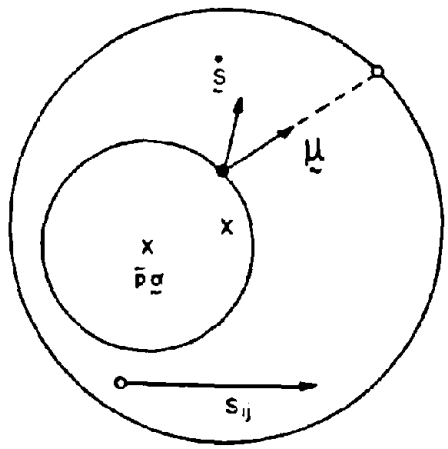

Figure 5.3 Yield Surface Translation by the Stress Point in Deviatoric Stress Space

combining Eqs 1,7 and 9, one finally gets:

$$\dot{\lambda} = \frac{1}{H'} \mathbf{Q} : \dot{\sigma} = \frac{1}{H' + H_0} \mathbf{Q} : \mathbf{E} : \dot{\varepsilon} \tag{12}$$

with

$$H_0 = \mathbf{Q} : \mathbf{E} : \mathbf{P} = 2G + B\,(3P'')\,(3Q'') \tag{13}$$

and H' = plastic modulus.

5.2.6 Remarks:

(i) Under the assumptions spelled above, the elastic-plastic relations write in expanded form as

$$\dot{\sigma} = 2G\,\dot{\varepsilon} + (B - \frac{2G}{3})\,\dot{\varepsilon}_v\,\delta - <\dot{\lambda}>(2G\;Q' + B\;3P''\;\delta) \tag{14}$$

with

$$\dot{\lambda} = \frac{1}{H' + H_o} \left(2G\, \mathbf{Q}' : \dot{\boldsymbol{\varepsilon}} + B\, 3Q''\, \dot{\varepsilon}_v \right) \tag{15}$$

where $\dot{\varepsilon}_v = tr\ \dot{\boldsymbol{\varepsilon}}$. Or equivalently, in terms of deviatoric and dilatational components

$$\dot{\mathbf{s}} = 2G\, \dot{\mathbf{e}} - \langle \dot{\lambda} \rangle 2G\, \mathbf{Q}' \tag{16a}$$

$$\dot{p} = B\, \dot{\varepsilon}_v - \langle \dot{\lambda} \rangle B\, 3P'' \tag{16b}$$

where $\dot{\mathbf{e}} = \dot{\boldsymbol{\varepsilon}} - \frac{1}{3} \dot{\varepsilon}_v\, \boldsymbol{\delta}$ = deviatoric rate of deformation tensor.

(ii) It is assumed that no pure elastic domain exits. The first yield surface is thus chosen as a degenerate yield surface of size zero which coincides with the stress point. The normal associated with that yield surface is assumed to be purely dilatational. (i.e., from Eq. 4, $\mathbf{Q}' = 0$ and $3Q'' = -\sqrt{3}$). The plastic loading function associated with the stress point is defined through

$$\dot{\lambda} = \frac{1}{H' + 3B}\, B\, 3Q''\, \dot{\varepsilon}_v \tag{17}$$

(iii) The dependence of the moduli upon the effective mean normal stress is assumed of the following form

$$G = G_1 \left(\frac{p}{p_1} \right)^n \qquad B = B_1 \left(\frac{p}{p_1} \right)^n \qquad H' = H'_1 \left(\frac{p}{p_1} \right)^n \tag{18}$$

respectively, where n = experimental parameter ($n = 0.5$ for most cohesionless soils, and $n = 1$ for cohesive soils (Richard et al., 1970)); p_1 = reference effective mean normal stress. The assumed dependence of the elastic moduli on the material state renders the material's elasticity (Eq. 1) hypoelastic.

5.3 MODEL PARAMETERS IDENTIFICATION

In addition to the usual state parameters (*i.e.,* mass density, porosity, permeability), the constitutive parameters required to model the behavior of the solid porous soil skeleton are as summarized hereafter:

(i) Elastic Parameters:

- *Shear Modulus:* G
- *Bulk Modulus:* B
- *Power Exponent:* n

(ii) Plastic Parameters:

- *Dilation Parameters:* $\bar{\eta}_C$, $\bar{\eta}_E$
- *Yield Surfaces Parameters:*
  - *Position:* α
  - *Size:* M
  - *Plastic Modulus:* H'

The constitutive parameters required to characterize the behavior of any given soil are to be determined by fitting the model to available experimental soil test data.

The (hypo-)elastic shear G and bulk B moduli (low strain moduli) are best determined through seismic (wave velocity)-type measurements. Their dependence on the mean stress with the power of n (Eq. 18) is empirical in nature, and is suggested by Richard et al. (1970). Correlation formula (relating moduli to initial void ratio, confining stress, overconsolidation ratio, *etc...)* based on the results of resonant column tests are also available (see, *e.g.,* Hardin and Drenevitch (1972)). Typically, $B = 2G / 3$.

All required plastic model parameters can be derived entirely from the results of conventional soil tests (*e.g.,* "triaxial" or simple shear soil tests). In the following, a sys-

tematic calibration procedure of the required plastic parameters is proposed.

REMARKS:

(i) Because $\alpha_{ij} \neq 0$ in general, the yielding of the material is anisotropic. The yield surfaces' initial position is a direct expression of the material "memory" of its past loading history. Since $\boldsymbol{\alpha}$ is a symmetric second-order tensor, it posseses in general three distinct orthogonal principal directions. The material is therefore *orthotropic* in general (it possesses three distinct perpendicular principal axes of anisotropy). If $\boldsymbol{\alpha}$ has two equal principal values, the material is *cross-anisotropic* (or transverse anisotropic), and the material then possesses a principal axis of anisotropy perpendicular to a plane of isotropy. Finally, if the three principal values of $\boldsymbol{\alpha}$ are all equal, the material is *isotropic*.

The initial anisotropy originally develops during the soil deposition and subsequent consolidation which, in most practical cases, occurs under no lateral deformations. In the following, for simplicity, the material is therefore assumed to be initially cross-anisotropic. Further, most conventional soil tests (*e.g.*, "triaxial", simple shear soil tests) require the material to be initially cross-anisotropic. The vertical 1-axis is assumed to coincide with the principal direction of consolidation. The horizontal (2-3)-plane is thus a plane of isotropy and the material's anisotropy initially exhibits rotational symmetry about the vertical 1-axis. In that case, the initial position of the yield surfaces is defined by the sole determination of the parameter α :

$$\alpha = (\alpha_1 - \alpha_3) = 3 \alpha_1 / 2$$

since $\alpha_{ij} = 0$ for $i \neq j$, and

$$\alpha_2 = \alpha_3 = - \alpha_1 / 2 = - \alpha / 3$$

(ii) In general, the model allows different dilation parameters $\bar{\eta}_C$ and $\bar{\eta}_E$ to be associated with each yield surface. However, such a level of sophistication is usually unwarranted because of the rather inaccurate experimental measurements of the detailed volumetric strains observed in conventional soil tests (especially in extension). Therefore, in the following, one averaged value for η_C and η_E is used, and assumed to pertain to all yield surfaces.

5.3.1 "Triaxial" Soil Test:

In this section, attention is restricted to the "triaxial" soil test for which the two effective (lateral) principal stresses are equal, $\sigma_2 = \sigma_3$. In order for the soil specimen to deform in an axisymmetric fashion ($\varepsilon_2 = \varepsilon_3$), the axes of loading must coincide with the principal axes of the anisotropic tensor α, and $\alpha_2 = \alpha_3$. In the following, in order to

follow common usage in soil mechanics, compressive stresses and strains are counted as positive and the discussion is presented in terms of the following stress and strain variables:

$$q = (\sigma_1 - \sigma_3) \qquad p = (\sigma_1 + 2\sigma_3)/3 \tag{19}$$

$$\bar{\varepsilon} = (\varepsilon_1 - \varepsilon_3) \qquad \varepsilon_v = \varepsilon_1 + 2\varepsilon_3 \tag{20}$$

where the reference axes 1 and 3 are assumed to be in the vertical and horizontal directions, respectively. Eq. 3 then simplifies to:

$$f(\sigma, \alpha, M) = |q - \alpha \bar{p}| - M\bar{p} = 0 \qquad viz., \qquad q/\bar{p} = (\alpha \pm M) \tag{21}$$

where $\alpha = (\alpha_1 - \alpha_3) = 3\alpha_1/2$. The trace of the yield surface onto the triaxial (q, p) stress plane consists of two straight lines of slopes $(\alpha + M)$ and $(\alpha - M)$, respectively. The two lines are anchored along the hydrostatic p – axis at location $p = -a$. This is illustrated in Fig. 5.4. In the "triaxial" soil test loading condition, the mobilized stress ratio η is defined as follows:

$$\eta = q/\bar{p} \tag{22}$$

such that $\eta > 0$ in compression tests $(\sigma_1 > \sigma_3)$; and $\eta < 0$ in extension tests $(\sigma_1 < \sigma_3)$. Yielding, accordingly with the proposed model, is therefore directly related to the mobilized stress ratio, since the yield function can be rewritten as (from Eqs 21 and 22):

$$f(\sigma, \alpha, M) = f(\eta, \alpha, M) = \eta - (\alpha \pm M) = 0 \tag{23}$$

The mobilized stress ratio η is related to the mobilized friction angle ϕ commonly used in soil mechanics, *viz.*,

$$\sin\phi = \frac{|(\sigma_1 - \sigma_3)|/2}{a + (\sigma_1 + \sigma_3)/2} \tag{24}$$

by the following relation (combining Eqs 19,22 and 24):

$$\sin\phi = \frac{3\,|\eta|}{6 + \eta} \tag{25}$$

inversely, one can also write (from Eqs 23 and 25):

$$\eta_C = \left(\frac{q}{\bar{p}}\right)_C = + \frac{6\sin\phi_C}{3 - \sin\phi_C} = \alpha + M \qquad \textit{in compression tests} \tag{26a}$$

$$\eta_E = \left(\frac{q}{\bar{p}}\right)_E = - \frac{6\sin\phi_E}{3 + \sin\phi_E} = \alpha - M \qquad \textit{in extension tests} \tag{26b}$$

where ϕ_C and ϕ_E = mobilized friction angles in compression and extension loading conditions, respectively.

Model calibration is to be achieved by matching directly the model equations (Eqs 1-18) with the experimental test data. For that purpose, the following are first derived by direct substitutions of Eqs 19 and 20 into the appropriate expressions:

$$|\,\mathbf{s} - \bar{p}\,\boldsymbol{\alpha}\,| = \sqrt{\frac{2}{3}}\,|\,q - \bar{p}\,\alpha\,| \tag{27}$$

$$(\mathbf{s} - \bar{p}\,\boldsymbol{\alpha}) : \boldsymbol{\alpha} = \frac{2}{3}\,(q - \bar{p}\,\alpha)\,\alpha \tag{28}$$

$$(Q'_1 - Q'_3) = \sqrt{\frac{3}{2}}\,\frac{(q - \bar{p}\,\alpha)}{|\,q - \bar{p}\,\alpha\,|} \tag{29}$$

$$3\,Q'' = \sqrt{\frac{2}{3}}\,\left(M - \frac{(q - \bar{p}\,\alpha)}{|\,q - \bar{p}\,\alpha\,|}\,\alpha\right) \tag{30}$$

$$\begin{aligned} \mathbf{Q} : \dot{\boldsymbol{\sigma}} &= \mathbf{Q}' : \dot{\mathbf{s}} + 3\,Q''\,\dot{p} \\ &= \frac{2}{3}\,(Q'_1 - Q'_3)\,\dot{q} + 3\,Q''\,\dot{p} \\ &= \sqrt{\frac{2}{3}}\,\frac{(q - \bar{p}\,\alpha)}{|\,q - \bar{p}\,\alpha\,|}\,(\dot{q} - \eta\,\dot{p}) \end{aligned} \tag{31}$$

and the stress-strain relations (Eq. 1) simplify to:

$$\frac{\dot{\bar{\varepsilon}}}{\dot{q}} = \frac{1}{2G} + \frac{1}{H'}\left(1 - \eta \dot{p} / \dot{q}\right) \tag{32}$$

$$\frac{\dot{\varepsilon}_v}{\dot{p}} = \frac{1}{B} \pm \frac{1}{H'}\sqrt{\frac{2}{3}}\,\frac{1-(\eta/\bar{\eta})^2}{1+(\eta/\eta)^2}\left(\dot{q}/\dot{p} - \eta\right) \tag{33}$$

for the shear and dilatational components, respectively. In Eq. 33, the plus (+) sign is for compression, and the minus (−) sign for extension loading conditions; $\bar{\eta} = \bar{\eta}_C$ in compression; and $\bar{\eta} = \bar{\eta}_E$ in extension.

Yielding, *i.e.*, plastic flow, occurs on the yield surface f (Eq. 23) with associated plastic parameters (α, M, H') when the mobilized stress ratios $\eta = (\alpha \pm M)$, and when the loading index (Eq. 12) $\dot{\lambda} > 0$, *i.e.*, (from Eqs 12 and 31) when

$$\dot{q} - \eta \dot{p} = \bar{p}\,\dot{\eta} \tag{34}$$

is positive in compression $(\eta = \eta_C = \alpha + M)$, and negative in extension $(\eta = \eta_E = \alpha - M)$, respectively. The plastic modulus H' associated with the yield level defined by the parameters α and M is obtained as follows. Given the shear stress-strain curve (q *vs* $\bar{\varepsilon}$), and the particular stress path (q *vs* p) followed in the test, it is possible to backfigure the functional dependence of the plastic modulus H' on the mobilized stress ratio η, *i.e.*, $H' = H'(\eta)$ in both compresssion and extension loading conditions by inverting Eq. 32 as:

$$H' = \frac{2GH}{2G - H}\left(1 - \eta / s\right) \tag{35}$$

where $s = \dot{q} / \dot{p}$ = slope of the effective stress path followed in the (q, p) plane; and $H = \dot{q} / \dot{\bar{\varepsilon}}$ = slope of the shear stress-strain curve. Clearly, for monotonic stress paths:

$$H = H(q,p) = H(\eta) \qquad \text{and} \qquad s = s(q,p) = s(\eta) \tag{36}$$

and therefore, the variation of the plastic modulus H' with the mobilized stress ratio η can be computed from the test results. This is illustrated in Fig. 5.4.

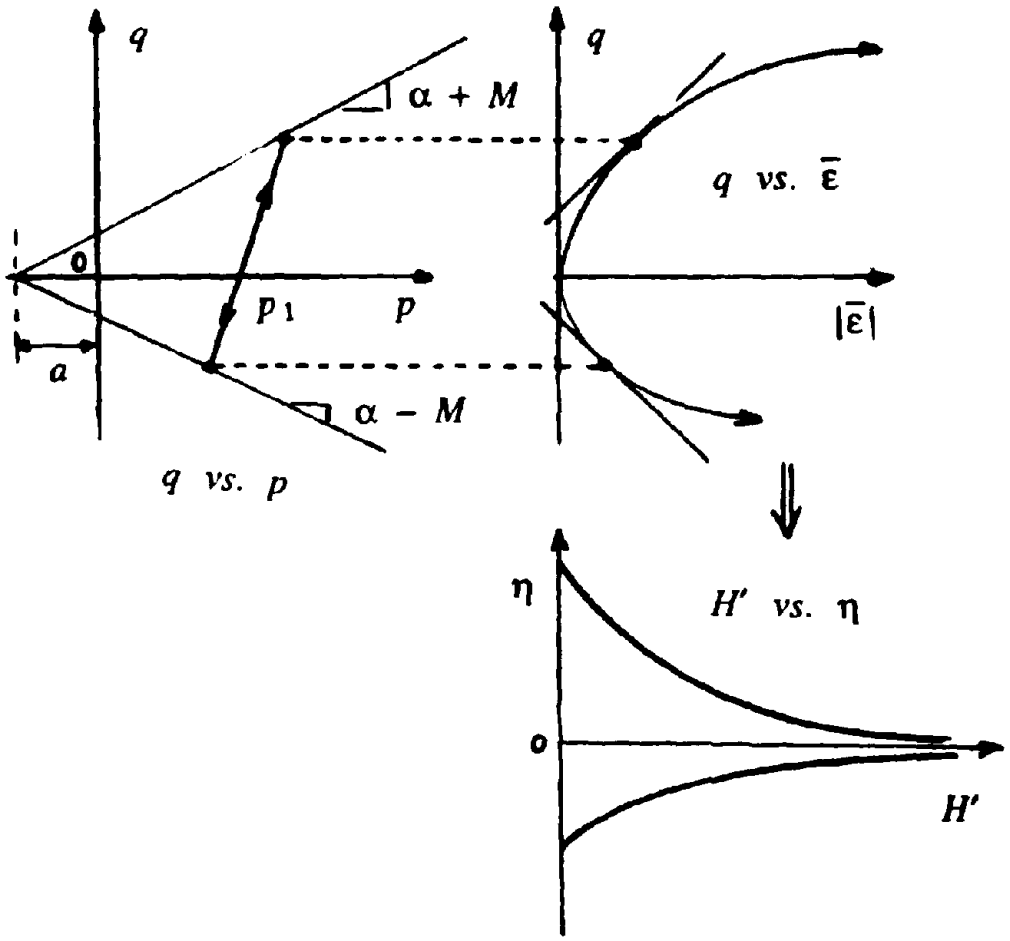

Figure 5.4 Model Interpretation - Triaxial Soil Test

The proposed constitutive model *approximates* the (measured) smooth functional dependence of the plastic modulus H' on the stress ratio η, by requiring that H' be constant between each selected yield levels. Evidently, the degree of accuracy achieved by such a representation of the experimental curve $H' = H'(\eta)$ is directly dependent upon the number of selected yield levels. For a given H', the associated yield parameters (α, M), are computed from the corresponding mobilized stress ratios $\eta = \eta_C$ in compression ($\dot{\eta} > 0$), and $\eta = \eta_E$ in extension ($\dot{\eta} < 0$), respectively, as (from Eq. 26):

$$\alpha = (\eta_C + \eta_E)/2 \qquad M = (\eta_C - \eta_E)/2 \tag{37}$$

Therefore, once the number of yield levels has been selected, the identification of the plastic parameters (α, M, H') associated with each yield level is straightforward and can easily be automated.

The dilation parameters $\bar{\eta}_C$ and $\bar{\eta}_E$ are obtained from Eq. 33, *viz.*,

$$\dot{p} = B\,\dot{\varepsilon}_v \qquad \textit{when} \quad \eta = \bar{\eta} \tag{38}$$

In undrained tests (constant volume tests), they correspond to the effective stress ratios at which the effective stress path changes concavity (*i.e.*, $s = \dot{q}/\dot{p} = \infty$). In drained tests, they are close to the effective stress ratios at which the material experiences maximum compaction. The dilation parameters are related to the dilatancy angles $\bar{\phi}_C$ and $\bar{\phi}_E$ commonly used in soil mechanics as (from Eq. 26)

$$\bar{\eta}_C = +\frac{6\sin\bar{\phi}_C}{3 - \sin\phi_C} \qquad \bar{\eta}_E = -\frac{6\sin\bar{\phi}_E}{3 + \sin\phi_E} \tag{39}$$

Typically, (see *e.g.*, Rowe (1962)) $\bar{\phi}_C = \bar{\phi}_E = 30$ *degrees* (which in cohesionless soils corresponds to $\frac{\sigma_I}{\sigma_{III}} = 3$), and (from Eq. 39) $\bar{\eta}_C = 1.2$; $\bar{\eta}_E = -0.86$.

REMARKS:

(i) The plastic bulk modulus H', associated with the stress point is determined by measuring the slopes $\dot{p} / \dot{\varepsilon}_v$ of small hydrostatic load-unload cycles at selected hydrostatic pressures, viz.,

$$\frac{\dot{p}}{\dot{\varepsilon}_v} = B \frac{H'}{H' + 3B} \qquad (Load)$$

$$\frac{\dot{p}}{\dot{\varepsilon}_v} = B \qquad (Unload)$$

Typically, $H' = 3B$.

(ii) The dependence of the moduli on the mean effective stress (Eq. 18) is taken into account by simply referring all moduli in Eqs 32, 33 and 35 to the reference mean stress p_1 as:

$$G_1 = G \left(\frac{p_1}{p} \right)^n \qquad B_1 = B \left(\frac{p_1}{p} \right)^n \qquad H_1 = H \left(\frac{p_1}{p} \right)^n$$

and finally,

$$H'_1 = H' \left(\frac{p_1}{p} \right)^n$$

(iii) On the last outermost yield surface, $H' = 0$, and the last yield surface therefore plays the role of a failure surface. If the mobilized friction angle at failure is to be the same in compression and extension loading conditions, *viz.*,

$$\phi_C{}^f = \phi_E{}^f$$

then (from Eq. 25):

$$\eta_E{}^f = - \frac{3 \eta_C{}^f}{3 + \eta_C{}^f}$$

and (from Eq. 37)

$$\alpha^f = \frac{1}{2} \frac{(\eta_C{}^f)^2}{3 + \eta_C{}^f} \qquad M^f = \frac{1}{2} \eta_C{}^f \frac{6 + \eta_C{}^f}{3 + \eta_C{}^f}$$

where (from Eq. 26)

$$\eta_C{}^f = \frac{6 \sin \phi_C{}^f}{3 - \sin \phi_C{}^f}$$

(iv) For pure shear loading conditions *(i.e.,* $\dot{p} = 0$), Eq. 35 reduces to

$$H' = \frac{2\,G\,H}{2\,G - H}$$

and the approximation procedure *(viz.* H' = constant between each selected yield levels) reduces to a piecewise linearization of the shear stress-strain curves. The various yield levels are then simply identified by the condition that the slopes $H = \dot{q} / \dot{\bar{\epsilon}}$ be the same in compression and extension tests (see *e.g.,* Prevost (1977)).

5.4 REFERENCES

1. Baladi, G.Y. and Rohani, B., "Elastic-Plastic Model for Saturated Sand," *J. Geotech. Eng. Div.*, ASCE, Vol. 105, No. GT4, April 1979, pp. 465-480.
2. Coon, M.D. and Evans, R.J., "Recoverable Deformations of Cohesionless Soils," *J. Soil Mech. Found. Eng.*, ASCE, Vol. 97, No. SM2, Feb. 1971, pp. 375-390.
3. Dafalias, Y.F., "Bounding Surface Plasticity: Mathematical Foundation and Hypoplasticity," *J. Eng. Mech.*, ASCE, Vol. 112, No. 9, 1986, pp. 966-987.
4. DiMaggio, F.L. and Sandler, I.S., "Material Models for Granular Soils," *J. Eng. Mech. Div.*, ASCE, Vol. 97, No. EM3, June 1971, pp. 935-950.
5. Drucker, D.C., Gibson, R.E., and Henkel, D.J., "Soil Mechanics and Work-Hardening Theories of Plasticity," *Proceedings*, ASCE, Vol. 81, 1955, pp. 1-14, also *Transactions*, ASCE, Vol. 122, 1957, pp. 338-346.
6. Duncan, J.M., and Chang, C.Y., "Nonlinear Analysis of Stress and Strain in Soils," *J. Soil Mech. Found. Eng.*, ASCE, Vol. 96, No. SM5, Sept. 1970, pp. 1629-1653.
7. Ghaboussi, J. and Momen, H., "Modelling and Analysis of Cyclic Behavior of Sands," *Soil Mechanics - Transient and Cyclic Loads*, Eds. G.N. Pande and O.C. Zienkiewicz, Wiley, 1982, pp. 313-342.
8. Hicher, P.Y., "Comportement Mecanique des argiles saturees sur divers chemins de sollicitations monotones et cycliques. Application a une modelisation elastoplastique et viscoplastique," These de Doctorat d'Etat, Universite Paris 6, Paris, France, December 1985.
9. Hardin, B.O. and Drnevich, V.P., "Shear Modulus and Damping in Soils: Design Equations and Curves," *J. Soil Mech. Found. Div.*, ASCE, Vol. 98, No. SM7, 1972, pp. 667-692.
10. Lade, P.V. and Duncan, J.M., "Elastoplastic Stress-Strain Theory for Cohesionless Soil," *J. Geotech. Eng. Div.*, ASCE, Vol. 101, 1975, pp. 1037-1053.
11. Luoung, M.P., "Phenomenes Cycliques dans les Sols Pulverulents," *Revue Francaise de Geotechnique*, Vol. 10, 1980, pp. 39-53.
12. Luong, M.P. and Touati, A., "Sols Grenus sous Fortes Constsraintes," *Revue Francaise de Geotechnique*, No. 23, 1983, pp. 51-63.
13. Mroz, Z., "On the Description of Anisotropic Work-Hardening," *J. Mech. Phys. Solids*, Vol. 15, 1967, pp. 163-175.
14. Mroz, Z. and Pietruszak, S.T., "A Constitutive Model for Sand with Anisotropic Hardening Rule," *Int. J. Num. Meth. Geom.*, Vol. 7, 1983, pp. 305-320.
15. Nemat-Nasser, S., "On Dynamic and Static Behavior of Granular Materials," *Soil Mechanics-Transient and Cyclic Loads*, Eds. G.N. Pande and O.C. Zienkiewicz, Wiley, 1982, pp. 439-458.
16. Prevost, J.H., "A Simple Plasticity Theory for Frictional Cohesionless Soils," *Soil Dynamics and Earthquake Engineering*, Vol. 4, No. 1, 1985, pp. 9-17.
17. Prevost, J.H., "Two-Surface vs. Multi-Surface Plasticity Theories," *Int. J. Num. Meth. Geom.*, Vol. 6, 1982, pp. 323-338.
18. Prevost, J.H., "Anisotropic Undrained Stress-Strain Behavior of Clays," *J. Geotech. Eng. Div.*, ASCE, Vol. 104, No. GT8, 1978, pp. 1075-1090.
19. Prevost, J.H., "Mathematical Modeling of Monotonic and Cyclic Undrained Clay Behavior," *Int. J. Num. Meth. Geom.*, Vol. 1, No. 2, 1977, pp. 195-216.

20. Richard, R.E., Woods, R.D. and Hall, J.R., *Vibrations of Soils and Foundations,* Prentice-hall, N.J., 1970.

21. Roscoe, K.H. and Burland, J.B., "On the Generalized Stress-Strain Behavior of Wet Clay," *Engineering Plasticity,* J. Heyman and F. Leckie, eds., Cambridge University Press, Cambridge, England, 1968, pp. 535-609.

22. Rowe, P.W., "The Stress-Dilatancy Relation for Static Equilibrium of an Assembly of Particles in Contact," *Proc. Roy. Soc.,* Vol. A269, 1962, pp. 500-527.

23. Schofield, A.N. and Wroth, C.P., *Critical State Soil Mechanics,* McGraw Hill, Inc., London, England, 1968.

24. Valanis, K.C. and Read, H.J.E., "A New Endochronic Plasticity Model for Soils," *Soil Mechanics-Transient and Cyclic Loads,* Eds. G.N. Pande and O.C. Zienkiewicz, Wiley, 1982, pp. 375-417.

SECTION 6
SHEAR STRESS-STRAIN CURVE GENERATION FROM SIMPLE MATERIAL PARAMETERS

6.1 INTRODUCTION

The calibration of elaborate constitutive soil models, especially those using multiple yield levels (see e.g., Mroz (1967); Prevost (1977, 1985)), require that stress-strain curves (typically obtained from triaxial or simple shear soil tests) be available. However, budget constraints often prevent detailed laboratory tests to be conducted on every soil type present at a given site. Further, usual parcity of field information, randomness and spatial variability of natural deposits require in every design situation that parametric studies and/or Monte Carlo type simulations be conducted. Therefore, generation of the stress-strain curves required for the analysis, from limited field information, is a common and significant problem. In this section attention is focused on shear stress-strain curve generation.

Minimum information for the generation of the curve requires knowledge of (1) the initial gradient, and (2) the stress and strain levels at failure. The initial gradient, G_o, is usually available from seismic type measurements (see e.g., Richard et al. (1970)). (See Fig. 6.1.) The maximum shear stress at failure, τ_{max}, is commonly determined through correlations with in-situ test results like the SPT and/or the cone penetration test (see e.g., Das (1985) for a recent survey of available correlation formula). The maximum shear strain γ_{max} at failure can also be estimated. Therefore, the problem to be addressed is that of finding a functional relationship between the shear stress τ and the shear strain γ, $\tau = \tau(\gamma)$, such that:

- at the origin:

1) $\tau|_{\gamma=0} = 0$

2) $\frac{\partial \tau}{\partial \gamma}|_{\gamma=0} = G_o$

- at failure:

3) $\tau|_{\gamma=\gamma_{max}} = \tau_{max}$

4) $\frac{\partial \tau}{\partial \gamma}|_{\gamma=\gamma_{max}} = 0$

- between the origin and failure:

5) $\frac{\partial \tau}{\partial \gamma} > 0$ and $\frac{\partial^2 \tau}{\partial \gamma^2} < 0 \qquad 0 \leq \gamma < \gamma_{max}$

Conditions (1) through (4) define two points through which the curve must pass with prescribed gradients. Condition (5) merely states that the curve must be smooth without points of inflection.

The best known and most widely used function is hyperbolic (Kondner (1963); Hardin and Drnevich (1972)). The function is simple but, as shown hereafter, far from ideal since it is not able to model failure accurately (conditions 3 and 4). Therefore, a modified hyperbolic function including a power term is proposed in the following. This function is shown to offer great versatility for modeling stress-strain behavior in both monotonic and cyclic loading conditions; at both low and high strain levels.

It is convenient to non-dimensionalize the stress-strain relation. This is achieved by normalizing the stress as $y = \tau/(G_o\gamma_1)$ and the strain as $x = \gamma/\gamma_1$ where γ_1 is a specific strain value. (See Fig. 6.1.) The shear stress-strain relation is then expressed in terms of the dimensionless quantities, x and y as $y = y(x)$, and

$$\frac{\partial \tau}{\partial \gamma} = G_o \frac{\partial y}{\partial x} \qquad \frac{\partial^2 \tau}{\partial \gamma^2} = \frac{G_o}{\gamma_1} \frac{\partial^2 y}{\partial x^2}. \tag{1}$$

In terms of the quantities x and y, the desirable properties of the normalized stress-strain curve parallel the restrictions stated previously. Specifically, the normalized curve must begin at the origin with an initial slope equal to 1; have a positive slope and negative curvature until the failure point at which the slope must equal 0.

6.2 HYPERBOLIC FUNCTION

The basic equation has the form

$$\tau = \tau_{max}\frac{\gamma}{\gamma_r + \gamma} \tag{2}$$

where $\gamma_r = \tau_{max}/G_o$ is the reference strain. (See e.g., Das (1983).) Through the normalization procedure previously described with $\gamma_1 = \gamma_r$, the hyperbolic function takes the following form:

$$y = \frac{x}{1 + x}, \tag{3}$$

where $y = \tau/(G_o\gamma_r)$ and $x = \gamma/\gamma_r$. The slope and curvature are given by

$$\frac{\partial y}{\partial x} = \frac{1}{(1 + x)^2} \tag{4}$$

and

$$\frac{\partial^2 y}{\partial x^2} = -\frac{2}{(1 + x)^3} \tag{5}$$

respectively. Examining the functional forms, one sees that the requirements (1), (2), and (5), viz., $y|_{x=0} = 0$; $\frac{\partial y}{\partial x}|_{x=0} = 1$; $\frac{\partial y}{\partial x} > 0$ and $\frac{\partial^2 y}{\partial x^2} < 0$ for any x are satisfied. However, the requirements (3) and (4), that the curve must pass through a failure point with zero slope cannot be met (unless $\gamma_{max} = \infty$). Therefore, although the hyperbolic function is a simple method of curve generation which is easily fitted to the initial conditions, it cannot model failure accurately.

6.3 MODIFIED HYPERBOLIC FUNCTION

Introduced as an alternative to the hyperbolic relation for the purpose of curve generation, the modified hyperbolic function has the following form:

$$\tau = \tau_1 \frac{\gamma}{\tau_1/G_o + \gamma} - \tau_1 \frac{\tau_1/G_o}{(\tau_1/G_o + \gamma_{max})^2} \frac{1}{\gamma_{max}^m} \frac{\gamma^{m+1}}{(m+1)} \tag{6}$$

where τ_1 and m are real and positive parameters. The equation is normalized using $\gamma_1 = \gamma_{max}$. By letting $y_1 = \tau_1/(G_o\gamma_{max})$, and $y = \tau/(G_o\gamma_{max})$ and $x = \gamma/\gamma_{max}$ as before, the equation can be expressed as

$$y = y_1 \frac{x}{y_1 + x} - \frac{y_1^2}{(y_1+1)^2} \frac{x^{m+1}}{(m+1)}. \tag{7}$$

Differentiation results in the following expressions for the slope and curvature:

$$\frac{\partial y}{\partial x} = \frac{y_1^2}{(y_1+x)^2} - \frac{y_1^2}{(y_1+1)^2} x^m \tag{8}$$

and

$$\frac{\partial^2 y}{\partial x^2} = -\frac{2y_1^2}{(y_1+x)^3} - \frac{y_1^2}{(y_1+1)^2} m x^{m-1}. \tag{9}$$

Considering the restrictions on the functional form of the normalized equation, we find the $_{,x=0} = 0$, $\frac{\partial y}{\partial x}|_{x=0} = 1$, $\frac{\partial y}{\partial x} > 0$ for $0 \le x < 1$, $\frac{\partial^2 y}{\partial x^2} < 0$ for $0 \le x < 1$, and $\frac{\partial y}{\partial x}|_{x=1} = 0$ are all satisfied. The parameter y_1 is determined by requiring that $y|_{x=1} = y_{max}$ where $y_{max} = \tau_{max}/(G_o\gamma_{max}) = \gamma_r/\gamma_{max}$. This results in

$$y_{max} = \frac{y_1}{y_1+1} - \frac{y_1^2}{(y_1+1)^2} \frac{1}{(m+1)}. \tag{10}$$

Rearranging in order to solve for y_1 yields

$$y_1^2(y_{max} - \frac{m}{m+1}) + 2y_1(y_{max} - \frac{1}{2}) + y_{max} = 0. \tag{11}$$

Requiring the roots to be real results in the inequality

$$m \ge 4y_{max} - 1. \tag{12}$$

Solving for a positive y_1 by taking the appropriate square root,

$$y_1 = \frac{y_{max} - \frac{1}{2} + \sqrt{\frac{1}{4} - y_{max}/(m+1)}}{m/(m+1) - y_{max}}. \tag{13}$$

Considering the sign of the numerator and the denominator in turn over the subintervals of y to guarantee a positive y_1, it can be shown that

- when $0 < y_{max} = \gamma_r/\gamma_{max} \leq \frac{1}{4}$ $\quad m > 0$
- when $\frac{1}{4} < y_{max} = \gamma_r/\gamma_{max} < \frac{1}{2}$ $\quad m \geq 4y_{max} - 1$
- when $\frac{1}{2} \leq y_{max} = \gamma_r/\gamma_{max} < 1$ $\quad m > y_{max}/(1 - y_{max})$.

Satisfying these conditions will ensure that $y|_{x=1} = y_{max} = \gamma_r/\gamma_{max}$. Therefore, all necessary conditions on the functional relationship can be satisfied with the modified hyperbolic function. Further examination using a variety of values for the parameter m shows that m has no significant effect on the characteristics of the shear stress-strain curve. Thus the parameter m can be selected as

$$m = y_{max}/(1 - y_{max}) \qquad \text{when} \quad 0 < y_{max} = \gamma_r/\gamma_{max} < \tfrac{1}{2}$$

and

$$m = 1.1\{y_{max}/(1 - y_{max})\} \qquad \text{when} \quad \tfrac{1}{2} \leq y_{max} = \gamma_r/\gamma_{max} < 1$$

which satisfy the restrictions on m in each subinterval.

Fig. 6.2 shows the stress-strain curves generated for various values of the quantity $\gamma_r/\gamma_{max} = \tau_{max}/G_o\gamma_{max}$. Low values of γ_r/γ_{max} result in highly nonlinear curves. The degree of nonlinearity decreases as γ_r/γ_{max} increases until $\gamma_r/\gamma_{max} = 1.0$, which corresponds to a linear stress-strain relation. Normally, γ_r/γ_{max} is to be selected such that the generated stress-strain curve matches experimental test data. Fig. 6.3 shows the variation of the secant modulus $G = \tau/\gamma$ with the strain level γ for various γ_r/γ_{max} as dimensionless plots G/G_o versus γ/γ_{max} (Fig. 6.3a) and $G/(\tau_{max}/\gamma_{max})$ versus γ/γ_{max} (Fig. 6.3b). Shear moduli variations for sands and clays are usually presented in the forms of Fig. 6.3a and 6.3b, respectively. Clearly, the curves shown in Fig. 6.3 span all known soil test data.

6.4 EQUIVALENT VISCOUS DAMPING

The material behavior is assumed to be nonlinear and hysteretic. Hysteresis loops are constructed from the monotonic shear stress-strain curve by using the Masing Rule (Masing (1926)). The shear stress-strain curve then plays the role of the backbone or skeleton curve. An equivalent viscous damping, ξ_1, for the hysteretic material can be computed as (see e.g., Jacobsen (1958)):

$$\xi_1 = \frac{1}{4\pi}\frac{\Delta W}{W_1} \tag{14}$$

where ΔW is the frictional work area, i.e., the area enclosed by the hysteresis loop, and W_1 is defined as the work area under the corresponding backbone stress-strain curve as illustrated in Fig. 4,

$$W_1 = \int_0^{\gamma} \tau d\gamma. \tag{15}$$

Let W_2 denote the work area under the secant line as illustrated in Fig. 4, viz.,

$$W_2 = \frac{1}{2}\tau\gamma. \tag{16}$$

Using these definitions, the expression for equivalent viscous damping becomes:

$$\xi_1 = \frac{2}{\pi}(1 - \frac{W_2}{W_1}). \tag{17}$$

Another expression for an equivalent viscous damping is often used as:

$$\xi_2 = \frac{1}{4\pi}\frac{\Delta W}{W_2} = \frac{2}{\pi}(\frac{W_1}{W_2} - 1). \tag{18}$$

Conveniently, ξ_1 and ξ_2 are related through the equation (from Eqs. 17 and 18)

$$\xi_2 = \frac{\xi_1}{1 - \frac{\pi}{2}\xi_1}. \tag{19}$$

It can be shown that $1 \leq W_1/W_2 \leq 2$. Therefore, as W_1/W_2 approaches its maximum value of 2, ξ_1 is bounded by 32% and ξ_2 by 64%.

Using the relations $x = \gamma/\gamma_1$ and $y = \tau/(G_o\gamma_1)$, W_1 and W_2 can be expressed in terms of the normalized quantities x and y as:

$$W_1 = G_o\gamma_1^2 \int_0^x y dx \tag{20}$$

and

$$W_2 = \frac{1}{2} G_o \gamma_1^2 y x. \tag{21}$$

Specifically, for the curve generated with the modified hyperbolic equation, it is found that

$$W_1 = G_o \gamma_1^2 \{ y_1 x - y_1^2 \ln(\frac{y_1 + x}{y_1}) - \frac{y_1^2}{(y_1 + 1)^2} \frac{x^{m+2}}{(m+1)(m+2)} \} \tag{22}$$

and

$$W_2 = \frac{1}{2} G_o \gamma_1^2 \{ y_1 \frac{x^2}{y_1 + x} - \frac{y_1^2}{(y_1 + 1)^2} \frac{x^{m+2}}{(m+1)} \} \tag{23}$$

when $x \leq 1$, and

$$W_1 = W_1|_{x=1} + y_{max}(x - 1) \tag{24}$$

and

$$W_2 = \frac{1}{2} y_{max} x \tag{25}$$

when $x > 1$. Fig. 6.5 shows variations of damping ratios with strain levels for various γ_r/γ_{max}. Again, the curves shown in Fig. 6.5 clearly span all known soil test data.

6.5 CONCLUSIONS

Two equations for curve generation have been examined. The popular hyperbolic function has been shown to be easily fitted to the initial conditions but not able to model failure accurately. A modified hyperbolic function including a power term was proposed. This function has been shown to offer great versatility and accuracy in modeling shear stress-strain behavior in both monotonic and cyclic conditions; at both low and high strain levels.

6.6 REFERENCES

1. Das, Braja M., *Fundamentals of Soil Dynamics*, Elsevier Science Publishing Co., Inc., 1983.
2. Das, Braja M., *Principles of Geotechnical Engineering*, PWS Publishers, 1985.
3. Hardin, B. O., and Drnevich, V.P., "Shear Modulus and Damping in Soils: Design Equations and Curves," *Journal of the Soil Mechanics and Foundations Division, ASCE*, Vol. 98, No. SM7, 1972, pp. 667-692.
4. Kondner, R. L., "Hyperbolic Stress-Strain Response: Cohesive Soils," *J. Soil Mech. Found. Div., ASCE*, Vol. 89, No. SM1, 1963, pp. 115-143.
5. Masing, G., "Eigenspannungen und verfestigung beim Messing," *Proc. Second Internatl. Congr. App. Mechs.*, Zurich, 1926.
6. Mróz, Z., "On the Description of Anisotropic Work Hardening," *J. Mech. Phys. solids*, Vol. 15, 1967, pp. 163-175.
7. Prévost, J. H., "Numerical Modeling of Monotonic and Cyclic Undrained Clay Behavior," *Int. J. Num. Meth. Geom.*, Vol. 1, No. 2, 1977, pp. 195-216.
8. Prévost, J. H., "A Simple Plasticity Theory for Frictional Cohesionless Soils," *Soil Dyn. Earthq. Eng.*, Vol. 4, No. 1, 1985, pp. 9-17.
9. Richart, Jr., F. E., Woods, R. D., and Hall, Jr., J. R., *Vibrations of Soils and Foundations*, Prentice-Hall, Inc., 1970.

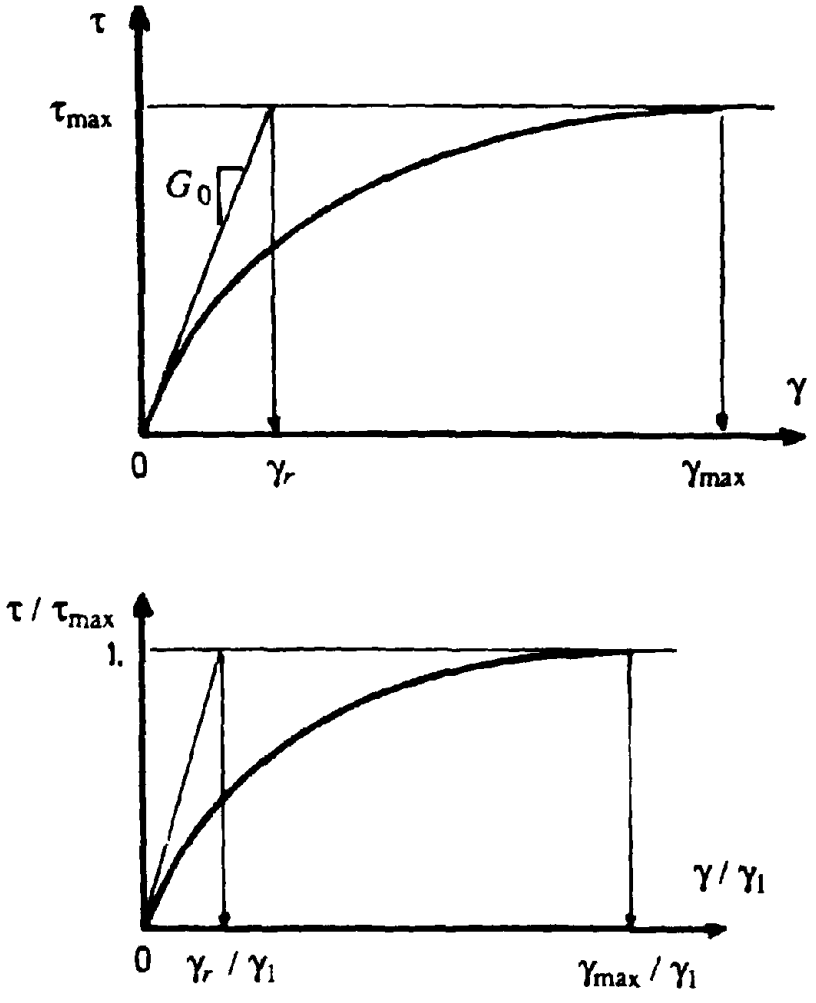

Figure 6.1 Shear Stress-Strain Curve - Notation Definition

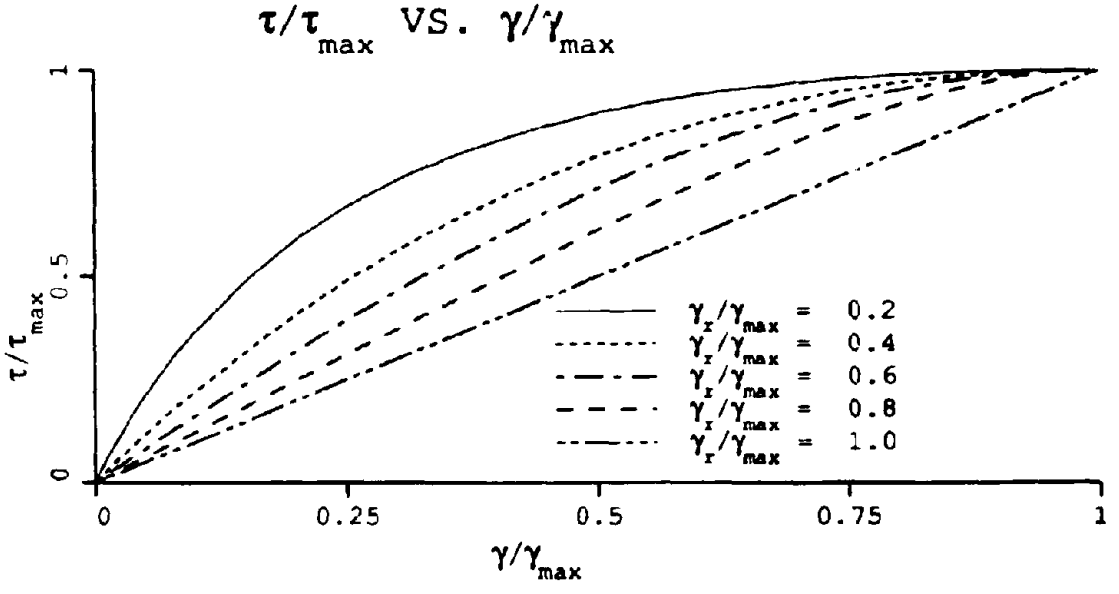

Figure 6.2 Generated Shear Stress-Strain Curves

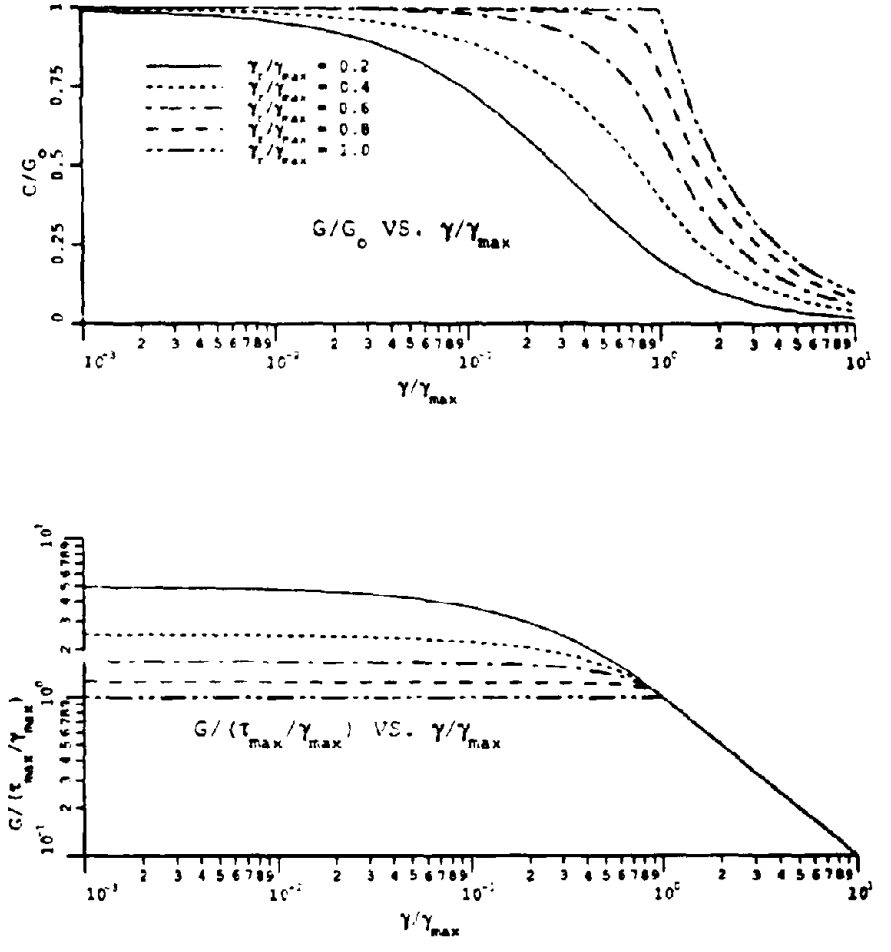

Figure 6.3 Secant Modulus vs. Shear Strain Level

(a) G / G_0 *vs* γ / γ_{max}

(b) $G / (\tau_{max} / \gamma_{max})$ *vs* γ / γ_{max}

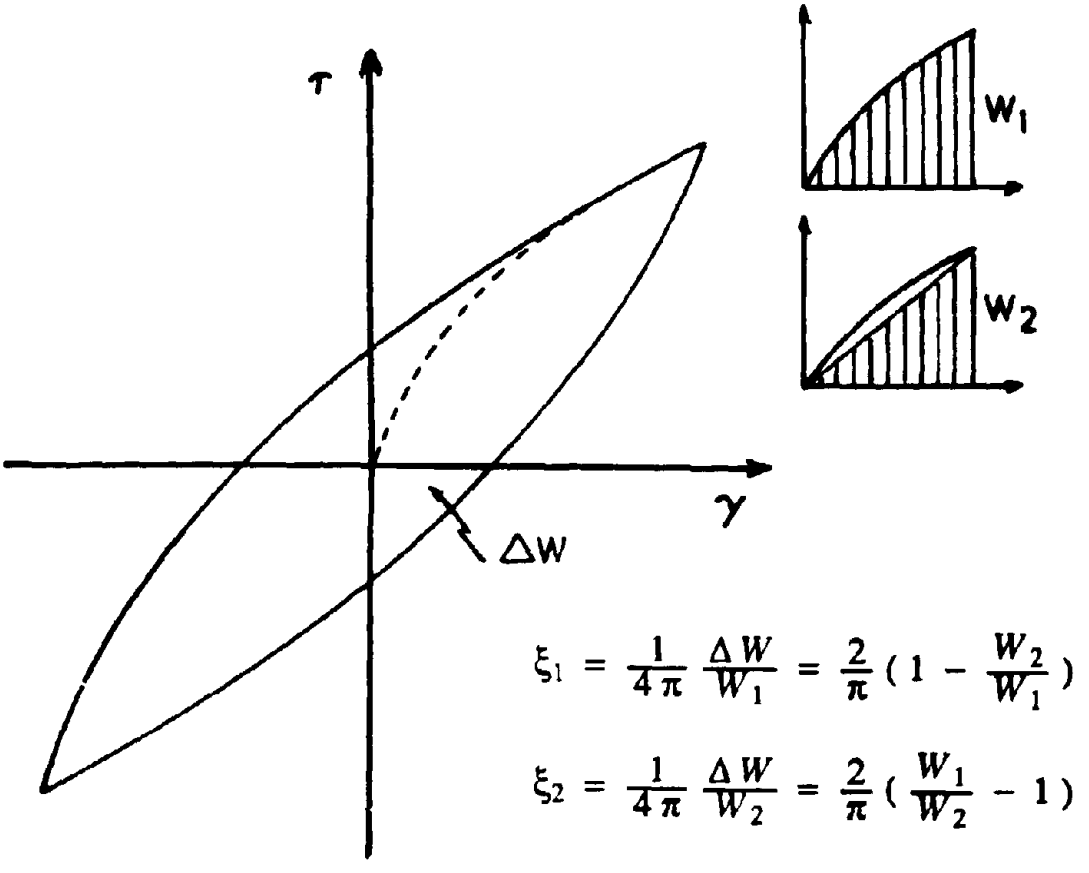

$$\xi_1 = \frac{1}{4\pi}\frac{\Delta W}{W_1} = \frac{2}{\pi}\left(1 - \frac{W_2}{W_1}\right)$$

$$\xi_2 = \frac{1}{4\pi}\frac{\Delta W}{W_2} = \frac{2}{\pi}\left(\frac{W_1}{W_2} - 1\right)$$

Figure 6.4 Hysteresis Loops - Equivalent Viscous Damping Definition

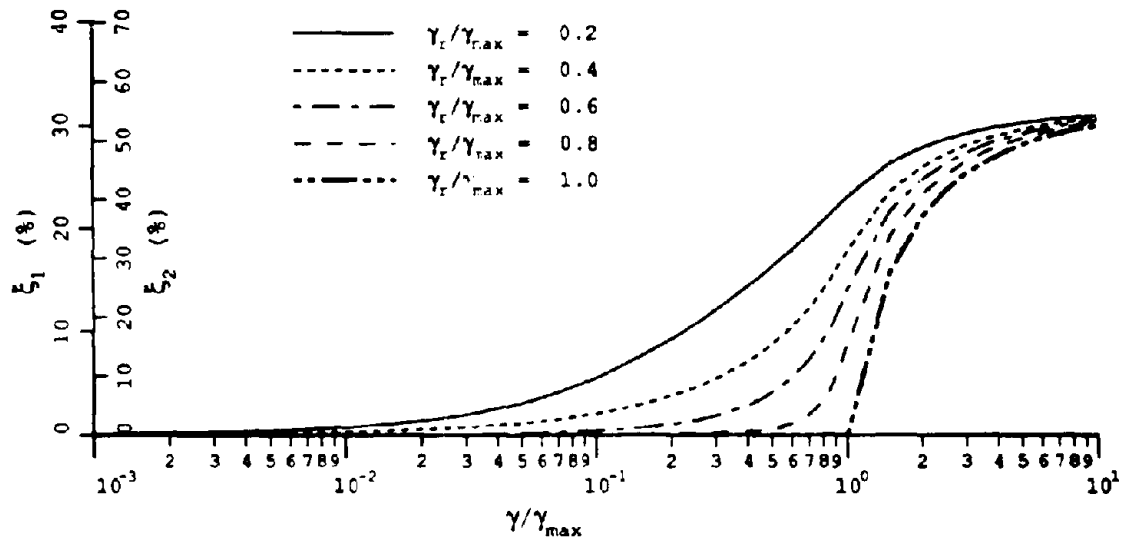

Figure 6.5 Equivalent Viscous Damping vs. Shear Strain Level

SECTION 7

INTEGRATION ALGORITHMS

FOR ELASTIC-PLASTIC CONSTITUTIVE RELATIONS

7.1 INTRODUCTION

Plasticity theory has recently gained widespread acceptance in large-scale numerical simulations of practical geotechnical engineering problems, due to its extreme versatility and accuracy in modeling real engineering materials behavior. Building upon the pioneering works of Drucker and Prager (1952) on soil plasticity, the modern trend has been toward the development of more and more elaborate and complicated elastoplastic constitutive models which resemble the behavior of real engineering materials more closely.

The numerical solution of elastic-plastic boundary value problems is based on an iterative solution of the discretized momentum balance equations. Typically, for every load/time step, solution involves the following steps: Given a converged configuration at step n:

(i) The discretized momentum equations are used to compute a new configuration for step $(n+1)$ via an incremental motion which is used to compute at every stress point incremental strains $\Delta\varepsilon$;

(ii) At every stress point, for the *given* incremental strains $\Delta\varepsilon$, new values of the state variables (σ_{n+1}, S_{n+1}) and ε^p_{n+1} are obtained by integration of the local constitutive equations;

(iii) From the new computed stresses, balance of momentum is checked and if violated iterations are performed by returning to step (i).

In this section, attention is focused on step (ii) which may be regarded as the central problem of computational plasticity since it is the main role played by the constitutive equations in the computations. In finite difference / finite element computer codes the

elastoplastic constitutive equations are usually incorporated through a separate set of constitutive subroutines. The purpose of these subroutines is the integration of the elastic-plastic constitutive equations. That is, at every stress point, given a deformation history, the role of the constitutive-equation subroutine is to return the corresponding stress history. Exact analytical solutions for the elastic-plastic evolution problem are available only for the simplest elastic-plastic models. The first exact solution was obtained by Krieg and Krieg (1977) for the case of the isotropic elastic-perfectly plastic von Mises model. Later, Yoder and Whirley (1984) extended the solution to apply to the von Mises model with arbitrary combination of kinematic and isotropic hardening. Recently, Loret and Prevost (1986) developed an exact solution for the isotropic Drucker-Prager model with linear hardening and arbitrary degree of nonassociativity. Although error-free, these solutions are computationally too slow to be used routinely in actual calculations. Further, exact analytical solutions are not available for more complex models. Therefore, all elastic-plastic models are implemented in analysis programs with some error, via an integration algorithm called the stress-point algorithm. Evidently, the accuracy and stability of the global solutions is to be strongly affected by the accuracy and stability of the stress-point algorithm. Also, the cost of the analysis is most strongly affected by the efficiency of the stress-point algorithm. The best algorithm, the one to be favored, is therefore the one which combines computational efficiency with accuracy.

The first stress-point algorithm to be developed was the radial return algorithm proposed by Wilkins (1964) for the elastic-perfectly plastic von Mises model. The algorithm was subsequently extended by Krieg and Key (1976) to accommodate isotropic and kinematic hardening laws. The algorithms are analysed in Krieg and Krieg (1977); Schreyer et al. (1979); Yoder and Wirley (1984); and Ortiz and Popov (1985). Algorithms for the Drucker-Prager model have also been proposed. Approximate elaborate

subincrementation strategies with successive radial stress corrections have been proposed (see e.g., Nayak and Zienkiewicz, 1972). Other somewhat arbitrary stress corrections have also been attempted (see e.g., Chen, 1975; Vermeer, 1980) to correct for the inherent stress drift away from the yield surface. However, all these procedures tend to be quite expensive and are not *error-free*. They are analyzed in Loret and Prevost (1986). Integration algorithms for more complex models have also been developed, typically on a case-by-case basis (see e.g., Sandler and Rubin (1979) for the cap model). However, no general framework for developing consistent, accurate and stable algorithms was available until recently. It was therefore difficult to assess in general the relative merits and/or shortcomings of the various proposed procedures.

In this section, stress-point numerical algorithms are developed as the basis for computer modules designed to interface with large scale finite element/finite difference computer programs for solution of boundary value problems. Since the elastic-plastic evolution problem is of a strain driven nature, the integration process is split into an elastic predictor and a return map to restore plastic consistency. The return mapping is achieved by integrating the nonlinear plastic evolution equations, and there are several ways this can be implemented (see *e.g.*, Nguyen, 1977; Simo and Ortiz, 1985; Simo and Taylor, 1986; Ortiz and Simo, 1986; Simo and Hughes, 1987). In the following, attention is focused on the so-called "cutting-plane" algorithm (see e.g., Simo and Hughes (1987)). One yield surface and multiple-yield surface plasticity theories are considered. Finally, a generalization to account for visco-plastic effects is considered. For that purpose, the visco-plastic setup proposed by Duvaut and Lions (1972), is adopted. It leads to a closed-form unconditionally stable algorithm, in which the visco-plastic update can be constructed from the trial state and the solution to the rate-independent elasto-plastic problem (Simo et al. (1988)).

7.2 THEORY

The main equations of the theory are summarized as follows:

$$\dot{\sigma} = \mathbf{E} : (\dot{\varepsilon} - \dot{\varepsilon}^{p}) \qquad \textit{constitutive equation} \qquad (1)$$

$$f(\sigma, \mathbf{S}) = 0 \qquad \textit{yield function} \qquad (2)$$

$$\dot{\varepsilon}^{p} = \langle \dot{\lambda} \rangle \mathbf{P}(\sigma, \mathbf{S}) \qquad \textit{flow rule} \qquad (3)$$

$$\dot{\mathbf{S}} = \langle \dot{\lambda} \rangle \bar{\mathbf{S}}(\sigma, \mathbf{S}) \qquad \textit{hardening rule} \qquad (4)$$

where $\mathbf{S}$ denotes the collection of structure (hidden or "internal") variables, assumed to consist of second-order tensors α and scalars M, *viz.*,

$$\mathbf{S} = [\alpha, M]$$

In Eq.1 $\mathbf{E}$ is the fourth-order isotropic elastic coefficient tensor. For plastic flow to occur, the yield function (Eq. 2) must be satisfied and $\dot{\lambda}$ must be positive. The plastic loading index $\dot{\lambda}$ is obtained via the consistency condition which emanates from time differentiation of Eq. 2, *viz.*,

$$\dot{\lambda} = \frac{\partial_{\sigma} f : \mathbf{E} : \dot{\varepsilon}}{\partial_{\sigma} f : \mathbf{E} : \mathbf{P} - \partial_{\mathbf{S}} f : \mathbf{S}} \qquad (5)$$

In the sequel the following notation is used:

$$\partial_{\sigma} f = \mathbf{Q} = \mathbf{Q}' + Q'' \boldsymbol{\delta} \qquad (6)$$

$$H' = -\partial_{\mathbf{S}} f : \bar{\mathbf{S}} \qquad (7)$$

$$H_0 = \mathbf{Q} : \mathbf{E} : \mathbf{P} = B\,(tr\,\mathbf{P})\,(tr\,\mathbf{Q}) + 2G\,\mathbf{P}' : \mathbf{Q}' \qquad (8)$$

where B, G = Elastic bulk and shear moduli, respectively.

7.3 ALGORITHMS

The problem to be addressed is as follows:

- Given the known state variables associated with a converged configuration at step n :

$$(\sigma_n , S_n) \qquad \text{and} \qquad (\varepsilon_n^p , \varepsilon_n)$$

and a new configuration at step $(n + 1)$, via ε_{n+1},

- Find the new values of the state variables:

$$(\sigma_{n+1} , S_{n+1}) \qquad \text{and} \qquad \varepsilon_{n+1}^p$$

In the process, the incremental strains $\Delta \varepsilon = (\varepsilon_{n+1} - \varepsilon_n)$ defining the state update are assumed given. Further, it is assumed that the loading strain rate $\dot{\varepsilon}$ is constant over the time interval, viz,

$$\Delta \varepsilon = \int_0^{\Delta t} \dot{\varepsilon} \, dt = \dot{\varepsilon} \, \Delta t \tag{9}$$

where Δt = *time step* $(= t_{n+1} - t_n)$. As summarized by Ortiz and Popov (1985) an acceptable algorithm for the integration of Eqs. 1-4 should satisfy the following three basic requirements:

(i) Consistency with the constitutive relations to be integrated (i.e., first-order accuracy),
(ii) Numerical stability, and
(iii) Incremental plastic consistency.

Conditions (i) and (ii) are necessary for attaining convergence of the numerical solution as the time step becomes vanishingly small. Condition (iii) is the algorithmic counterpart of the plastic consistency condition which requires the yield function to be satisfied by the updated state variables.

Integration of Eqs. 1 - 4 is achieved by a stress relaxation procedure by which Eq. 1 is first used to obtain an elastic predictor, hereafter referred to as the trial stress σ^{tr}_{n+1}, viz.,

$$\sigma^{tr}_{n+1} = \mathbf{E} : (\varepsilon_{n+1} - \varepsilon^{p}_{n}) = \sigma_{n} + \mathbf{E} : \Delta \varepsilon \tag{10}$$

Clearly, if $f (\sigma^{tr}_{n+1}, \mathbf{S}_{n}) \leq 0$ the process is elastic and the trial stress is in fact the final state. Otherwise, the trial stress lies outside the yield surface and must be relaxed onto the yield surface to restore plastic consistency. For that purpose, the trial stress is taken as the initial condition for the following plastic relaxation:

$$\sigma_{n+1} = \sigma^{tr}_{n+1} - \Delta \sigma^{p} \tag{11}$$

where (from Eqs. 1 and 3)

$$\Delta \sigma^{p} = \int_{0}^{\Delta t} \mathbf{E} : \dot{\varepsilon}^{p} \, dt = \int_{0}^{\Delta t} \dot{\lambda} \, \mathbf{E} : \mathbf{P} \, dt \tag{12}$$

such that

$$f (\sigma_{n+1}, \mathbf{S}_{n+1}) = 0 \tag{13}$$

to restore plastic consistency. The resulting procedure is shown schematically in Fig. 7.1, and consists of *returning back* the trial stress onto the yield surface. In general, the return path defined by $\mathbf{P}$ in Eq. 12 is not known in advance nor can it be determined analytically, and it is therefore necessary to integrate Eq. 12 numerically.

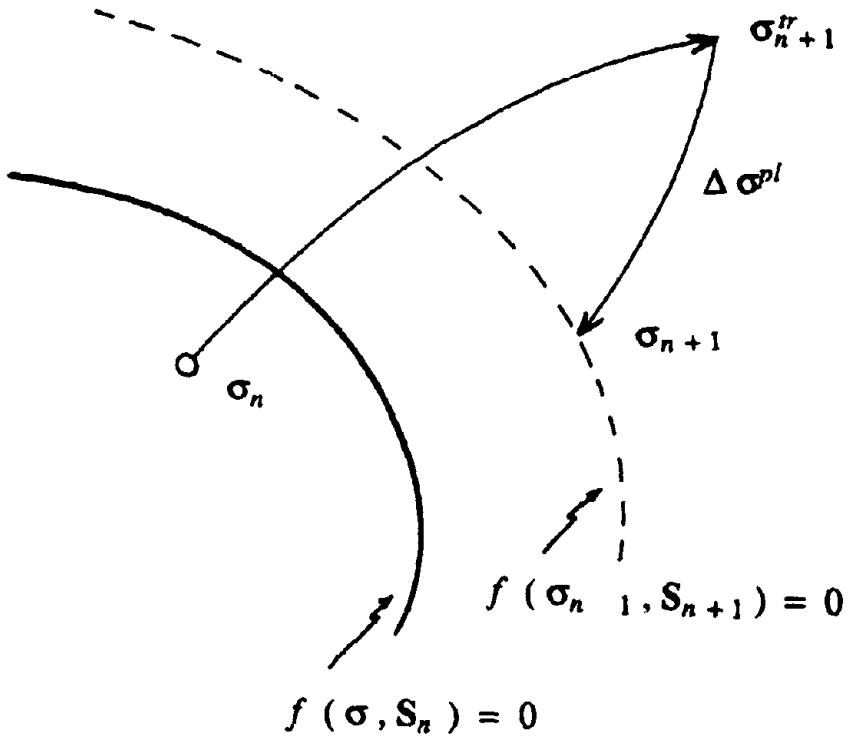

Figure 7.1 Schematic of the Elastic Predictor / Plastic Stress Relaxation

7.3.1 Algorithmic Set-up

An efficient and simple procedure for performing the return mapping was proposed by Simo and Ortiz (1985), and further analysed by Ortiz and Simo (1986). In this algorithm the return mapping is defined iteratively by employing linearized equations iteratively about the current trial state. At every iteration, the plastic corrector problem is integrated about the current trial values of the state variables by an *explicit* forward Euler difference scheme over the length $\tilde{\lambda}$ to be determined by requiring that the updated state variables satisfy a linearized version of the constraint equation, *viz.*, let i denote the iteration counter:

$$\boldsymbol{\sigma}_{n+1}^{(i)} = \mathbf{E} : (\boldsymbol{\varepsilon}_{n+1} - \boldsymbol{\varepsilon}_{n+1}^{p\,(i)}) \tag{14}$$

$$\boldsymbol{\varepsilon}_{n+1}^{p\,(i+1)} = \boldsymbol{\varepsilon}_{n+1}^{p\,(i)} + \tilde{\lambda}_{n+1}^{(i)} \mathbf{P} (\boldsymbol{\sigma}_{n+1}^{(i)}, \mathbf{S}_{n+1}^{(i)}) \tag{15}$$

$$\mathbf{S}_{n+1}^{(i+1)} = \mathbf{S}_{n+1}^{(i)} + \tilde{\lambda}_{n+1}^{(i)} \bar{\mathbf{S}} (\boldsymbol{\sigma}_{n+1}^{(i)}, \mathbf{S}_{n+1}^{(i)}) \tag{16}$$

with the constraint condition:

$$f (\boldsymbol{\sigma}_{n+1}^{(i+1)}, \mathbf{S}_{n+1}^{(i+1)}) = 0 \tag{17}$$

Initially:

$$\boldsymbol{\sigma}_{n+1}^{(0)} = \boldsymbol{\sigma}_{n+1}^{tr} \qquad \boldsymbol{\varepsilon}_{n+1}^{p\,(0)} = \boldsymbol{\varepsilon}_{n}^{p} \qquad \mathbf{S}_{n+1}^{(0)} = \mathbf{S}_{n} \tag{18}$$

Let

$$f_{n+1}^{(i)} := f (\boldsymbol{\sigma}_{n+1}^{(i)}, \mathbf{S}_{n+1}^{(i)}) \tag{19}$$

At every iteration the yield function f (the constraint equation, Eq. 31) is linearized about the current trial values of the state variables, $(\boldsymbol{\sigma}_{n+1}^{(i)}, \mathbf{S}_{n+1}^{(i)})$ to obtain the following:

$$f (\boldsymbol{\sigma}_{n+1}^{(i+1)}, \mathbf{S}_{n+1}^{(i+1)}) \approx$$

$$f_{n+1}^{(i)} + \partial_{\boldsymbol{\sigma}} f_{n+1}^{(i)} : (\boldsymbol{\sigma}_{n+1}^{(i+1)} - \boldsymbol{\sigma}_{n+1}^{(i)}) + \partial_{\mathbf{S}} f_{n+1}^{(i)} : (\mathbf{S}_{n+1}^{(i+1)} - \mathbf{S}_{n+1}^{(i)}) = 0 \tag{20}$$

Combining Eqs 14-16 and 20, one finds:

$$\tilde{\lambda}_{n+1}^{(i)} = \frac{f_{n+1}^{(i)}}{\partial_\sigma f_{n+1}^{(i)} : \mathbf{E} : \mathbf{P}_{n+1}^{(i)} - \partial_S f_{n+1}^{(i)} : \bar{\mathbf{S}}_{n+1}^{(i)}} \tag{21}$$

and (from Eq. 14) the updated stress state is computed as:

$$\sigma_{n+1}^{(i+1)} = \sigma_{n+1}^{(i)} - \tilde{\lambda}_{n+1}^{(i)} \; \mathbf{E} : \mathbf{P}_{n+1}^{(i)} \tag{22}$$

The iterations continue until plastic consistency is restored to within a prescribed tolerance, *viz.*, $| f_{n+1}^{(i+1)} / f_{n+1}^{(0)} | \leq TOL$ *with* $TOL << 1$. The procedure is summarized in Flowchart 7-1 (from Simo and Hughes, 1987). The algorithm is consistent, *first-order accurate*, only conditionally stable but achieves a quadratic convergence rate for the update.

FLOWCHART 7-1. - CUTTING PLANE PROJECTION ITERATIONS

1. Initialize: $i = 0$ $\qquad \boldsymbol{\varepsilon}_n^{p\,(0)}_{n+1} = \boldsymbol{\varepsilon}_n^p \qquad \mathbf{S}_n^{(0)}_{n+1} = \mathbf{S}_n$

2. Update stress and check yield condition / plastic consistency:

$$\boldsymbol{\sigma}_n^{(i)}_{n+1} = \mathbf{E} : (\boldsymbol{\varepsilon}_{n+1} - \boldsymbol{\varepsilon}_n^{p\,(i)}_{n+1})$$

$$f_n^{(i)}_{n+1} := f\,(\boldsymbol{\sigma}_n^{(i)}_{n+1}, \mathbf{S}_n^{(i)}_{n+1})$$

IF $[\, f_n^{(i)}_{n+1} \le 0$ *.OR.* $| f_n^{(i)}_{n+1} / f_n^{(0)}_{n+1} | < TOL\,]$ *EXIT*; *OTHERWISE*:

3. Compute new plastic loading function:

$$\tilde{\lambda}_n^{(i)}_{n+1} = \frac{f_n^{(i)}_{n+1}}{\partial_{\boldsymbol{\sigma}} f_n^{(i)}_{n+1} : \mathbf{E} : \mathbf{P}_n^{(i)}_{n+1} - \partial_{\mathbf{S}} f_n^{(i)}_{n+1} : \bar{\mathbf{S}}_n^{(i)}_{n+1}}$$

4. Update plastic strains and state variables:

$$\boldsymbol{\varepsilon}_n^{p\,(i+1)}_{n+1} = \boldsymbol{\varepsilon}_n^{p\,(i)}_{n+1} + \tilde{\lambda}_n^{(i)}_{n+1}\, \mathbf{P}_n^{(i)}_{n+1}$$

$$\mathbf{S}_n^{(i+1)}_{n+1} = \mathbf{S}_n^{(i)}_{n+1} + \tilde{\lambda}_n^{(i)}_{n+1}\, \bar{\mathbf{S}}_n^{(i)}_{n+1}$$

5. *Set*: $i = i + 1$ and *GOTO* 2.

7.3.2 Multi-Yield Surface Plasticity Case

Within the context of multi-yield surface plasticity models, it may occur that after completion of the preceeding calculations, it is found that the stress point lies outside the next larger yield surface. When this is the case, the iteration counter i must be reinitialized to $i = 0$, and calculations must begin again with respect to the next yield surface (step 3 in Flowchart 7-1). However, some small, but crucial correction to the stress must first be made to take account of the fact that the stress has actually been over relaxed. To see the origin of the necessary correction, assume that a stress relaxation has just been performed onto the yield surface $f^{(m)}$, and it is now found that the resulting stress point is outside surface $f^{(m+1)}$. This is illustrated in Fig. 7.2. Clearly, as a result of the stress overrelaxation, the yield surface $f^{(m)}$ now overlaps (or may even be totally outside) the surface $f^{(m+1)}$. However the relaxation should have performed onto the surface $f^{(m+1)}$ upon contact of the two surfaces. The correction thus becomes:

$$\varepsilon^{p\,(i+1)} = \varepsilon^{p\,(i)} - \tilde{\lambda}_m^{(i)}\,\mathbf{P}^{(m)}(\sigma^{(i)}, \mathbf{S}_m^{(i)}) + \tilde{\lambda}_{m+1}^{(i)}\,\mathbf{P}^{(m+1)}(\sigma^{(i)}, \mathbf{S}_{m+1}^{(i)}) \qquad (23)$$

$$\mathbf{S}_m^{(i+1)} = \mathbf{S}_m^{(i)} - \tilde{\lambda}_m^{(i)}\,\bar{\mathbf{S}}^{(m)}(\sigma^{(i)}, \mathbf{S}_m^{(i)}) \qquad (24)$$

$$\mathbf{S}_{m+1}^{(i+1)} = \mathbf{S}_{m+1}^{(i)} + \tilde{\lambda}_{m+1}^{(i)}\,\bar{\mathbf{S}}^{(m+1)}(\sigma^{(i)}, \mathbf{S}_{m+1}^{(i)}) \qquad (25)$$

$$\sigma^{(i+1)} = \sigma^{(i)} + \tilde{\lambda}_m^{(i)}\,\mathbf{E} : \mathbf{P}^{(m)}(\sigma^{(i)}, \mathbf{S}_m^{(i)}) - \tilde{\lambda}_{m+1}^{(i)}\,\mathbf{E} : \mathbf{P}^{(m+1)}(\sigma^{(i)}, \mathbf{S}_{m+1}^{(i)}) \qquad (26)$$

where the subscript n has been omitted to simplify the notation. The length $\tilde{\lambda}_m^{(i)}$ is determined by linearizing the yield function $f^{(m)}$ about the current values of the state variables, *viz.*,

$$f^{(m)}(\sigma^{(i)}, \mathbf{S}_m^{(i+1)}) \simeq f^{(m)}(\sigma^{(i)}, \mathbf{S}_m^{(i)}) + \partial_{\mathbf{S}} f^{(m)} : (\mathbf{S}_m^{(i+1)} - \mathbf{S}_m^{(i)}) \qquad (27)$$

and by approximating the contact condition as:

$$f^{(m)}(\sigma^{(i)}, \mathbf{S}_m^{(i+1)}) = f^{(m+1)}(\sigma^{(i)}, \mathbf{S}_{m+1}^{(i)}) \qquad (28)$$

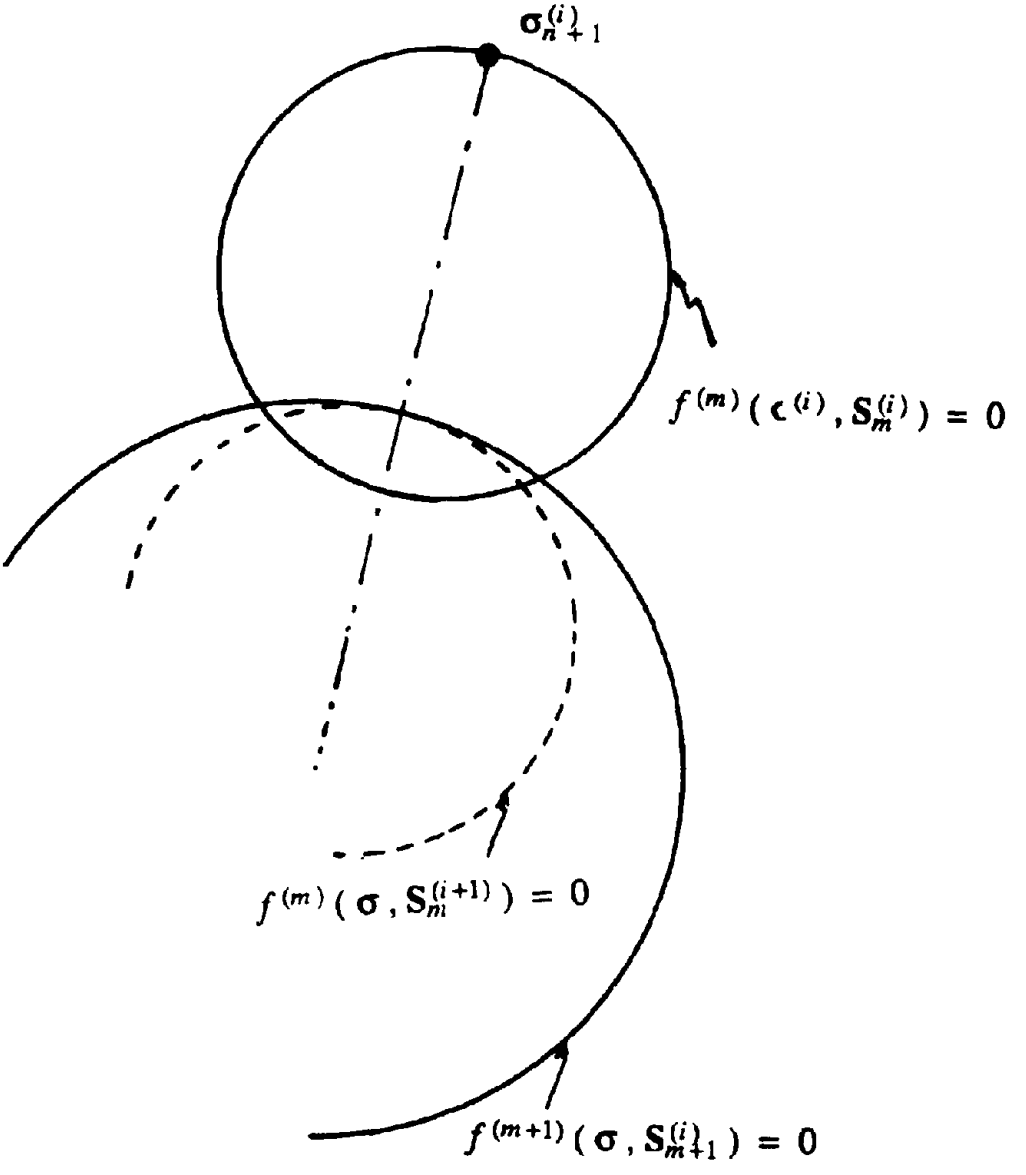

$$f^{(m)}(\sigma^{(i)}, S_m^{(i+1)}) = f^{(m+1)}(\sigma^{(i)}, S_{m+1}^{(i)})$$

Figure 7.2. Multi-Surface Plasticity Case - Schematic of Correction

Then, since $f^{(m)}(\boldsymbol{\sigma}^{(i)}, \mathbf{S}_m^{(i)}) = 0$, (from Eqs 24, 27 and 28):

$$\bar{\lambda}_m^{(i)} = -\frac{f^{(m+1)}(\boldsymbol{\sigma}^{(i)}, \mathbf{S}_{m+1}^{(i)})}{\partial_{\mathbf{S}} f^{(m)} : \bar{\mathbf{S}}^{(m)}(\boldsymbol{\sigma}^{(i)}, \mathbf{S}_m^{(i)})} = \frac{f^{(m+1)}(\boldsymbol{\sigma}^{(i)}, \mathbf{S}_{m+1}^{(i)})}{H'^{(i)}_m} \tag{29}$$

The length $\bar{\lambda}_{m+1}^{(i)}$ is determined by linearizing the yield function $f^{(m+1)}$ about the current values of the state variables, *viz.*,

$$f^{(m+1)}(\boldsymbol{\sigma}^{(i+1)}, \mathbf{S}_{m+1}^{(i+1)}) \approx$$

$$f^{(m+1)}(\boldsymbol{\sigma}^{(i)}, \mathbf{S}_{m+1}^{(i)}) + \partial_{\boldsymbol{\sigma}} f^{(m+1)} : (\boldsymbol{\sigma}^{(i+1)} - \boldsymbol{\sigma}^{(i)}) + \partial_{\mathbf{S}} f^{(m+1)} : (\mathbf{S}_{m+1}^{(i+1)} - \mathbf{S}_{m+1}^{(i)}) = 0 \tag{30}$$

Combining Eqs 23-26, 29 and 30, one finds:

$$\bar{\lambda}_{m+1}^{(i)} = \frac{f^{(m+1)}(\boldsymbol{\sigma}^{(i)}, \mathbf{S}_{m+1}^{(i)})}{\partial_{\boldsymbol{\sigma}} f^{(m+1)} : \mathbf{E} : \mathbf{P}^{(m+1)} - \partial_{\mathbf{S}} f^{(m+1)} : \bar{\mathbf{S}}^{(m+1)}} \left[1 + \frac{\partial_{\boldsymbol{\sigma}} f^{(m+1)} : \mathbf{E} : \mathbf{P}^{(m)}}{H'^{(i)}_m} \right] \tag{31}$$

The procedure is summarized in Flowchart 7-2.

FLOWCHART 7-2. - INTEGRATION ALGORITHM

MULTI-YIELD SURFACE PLASTICITY CASE

1. Initialize: $i = 0$ $\quad m = 1$ $\quad \varepsilon_n^{p\,(0)}{}_{+1} = \varepsilon_n^p$ $\quad \mathbf{S}_n^{(0)}{}_{+1} = \mathbf{S}_n$

2. Update stress and check yield condition / plastic consistency:

$$\boldsymbol{\sigma}_n^{(i)}{}_{+1} = \mathbf{E} : (\boldsymbol{\varepsilon}_{n+1} - \boldsymbol{\varepsilon}_n^{p\,(i)}{}_{+1})$$

$$f^{(m)}\,|_{n+1}^{(i)} := f^{(m)}(\boldsymbol{\sigma}_n^{(i)}{}_{+1}, \mathbf{S}_n^{(i)}{}_{+1})$$

IF $[f^{(m)}\,|_{n+1}^{(i)} \le 0$ *.OR.* $|\, f^{(m)}\,|_{n+1}^{(i)} / f^{(m)}\,|_{n+1}^{(0)}\,| < TOL\,]$ *GOTO* 6

OTHERWISE GOTO 3.

3. Compute new plastic loading function:

$$\tilde{\lambda}_n^{(i)}{}_{+1} = \left[\frac{f^{(m)}}{\partial_{\boldsymbol{\sigma}} f^{(m)} : \mathbf{E} : \mathbf{P}^{(m)} - \partial_{\mathbf{S}} f^{(m)} : \bar{\mathbf{S}}^{(m)}} \right]_{n+1}^{(i)}$$

4. Update plastic strains and state variables:

$$\boldsymbol{\varepsilon}_n^{p\,(i+1)}{}_{+1} = \boldsymbol{\varepsilon}_n^{p\,(i)}{}_{+1} + \tilde{\lambda}_n^{(i)}{}_{+1}\, \mathbf{P}^{(m)}\,|_{n+1}^{(i)}$$

$$\mathbf{S}_n^{(i+1)}{}_{+1} = \mathbf{S}_n^{(i)}{}_{+1} + \tilde{\lambda}_n^{(i)}{}_{+1}\, \bar{\mathbf{S}}^{(m)}\,|_{n+1}^{(i)}$$

5. *Set*: $i = i + 1$ and *GOTO* 2.

6. Check for overshooting of next yield surface, $f^{(m+1)}$:

IF $[m = NYS\,]$ *EXIT*

IF $[f^{(m+1)}(\boldsymbol{\sigma}_n^{(i)}{}_{+1}, \mathbf{S}_n^{(i)}{}_{+1}) \le 0\,]$ *EXIT*

OTHERWISE GOTO 7.

FLOWCHART 7-2. - Cont'd

7. Compute new plastic loading functions:

$$H_0^{(m)} := \partial_\sigma f^{(m)} : \mathbf{E} : \mathbf{P}^{(m)} \qquad H'^{(m)} := -\partial_S f^{(m)} : \bar{\mathbf{S}}^{(m)}$$

$$\tilde{\lambda}^{(m)} = \left[\frac{f^{(m+1)}}{H'^{(m)}} \right]_{n+1}^{(i)}$$

$$\tilde{\lambda}^{(m+1)} = \left[\frac{f^{(m+1)}}{H_0^{(m+1)} + H'^{(m+1)}} \left[1 + \frac{H_0^{(m)}}{H'^{(m)}} \right] \right]_{n+1}^{(i)}$$

8. Update plastic strains and state variables:

$$\boldsymbol{\varepsilon}_{n+1}^{p\,(i+1)} = \boldsymbol{\varepsilon}_{n+1}^{p\,(i)} - \tilde{\lambda}^{(m)} \mathbf{P}^{(m)} \Big|_{n+1}^{(i)} + \tilde{\lambda}^{(m+1)} \mathbf{P}^{(m+1)} \Big|_{n+1}^{(i)}$$

$$\mathbf{S}_{n+1}^{(i+1)} = \mathbf{S}_{n+1}^{(i)} + \tilde{\lambda}^{(m+1)} \bar{\mathbf{S}}^{(m+1)} \Big|_{n+1}^{(i)}$$

9. *Set*: $m = m + 1$; $i = i + 1$; and *GOTO* 2.

7.3.3 Application / Examples

Consider the case of yield functions of the type

$$f^{(m)}(\sigma, S^{(m)}) = |s - \bar{p}\,\alpha^{(m)}| + \sqrt{\frac{2}{3}}\,M^{(m)}\,\bar{p} = 0 \tag{32}$$

where

$$S^{(m)} = [\alpha^{(m)}, M^{(m)}] \tag{33}$$

$$s = \sigma - p\,\delta \qquad p = \frac{1}{3}\,tr\,\sigma \tag{34}$$

and $\bar{p} = (p - a)$ with a = attraction = material parameter; $\alpha^{(m)}$ = kinematic deviatoric tensor defining the coordinates of the center of the yield surface $f^{(m)}$ in deviatoric stress subspace; $M^{(m)}$ = material parameter. Then (from Eq. 32):

$$\partial_\sigma f^{(m)} := Q^{(m)} = \frac{(s - \bar{p}\,\alpha^{(m)})}{|s - \bar{p}\,\alpha^{(m)}|} + \frac{1}{3}\left[\sqrt{\frac{2}{3}}\,M^{(m)} - \frac{(s - \bar{p}\,\alpha^{(m)}) : \alpha^{(m)}}{|s - \bar{p}\,\alpha^{(m)}|}\right]\delta$$

$$= Q'^{(m)} + \zeta''^{(m)}\,\delta \tag{35}$$

The flow direction (Eq. 3) is assumed as follows:

$$P^{(m)} = P'^{(m)} + P''^{(m)}\,\delta \tag{36}$$

with

$$P'^{(m)} = Q'^{(m)} \qquad 3\,P''^{(m)} = \frac{(\eta / \bar{\eta})^2 - 1}{(\eta / \eta)^2 + 1} \tag{37}$$

where $\eta = (\frac{3}{2}s : s)^{1/2} / \bar{p}$ = mobilized stress ratio; and $\bar{\eta}$ = material parameter. A purely deviatoric kinematic hardening rule is assumed, and (from Eq. 32):

$$\partial_S f^{(m)} = \partial_\alpha f^{(m)} = -\bar{p}\,Q'^{(m)} \tag{38}$$

with

$$\dot{\alpha}^{(m)} = \langle \dot{\lambda} \rangle\,\bar{\alpha}^{(m)} = \langle \dot{\lambda} \rangle\,\frac{H'^{(m)}}{\bar{p}\,Q'^{(m)} : \mu^{(m)}}\,\mu^{(m)} \tag{39}$$

where $H'^{(m)}$ = plastic modulus; and $\mu^{(m)}$ = (deviatoric) tensor defining the direction of translation. Let NYS denote the number of yield functions used ($NYS \geq 1$). Then to avoid overlapping of the surfaces, the translation direction $\mu^{(m)}$ is given by

$$\mu^{(m)} = -\sqrt{\frac{2}{3}}\, M^{(m+1)}\, \bar{p}\, \frac{s - \bar{p}\,\alpha^{(m)}}{|\, s - \bar{p}\,\alpha^{(m)}\,|} - (s - \bar{p}\,\alpha^{(m+1)}) \qquad (40)$$

when surface $f^{(m)}$ translates towards surface $f^{(m+1)}$. On the last surface $m = NYS$ and usually $H' = 0$, and no motion is to take place, (the last surface then plays the role of a failure surface). Otherwise, $\mu^{(m)} = Q'^{(m)}$ on the last surface.

In order to illustrate the performance of the return mapping algorithm and assess its accuracy, we consider a cohesionless ($a = 0$) cross-anisotropic material with assumed friction angle at failure $\phi^f = 35\ degrees$ and dilation angle $\bar{\phi} = 30\ degrees$. The material is modelled by using 10 yield surfaces, and the following elastic moduli are assumed:

$$G_1 / p_1 = 150. \qquad B_1 / p_1 = 100.$$

where p_1 = reference mean effective stress. Following usual sign conventions in geomechanics, compressive stresses and strains are considered positive in the following. The material is assumed to be subjected, at constant volume, to a monotonically increasing and decreasing shear strain $\bar{\varepsilon}$ with maximum amplitude $\bar{\varepsilon} = 1.5\ 10^{-2}$ (undrained triaxial soil test). To assess accuracy and robustness of the algorithm, loading is achieved in N equal load steps $\Delta\bar{\varepsilon}$ with

$$\Delta\bar{\varepsilon} = \frac{\bar{\varepsilon}}{N}$$

with $N = 5$, 10 , and 100 . In all cases, the algorithm remained stable. The solution computed with 100 load steps is fully "converged", and can be considered "exact". Fig. 7.3a shows the computed shear stress versus shear strain curves. Very good agreement with the exact solution is obtained in all cases, even for the solutions constructed with

very large load steps. Fig. 7.3b shows the computed effective stress paths (shear stress versus mean effective stress). Clearly, the effective stress paths computed with large load steps differ from the exact stress path. This was to be expected, and is due to the assumed non-associativity and high degree of nonlinearity for the dilatational component of the plastic flow (Eq. 37). The algorithm only being first-order accurate, requires small load steps to return accurate answers in highly nonlinear situations. This point is clearly illustrated by the assumed nonlinearity in the dilatational component.

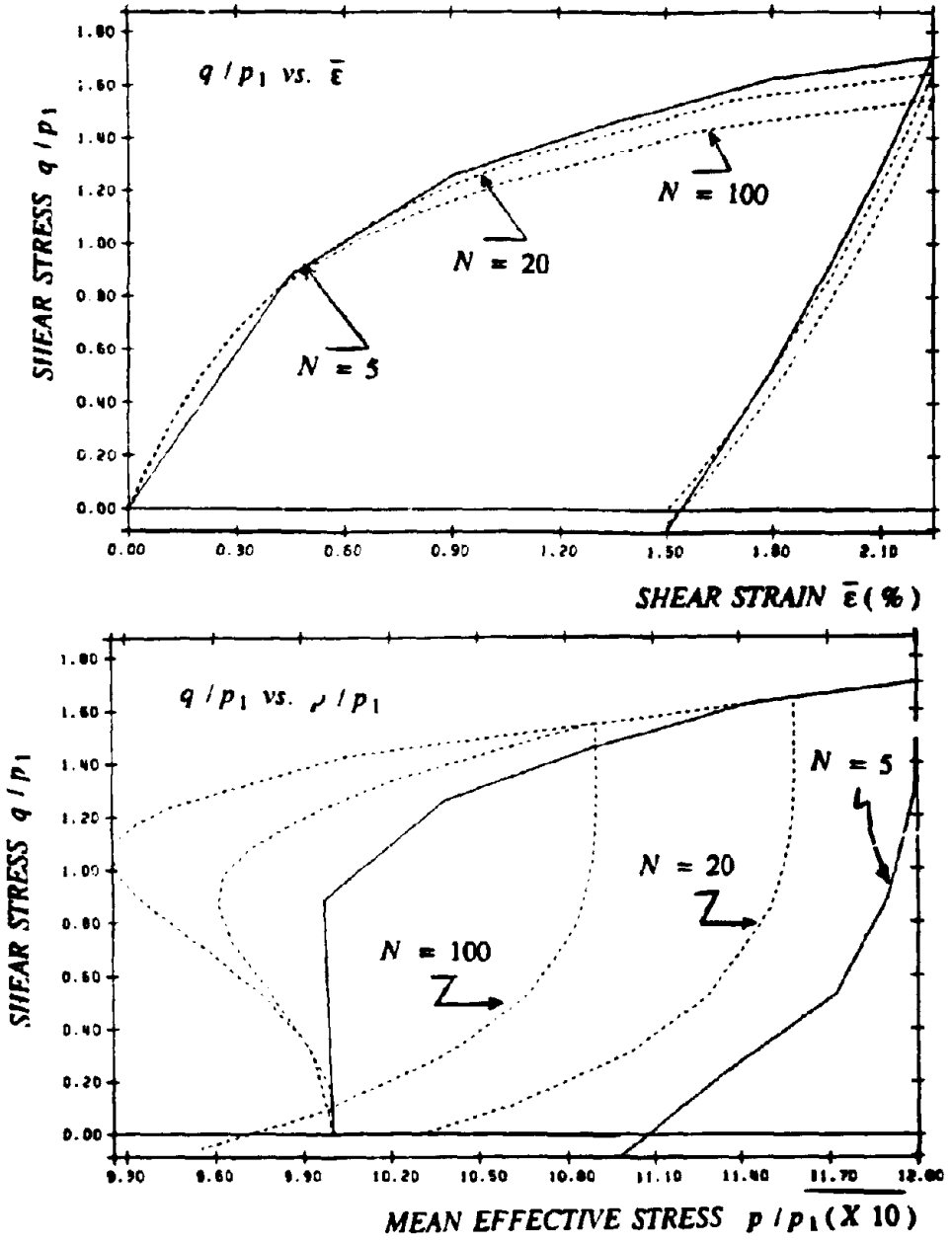

Figure 7.3 Multi-Surface Plasticity Case - Cutting Plane Algorithm
(*a*) Shear Stress-Strain Curves
(*b*) Effective Stress Paths

7.4 EXTENSION TO VISCO-PLASTICITY

The extension to visco-plasticity is based on the formulation proposed by Duvaut and Lions (1972). It is important to note that the visco-plastic formulation used here is different and not equivalent to Perzyna' s type formulation (Perzyna, 1966, 1971) commonly used in geomechanics (see *e.g.*, Katona, 1984). Let $[\ \sigma^{(*)}, S^{(*)}\ ]$ denote the *inviscid* solution of the elastoplastic problem. Then the visco-plastic constitutive equations are written in the following form:

$$\dot{\varepsilon}^{vp} = \frac{1}{\eta}\,\mathbf{E}^{-1} : (\sigma - \sigma^{(*)}) \qquad \dot{S} = \frac{-1}{\eta}\,(S - S^{(*)}) \qquad (41)$$

where η = relaxation time (= material constant). The exact integration of Eqs 1 and 41 is straightforward. The resulting algorithm is summarized in Flowchart 7-3. Note that the elastic and inviscid elasto-plastic solutions are recovered from the algorithm as:

- $\frac{\Delta t}{\eta} \rightarrow 0$; $\quad \sigma_{n+1} = \sigma_n + \mathbf{E} : \Delta\varepsilon_{n+1}$ $\quad$ (*Elastic*)
- $\frac{\Delta t}{\eta} \rightarrow \infty$; $\quad \sigma_{n+1} = \sigma_{n+1}^{(*)}$ $\quad$ (*Inviscid Elasto–Plastic*)

The algorithm is straightforward to implement.

FLOWCHART 7-3. - VISCO-PLASTIC ALGORITHM

1. Obtain the inviscid elasto-plastic solution: $[\ \sigma^{(*)}_{n+1}\ ,\ \mathbf{S}^{(*)}_{n+1}\ ]$

   using Flowcharts 7-1 or 7-2.

2. Compute the visco-plastic solution as:

$$\sigma_{n+1} = \exp(-\Delta t / \eta)\,\sigma_n + [\,1 - \exp(-\Delta t / \eta)\,]\,\sigma^{(*)}_{n+1} + \frac{1 - \exp(-\Delta t / \eta)}{\Delta t / \eta}\,\mathbf{E} : \Delta\varepsilon_{n+1}$$

$$\mathbf{S}_{n+1} = \exp(-\Delta t / \eta)\,\mathbf{S}_n + [\,1 - \exp(-\Delta t / \eta)\,]\,\mathbf{S}^{(*)}_{n+1}$$

3. *EXIT*.

7.5 REFERENCES

1. Chen, W.F., *Limit Analysis and Soil Plasticity, Developments in Geotechnical Engineering 7*, Elsevier Scientific, Amsterdam, 1975.
2. Drucker, D.C. and W. Prager, "Soil Mechanics and Plasticity Analysis or Limit Design," *Quart. Appl. Math.*, Vol. 10, No.2, 1952, pp. 157-165.
3. Duvaut, G. and Lions, J.L., *Les Inequations en Mecanique et en Physique*, Dunod, Paris, 1972.
4. Katona, M.G., "Evaluation of Viscoplastic Cap Model," *J. Geotech. Eng. Div.*, ASCE, Vol. 110, No. GT8, 1984, pp. 1106-1125.
5. Krieg, R.D. and S.M. Key, "Implementation of a Time Dependent Plasticity Theory into Structural Computer Programs," in *Constitutive Equations in Viscoplasticity: Computational and Engineering Aspects*, Eds J.A. Stricklin and K.J. Saczalski, ASME, New York, Vol. 20, 1976, pp. 125-137.
6. Krieg, R.D., and D.B. Krieg, "Accuracies of Numerical Solution Methods for the Elastic-Perfectly Plastic Model," *J. Pressure Vessel Technol.*, ASME, Vol. 99, 1977, pp. 510-515.
7. Loret, B. and J.H. Prevost, "Accurate Numerical Solutions for Drucker-Prager Elastic Plastic Models," *Comp. Meth. Appl. Mech. Eng.*, Vol. 54, No. 3, 1986, pp. 259-277.
8. Nayak, G.C. and O.C. Zienkiewicz, "Elastic-Plastic Stress Analysis: A Generalization for Various Constitutive Relations Including Strain Softening," *Int. J. Numer. Meths. Engrg*, Vol. 5, No. 1, 1972, pp. 113-135.
9. Nguyen, Q.S., "On the Elastic-Plastic Initial Boundary Value Problem and its Numerical Integration, *Int. J. Numer. Meths. Engrg.*, Vol. 11, 1977, pp. 817-832.
10. Ortiz, M., and J.C. Simo, "An Analysis of a New Class of Integration Algorithms for Elastoplastic Constitutive Relations," *Int. J. Num. Meth. Eng.*, Vol. 23, No. 3, 1986, pp. 353-366.
11. Ortiz, M., and E.P. Popov, "Accuracy and Stability of Integration Algorithms for Elastoplastic Constitutive Relations," *Int. J. Num. Meth. Eng.*, Vol. 21, No. 9, 1985, pp. 1561-1576.
12. Perzyna, P., "Fundamental Problems in Viscoplasticity," in *Advances in Applied Mechanics*, Vol. 9, Academic Press, New York, 1966, pp. 243-377.
13. Perzyna, P., "Thermodynamic Theory of Viscoplasticity," in *Advances in Applied Mechanics*, Vol. 11, Academic Press, New York, 1971, pp. 243-377.
14. Sandler, I.S. and D. Rubin, "An Algorithm and a Modular Subroutine for the Cap Model," *Int. J. Num. Analy. Methods in Geomech.*, Vol. 3, 1979, pp. 173-186.
15. Schreyer, H.L., R.F. Kulak and J.M. Kramer, "Accurate Numerical Solutions for Elastic-Plastic Models," *J. Pressure Vessel Technol.*, ASME, Vol. 101, 1979, pp. 226-234.
16. Simo, J.C. and Ortiz, M., "A Unified Approach to Finite Deformation Elastoplastic Analysis Based on the Use of Hyperelastic Constitutive Equations," *Comp. Meth. Appl. Mech. Eng.*, Vol. 49, 1985, pp. 221-245.
17. Simo, J.C. and Taylor, R.L., "A Consistent Return Mapping Algorithm for Plane Strain Elastoplasticity," *Int. J. Num. Methd. Engng.*, Vol. 22, 1986, pp. 649-670.

18. Simo, J.C. and Hughes, T.J.R., "General Return Mapping Algorithms for Rate-Independent Plasticity," in *Constitutive Laws for Engineering Materials: Theory and Applications*, Eds C.S. Desai, E. Krempl, P.D. Kiousis and T. Kundu, Elsevier, New York, Vol. 1, 1987, pp. 221-232.

19. Simo, J,C., Govindjee, J.G.K., and Hughes, T.J.R., "Unconditionally Convergent Algorithms for Non-Smooth MultiSurfcace Plasticity Amenable to Exact Linearization", in *Advances in Inelastic Analysis*, ASME Publication, AMD Vol. 88, 1987, pp. 87-95.

20. Vermeer, P.A., "Formulation and Analysis of Sand Deformation Problems," Ph.D. Thesis, Department of Civil Engineering, Delft University, The Netherlands, 1980.

21. Wilkins, M.L., "Calculation of Elastic-plastic Flow," in *Methods of Computational Physics*, Eds Alder B. et al., Academic Press, New York, Vol. 8, 1964.

22. Yoder, P.J. and B.G. Whirley, "On the Numerical Implementation of Elastoplastic Models," *J. Appl. Mech.*, ASME, Vol. 51, 1984, pp. 283-288.

NATIONAL CENTER FOR EARTHQUAKE ENGINEERING RESEARCH
LIST OF PUBLISHED TECHNICAL REPORTS

The National Center for Earthquake Engineering Research (NCEER) publishes technical reports on a variety of subjects related to earthquake engineering written by authors funded through NCEER. These reports are available from both NCEER's Publications Department and the National Technical Information Service (NTIS). Requests for reports should be directed to the Publications Department, National Center for Earthquake Engineering Research, State University of New York at Buffalo, Red Jacket Quadrangle, Buffalo, New York 14261. Reports can also be requested through NTIS, 5285 Port Royal Road, Springfield, Virginia 22161. NTIS accession numbers are shown in parenthesis, if available.

NCEER-87-0001 "First-Year Program in Research, Education and Technology Transfer," 3/5/87, (PB88-134275/AS).

NCEER-87-0002 "Experimental Evaluation of Instantaneous Optimal Algorithms for Structural Control," by R.C. Lin, T.T. Soong and A.M. Reinhorn, 4/20/87, (PB88-134341/AS).

NCEER-87-0003 "Experimentation Using the Earthquake Simulation Facilities at University at Buffalo," by A.M. Reinhorn and R.L. Ketter, to be published.

NCEER-87-0004 "The System Characteristics and Performance of a Shaking Table," by J.S. Hwang, K.C. Chang and G.C. Lee, 6/1/87, (PB88-134259/AS). This report is available only through NTIS (see address given above).

NCEER-87-0005 "A Finite Element Formulation for Nonlinear Viscoplastic Material Using a Q Model," by O. Gyebi and G. Dasgupta, 11/2/87, (PB88-213764/AS).

NCEER-87-0006 "Symbolic Manipulation Program (SMP) - Algebraic Codes for Two and Three Dimensional Finite Element Formulations," by X. Lee and G. Dasgupta, 11/9/87, (PB88-219522/AS).

NCEER-87-0007 "Instantaneous Optimal Control Laws for Tall Buildings Under Seismic Excitations," by J.N. Yang, A. Akbarpour and P. Ghaemmaghami, 6/10/87, (PB88-134333/AS).

NCEER-87-0008 "IDARC: Inelastic Damage Analysis of Reinforced Concrete Frame - Shear-Wall Structures," by Y.J. Park, A.M. Reinhorn and S.K. Kunnath, 7/20/87, (PB88-134325/AS).

NCEER-87-0009 "Liquefaction Potential for New York State: A Preliminary Report on Sites in Manhattan and Buffalo," by M. Budhu, V. Vijayakumar, R.F. Giese and L. Baumgras, 8/31/87, (PB88-163704/AS). This report is available only through NTIS (see address given above).

NCEER-87-0010 "Vertical and Torsional Vibration of Foundations in Inhomogeneous Media," by A.S. Veletsos and K.W. Dotson, 6/1/87, (PB88-134291/AS).

NCEER-87-0011 "Seismic Probabilistic Risk Assessment and Seismic Margins Studies for Nuclear Power Plants," by Howard H.M. Hwang, 6/15/87, (PB88-134267/AS). This report is available only through NTIS (see address given above).

NCEER-87-0012 "Parametric Studies of Frequency Response of Secondary Systems Under Ground-Acceleration Excitations," by Y. Yong and Y.K. Lin, 6/10/87, (PB88-134309/AS).

NCEER-87-0013 "Frequency Response of Secondary Systems Under Seismic Excitation," by J.A. HoLung, J. Cai and Y.K. Lin, 7/31/87, (PB88-134317/AS).

NCEER-87-0014 "Modelling Earthquake Ground Motions in Seismically Active Regions Using Parametric Time Series Methods," by G.W. Ellis and A.S. Cakmak, 8/25/87, (PB88-134283/AS).

NCEER-87-0015 "Detection and Assessment of Seismic Structural Damage," by E. DiPasquale and A.S. Cakmak, 8/25/87, (PB88-163712/AS).

NCEER-87-0016 "Pipeline Experiment at Parkfield, California," by J. Isenberg and E. Richardson, 9/15/87, (PB88-163720/AS).

NCEER-87-0017 "Digital Simulation of Seismic Ground Motion," by M. Shinozuka, G. Deodatis and T. Harada, 8/31/87, (PB88-155197/AS). This report is available only through NTIS (see address given above).

NCEER-87-0018 "Practical Considerations for Structural Control: System Uncertainty, System Time Delay and Truncation of Small Control Forces," J.N. Yang and A. Akbarpour, 8/10/87, (PB88-163738/AS).

NCEER-87-0019 "Modal Analysis of Nonclassically Damped Structural Systems Using Canonical Transformation," by J.N. Yang, S. Sarkani and F.X. Long, 9/27/87, (PB88-187851/AS).

NCEER-87-0020 "A Nonstationary Solution in Random Vibration Theory," by J.R. Red-Horse and P.D. Spanos, 11/3/87, (PB88-163746/AS).

NCEER-87-0021 "Horizontal Impedances for Radially Inhomogeneous Viscoelastic Soil Layers," by A.S. Veletsos and K.W. Dotson, 10/15/87, (PB88-150859/AS).

NCEER-87-0022 "Seismic Damage Assessment of Reinforced Concrete Members," by Y.S. Chung, C. Meyer and M. Shinozuka, 10/9/87, (PB88-150867/AS). This report is available only through NTIS (see address given above).

NCEER-87-0023 "Active Structural Control in Civil Engineering," by T.T. Soong, 11/11/87, (PB88-187778/AS).

NCEER-87-0024 Vertical and Torsional Impedances for Radially Inhomogeneous Viscoelastic Soil Layers," by K.W. Dotson and A.S. Veletsos, 12/87, (PB88-187786/AS).

NCEER-87-0025 "Proceedings from the Symposium on Seismic Hazards, Ground Motions, Soil-Liquefaction and Engineering Practice in Eastern North America," October 20-22, 1987, edited by K.H. Jacob, 12/87, (PB88-188115/AS).

NCEER-87-0026 "Report on the Whittier-Narrows, California, Earthquake of October 1, 1987," by J. Pantelic and A. Reinhorn, 11/87, (PB88-187752/AS). This report is available only through NTIS (see address given above).

NCEER-87-0027 "Design of a Modular Program for Transient Nonlinear Analysis of Large 3-D Building Structures," by S. Srivastav and J.F. Abel, 12/30/87, (PB88-187950/AS).

NCEER-87-0028 "Second-Year Program in Research, Education and Technology Transfer," 3/8/88, (PB88-219480/AS).

NCEER-88-0001 "Workshop on Seismic Computer Analysis and Design of Buildings With Interactive Graphics," by W. McGuire, J.F. Abel and C.H. Conley, 1/18/88, (PB88-187760/AS).

NCEER-88-0002 "Optimal Control of Nonlinear Flexible Structures," by J.N. Yang, F.X. Long and D. Wong, 1/22/88, (PB88-213772/AS).

NCEER-88-0003 "Substructuring Techniques in the Time Domain for Primary-Secondary Structural Systems," by G.D. Manolis and G. Juhn, 2/10/88, (PB88-213780/AS).

NCEER-88-0004 "Iterative Seismic Analysis of Primary-Secondary Systems," by A. Singhal, L.D. Lutes and P.D. Spanos, 2/23/88, (PB88-213798/AS).

NCEER-88-0005 "Stochastic Finite Element Expansion for Random Media," by P.D. Spanos and R. Ghanem, 3/14/88, (PB88-213806/AS).

NCEER-88-0006 "Combining Structural Optimization and Structural Control," by F.Y. Cheng and C.P. Pantelides, 1/10/88, (PB88-213814/AS).

NCEER-88-0007 "Seismic Performance Assessment of Code-Designed Structures," by H.H-M. Hwang, J-W. Jaw and H-J. Shau, 3/20/88, (PB88-219423/AS).

NCEER-88-0008 "Reliability Analysis of Code-Designed Structures Under Natural Hazards," by H.H-M. Hwang, H. Ushiba and M. Shinozuka, 2/29/88, (PB88-229471/AS).

NCEER-88-0009 "Seismic Fragility Analysis of Shear Wall Structures," by J-W Jaw and H.H-M. Hwang, 4/30/88, (PB89-102867/AS).

NCEER-88-0010 "Base Isolation of a Multi-Story Building Under a Harmonic Ground Motion - A Comparison of Performances of Various Systems," by F-G Fan, G. Ahmadi and I.G. Tadjbakhsh, 5/18/88, (PB89-122238/AS).

NCEER-88-0011 "Seismic Floor Response Spectra for a Combined System by Green's Functions," by F.M. Lavelle, L.A. Bergman and P.D. Spanos, 5/1/88, (PB89-102875/AS).

NCEER-88-0012 "A New Solution Technique for Randomly Excited Hysteretic Structures," by G.Q. Cai and Y.K. Lin, 5/16/88, (PB89-102883/AS).

NCEER-88-0013 "A Study of Radiation Damping and Soil-Structure Interaction Effects in the Centrifuge," by K. Weissman, supervised by J.H. Prevost, 5/24/88, (PB89-144703/AS).

NCEER-88-0014 "Parameter Identification and Implementation of a Kinematic Plasticity Model for Frictional Soils," by J.H. Prevost and D.V. Griffiths, to be published.

NCEER-88-0015 "Two- and Three- Dimensional Dynamic Finite Element Analyses of the Long Valley Dam," by D.V. Griffiths and J.H. Prevost, 6/17/88, (PB89-144711/AS).

NCEER-88-0016 "Damage Assessment of Reinforced Concrete Structures in Eastern United States," by A.M. Reinhorn, M.J. Seidel, S.K. Kunnath and Y.J. Park, 6/15/88, (PB89-122220/AS).

NCEER-88-0017 "Dynamic Compliance of Vertically Loaded Strip Foundations in Multilayered Viscoelastic Soils," by S. Ahmad and A.S.M. Israil, 6/17/88, (PB89-102891/AS).

NCEER-88-0018 "An Experimental Study of Seismic Structural Response With Added Viscoelastic Dampers," by R.C. Lin, Z. Liang, T.T. Soong and R.H. Zhang, 6/30/88, (PB89-122212/AS).

NCEER-88-0019 "Experimental Investigation of Primary - Secondary System Interaction," by G.D. Manolis, G. Juhn and A.M. Reinhorn, 5/27/88, (PB89-122204/AS).

NCEER-88-0020 "A Response Spectrum Approach For Analysis of Nonclassically Damped Structures," by J.N. Yang, S. Sarkani and F.X. Long, 4/22/88, (PB89-102909/AS).

NCEER-88-0021 "Seismic Interaction of Structures and Soils: Stochastic Approach," by A.S. Veletsos and A.M. Prasad, 7/21/88, (PB89-122196/AS).

NCEER-88-0022 "Identification of the Serviceability Limit State and Detection of Seismic Structural Damage," by E. DiPasquale and A.S. Cakmak, 6/15/88, (PB89-122188/AS).

NCEER-88-0023 "Multi-Hazard Risk Analysis: Case of a Simple Offshore Structure," by B.K. Bhartia and E.H. Vanmarcke, 7/21/88, (PB89-145213/AS).

NCEER-88-0024 "Automated Seismic Design of Reinforced Concrete Buildings," by Y.S. Chung, C. Meyer and M. Shinozuka, 7/5/88, (PB89-122170/AS).

NCEER-88-0025 "Experimental Study of Active Control of MDOF Structures Under Seismic Excitations," by L.L. Chung, R.C. Lin, T.T. Soong and A.M. Reinhorn, 7/10/88, (PB89-122600/AS).

NCEER-88-0026 "Earthquake Simulation Tests of a Low-Rise Metal Structure," by J.S. Hwang, K.C. Chang, G.C. Lee and R.L. Ketter, 8/1/88, (PB89-102917/AS).

NCEER-88-0027 "Systems Study of Urban Response and Reconstruction Due to Catastrophic Earthquakes," by F. Kozin and H.K. Zhou, 9/22/88.

NCEER-88-0028 "Seismic Fragility Analysis of Plane Frame Structures," by H.H-M. Hwang and Y.K. Low, 7/31/88, (PB89-131445/AS).

NCEER-88-0029 "Response Analysis of Stochastic Structures," by A. Kardara, C. Bucher and M. Shinozuka, 9/22/88, (PB89-174429/AS).

NCEER-88-0030 "Nonnormal Accelerations Due to Yielding in a Primary Structure," by D.C.K. Chen and L.D. Lutes, 9/19/88, (PB89-131437/AS).

NCEER-88-0031 "Design Approaches for Soil-Structure Interaction," by A.S. Veletsos, A.M. Prasad and Y. Tang, 12/30/88, (PB89-174437/AS).

NCEER-88-0032 "A Re-evaluation of Design Spectra for Seismic Damage Control," by C.J. Turkstra and A.G. Tallin, 11/7/88, (PB89-145221/AS).

NCEER-88-0033 "The Behavior and Design of Noncontact Lap Splices Subjected to Repeated Inelastic Tensile Loading," by V.E. Sagan, P. Gergely and R.N. White, 12/8/88, (PB89-163737/AS).

NCEER-88-0034 "Seismic Response of Pile Foundations," by S.M. Mamoon, P.K. Banerjee and S. Ahmad, 11/1/88, (PB89-145239/AS).

NCEER-88-0035 "Modeling of R/C Building Structures With Flexible Floor Diaphragms (IDARC2)," by A.M. Reinhorn, S.K. Kunnath and N. Panahshahi, 9/7/88, (PB89-207153/AS).

NCEER-88-0036 "Solution of the Dam-Reservoir Interaction Problem Using a Combination of FEM, BEM with Particular Integrals, Modal Analysis, and Substructuring," by C-S. Tsai, G.C. Lee and R.L. Ketter, 12/31/88, (PB89-207146/AS).

NCEER-88-0037 "Optimal Placement of Actuators for Structural Control," by F.Y. Cheng and C.P. Pantelides, 8/15/88, (PB89-162846/AS).

NCEER-88-0038 "Teflon Bearings in Aseismic Base Isolation: Experimental Studies and Mathematical Modeling," by A. Mokha, M.C. Constantinou and A.M. Reinhorn, 12/5/88, (PB89-218457/AS).

NCEER-88-0039 "Seismic Behavior of Flat Slab High-Rise Buildings in the New York City Area," by P. Weidlinger and M. Ettouney, 10/15/88.

NCEER-88-0040 "Evaluation of the Earthquake Resistance of Existing Buildings in New York City," by P. Weidlinger and M. Ettouney, 10/15/88, to be published.

NCEER-88-0041 "Small-Scale Modeling Techniques for Reinforced Concrete Structures Subjected to Seismic Loads," by W. Kim, A. El-Attar and R.N. White, 11/22/88, (PB89-189625/AS).

NCEER-88-0042 "Modeling Strong Ground Motion from Multiple Event Earthquakes," by G.W. Ellis and A.S. Cakmak, 10/15/88, (PB89-174445/AS).

NCEER-88-0043 "Nonstationary Models of Seismic Ground Acceleration," by M. Grigoriu, S.E. Ruiz and E. Rosenblueth, 7/15/88, (PB89-189617/AS).

NCEER-88-0044 "SARCF User's Guide: Seismic Analysis of Reinforced Concrete Frames," by Y.S. Chung, C. Meyer and M. Shinozuka, 11/9/88, (PB89-174452/AS).

NCEER-88-0045 "First Expert Panel Meeting on Disaster Research and Planning," edited by J. Pantelic and J. Stoyle, 9/15/88, (PB89-174460/AS).

NCEER-88-0046 "Preliminary Studies of the Effect of Degrading Infill Walls on the Nonlinear Seismic Response of Steel Frames," by C.Z. Chrysostomou, P. Gergely and J.F. Abel, 12/19/88, (PB89-208383/AS).

NCEER-88-0047 "Reinforced Concrete Frame Component Testing Facility - Design, Construction, Instrumentation and Operation," by S.P. Pessiki, C. Conley, T. Bond, P. Gergely and R.N. White, 12/16/88, (PB89-174478/AS).

NCEER-89-0001 "Effects of Protective Cushion and Soil Compliancy on the Response of Equipment Within a Seismically Excited Building," by J.A. HoLung, 2/16/89, (PB89-207179/AS).

NCEER-89-0002 "Statistical Evaluation of Response Modification Factors for Reinforced Concrete Structures," by H.H-M. Hwang and J-W. Jaw, 2/17/89, (PB89-207187/AS).

NCEER-89-0003 "Hysteretic Columns Under Random Excitation," by G-Q. Cai and Y.K. Lin, 1/9/89, (PB89-196513/AS).

NCEER-89-0004 "Experimental Study of 'Elephant Foot Bulge' Instability of Thin-Walled Metal Tanks," by Z-H. Jia and R.L. Ketter, 2/22/89, (PB89-207195/AS).

NCEER-89-0005 "Experiment on Performance of Buried Pipelines Across San Andreas Fault," by J. Isenberg, E. Richardson and T.D. O'Rourke, 3/10/89, (PB89-218440/AS).

NCEER-89-0006 "A Knowledge-Based Approach to Structural Design of Earthquake-Resistant Buildings," by M. Subramani, P. Gergely, C.H. Conley, J.F. Abel and A.H. Zaghw, 1/15/89, (PB89-218465/AS).

NCEER-89-0007 "Liquefaction Hazards and Their Effects on Buried Pipelines," by T.D. O'Rourke and P.A. Lane, 2/1/89, (PB89-218481).

NCEER-89-0008 "Fundamentals of System Identification in Structural Dynamics," by H. Imai, C-B. Yun, O. Maruyama and M. Shinozuka, 1/26/89, (PB89-207211/AS).

NCEER-89-0009 "Effects of the 1985 Michoacan Earthquake on Water Systems and Other Buried Lifelines in Mexico," by A.G. Ayala and M.J. O'Rourke, 3/8/89, (PB89-207229/AS).

NCEER-89-R010 "NCEER Bibliography of Earthquake Education Materials," by K.E.K. Ross, 3/10/89, (PB90-109901/AS).

NCEER-89-0011 "Inelastic Three-Dimensional Response Analysis of Reinforced Concrete Building Structures (IDARC-3D), Part I - Modeling," by S.K. Kunnath and A.M. Reinhorn, 4/17/89, (PB90-114612/AS).

NCEER-89-0012 "Recommended Modifications to ATC-14," by C.D. Poland and J.O. Malley, 4/12/89.

NCEER-89-0013 "Repair and Strengthening of Beam-to-Column Connections Subjected to Earthquake Loading," by M. Corazao and A.J. Durrani, 2/28/89, (PB90-109885/AS).

NCEER-89-0014 "Program EXKAL2 for Identification of Structural Dynamic Systems," by O. Maruyama, C-B. Yun, M. Hoshiya and M. Shinozuka, 5/19/89, (PB90-109877/AS).

NCEER-89-0015 "Response of Frames With Bolted Semi-Rigid Connections, Part I - Experimental Study and Analytical Predictions," by P.J. DiCorso, A.M. Reinhorn, J.R. Dickerson, J.B. Radziminski and W.L. Harper, 6/1/89, to be published.

NCEER-89-0016 "ARMA Monte Carlo Simulation in Probabilistic Structural Analysis," by P.D. Spanos and M.P. Mignolet, 7/10/89, (PB90-109893/AS).

NCEER-89-0017 "Preliminary Proceedings of the Conference on Disaster Preparedness - The Place of Earthquake Education in Our Schools, July 9-11, 1989," 6/23/89, (PB90-108606/AS).

NCEER-89-0018 "Multidimensional Models of Hysteretic Material Behavior for Vibration Analysis of Shape Memory Energy Absorbing Devices, by E.J. Graesser and F.A. Cozzarelli, 6/7/89.

NCEER-89-0019 "Nonlinear Dynamic Analysis of Three-Dimensional Base Isolated Structures (3D-BASIS)," by S. Nagarajaiah, A.M. Reinhorn and M.C. Constantinou, 8/3/89.

NCEER-89-0020 "Structural Control Considering Time-Rate of Control Forces and Control Rate Constraints," by F.Y. Cheng and C.P. Pantelides, 8/3/89.

NCEER-89-0021 "Subsurface Conditions of Memphis and Shelby County," by K.W. Ng, T-S. Chang and H-H.M. Hwang, 7/26/89.

NCEER-89-0022 "Seismic Wave Propagation Effects on Straight Jointed Buried Pipelines," by K. Elhmadi and M.J. O'Rourke, 8/24/89.

NCEER-89-0023 "Workshop on Serviceability Analysis of Water Delivery Systems," edited by M. Grigoriu, 3/6/89.

NCEER-89-0024 "Shaking Table Study of a 1/5 Scale Steel Frame Composed of Tapered Members," by K.C. Chang, J.S. Hwang and G.C. Lee, 9/18/89.

NCEER-89-0025 "DYNA1D: A Computer Program for Nonlinear Seismic Site Response Analysis - Technical Documentation," by Jean H. Prevost, 9/14/89.